[redacted]

NACA

RESEARCH MEMORANDUM

for the

Bureau of Aeronautics, Department of the Navy

STATIC LONGITUDINAL AND LATERAL STABILITY CHARACTERISTICS INCLUDING EFFECTS OF TRANSONIC AREA RULE AND WING MODIFICATION OF A 0.10-SCALE MODEL OF THE DOUGLAS A4D-1 AIRPLANE AT TRANSONIC SPEEDS

TED NO. NACA AD 3114

By Dewey E. Wornom and Thomas V. Bollech

Langley Aeronautical Laboratory
Langley Field, Va.

NATIONAL ADVISORY COMMITTEE
FOR AERONAUTICS

WASHINGTON

AUG 1 1956

[redacted]

NACA RM SL56G19

NATIONAL ADVISORY COMMITTEE FOR AERONAUTICS

RESEARCH MEMORANDUM

for the

Bureau of Aeronautics, Department of the Navy

STATIC LONGITUDINAL AND LATERAL STABILITY CHARACTERISTICS INCLUDING EFFECTS OF TRANSONIC AREA RULE AND WING MODIFICATION OF A 0.10-SCALE MODEL OF THE DOUGLAS A4D-1 AIRPLANE AT TRANSONIC SPEEDS

TED NO. NACA AD 3114

By Dewey E. Wornom and Thomas V. Bollech

SUMMARY

Force tests of a 0.10-scale model of the Douglas A4D-1 airplane were conducted in the Langley 8-foot transonic pressure tunnel to investigate the static longitudinal characteristics of wing and fuselage modifications and the static lateral characteristics of the basic model. The tests were conducted at Mach numbers of 0.60 to 1.20 with a maximum angle-of-attack range of -3° to 11°.

Addition of cross-sectional area to the aft fuselage section, extension of the wing trailing edge, and the combination of the two were effective in reducing the zero-lift drag around a Mach number of 0.975. These reductions were essentially maintained at least up to a lift coefficient of 0.4. Above a Mach number of 1.05, at lift coefficients up to 0.4, the addition of cross-sectional area to the aft fuselage section resulted in an increase in drag. The extension of the internal-flow duct inlets had no appreciable effect upon the drag characteristics of the model. Modifications involving the addition of cross-sectional area to the aft fuselage section and the extension of the wing trailing edge also resulted in a recovery of losses in lift-curve slope and static longitudinal stability exhibited by the basic model around a Mach number of 0.95. Wing leading-edge modifications, consisting of a tapered chord-extension with camber and a constant chord-extension with camber slightly improved the drag characteristics at lifting conditions. Addition of a tail cone fairing had no appreciable effect upon the longitudinal aerodynamic characteristics of the model. The basic model with a cambered and tapered chord-extension on the wing leading edge exhibited positive directional stability and positive effective dihedral throughout the angle-of-attack range.

INTRODUCTION

At the request of the Bureau of Aeronautics, Department of the Navy, longitudinal force and moment tests of a 0.10-scale model of the Douglas A4D-1 airplane were conducted in the Langley 8-foot transonic pressure tunnel. These tests were performed primarily as an attempt to improve the drag characteristics of the model through application of the transonic area rule of reference 1. The area-rule modifications, resulting in a minimum change in physical configuration, consisted of the addition of cross-sectional area to the fuselage aft of the wing, the addition of 10° forward sweep to the straight trailing edge of the delta wing, and the extension of duct inlets to improve the longitudinal area distribution of the model (ref. 2). Results from an investigation of the effects of wing leading-edge modifications, consisting of a tapered chord-extension with camber and a constant chord-extension with camber, on the drag characteristics, a tail cone fairing (designed for tail buffet alleviation) on the longitudinal aerodynamic characteristics, and transition on drag characteristics are also included.

In addition, results of static lateral stability tests of the basic model with and without empennage and some external-flow characteristics indicated by tuft studies are presented.

SYMBOLS

The stability system of axes used for the presentation of the data, together with the positive direction of force, moment, and angular measurements is shown in figure 1.

A	aspect ratio
A_e	duct exit area, sq ft
b	wing span, in.
c	local chord, in.
$\bar{c}$	mean aerodynamic chord, in.
D	measured drag corrected for internal drag and balance chamber buoyancy force, lb
D_i	internal drag, $\text{lb} = w\left(V_\infty - V_e\right) - A_e\left(p_e - p_\infty\right)$

$(L/D)_{max}$ maximum lift-drag ratio

M free-stream Mach number

p_e static pressure at duct exit, lb/sq ft

p_∞ free-stream static pressure, lb/sq ft

q_∞ free-stream dynamic pressure, lb/sq ft

R Reynolds number based on mean aerodynamic chord of 12.96 in.

S total basic wing area, sq ft

V_e velocity at duct exit, ft/sec

V_∞ free-stream velocity, ft/sec

w mass flow through inlets, slugs/sec

w_∞ mass flow in free-stream tube of area equal to minimum projected inlet area of both inlets at α and $\beta = 0^\circ$, slugs/sec

C_D drag coefficient, $\frac{D}{q_\infty S}$

C_{D_o} drag coefficient at zero lift, $\frac{\text{Drag at zero lift}}{q_\infty S}$

C_D' longitudinal-force coefficient, $\frac{\text{Longitudinal force}}{q_\infty S}$,

$C_D' = C_D$ when $\beta = 0^\circ$

C_{D_i} internal drag coefficient, $\frac{D_i}{q_\infty S}$

C_L lift coefficient, $\frac{\text{Lift}}{q_\infty S}$

$C_{L(L/D)_{max}}$ lift coefficient for maximum lift-drag ratio

C_{L_α} lift-curve slope per degree, averaged from $C_L = 0$ over linear portion of curve

C_l rolling-moment coefficient, $\frac{\text{Rolling moment}}{q_\infty Sb}$

C_{l_β} effective-dihedral derivative, $\partial C_l/\partial\beta$

C_n yawing-moment coefficient, $\frac{\text{Yawing moment}}{q_\infty Sb}$

C_{n_β} directional-stability derivative, $\partial C_n/\partial\beta$

C_m pitching-moment coefficient, $\frac{\text{Pitching moment about } 0.25\bar{c}}{q_\infty S\bar{c}}$

$C_{m_{C_L}}$ static longitudinal stability parameter, $\partial C_m/\partial C_L$ (averaged from $C_L = 0$ to 0.3)

C_Y lateral-force coefficient, $\frac{\text{Side force}}{q_\infty S}$

C_{Y_β} lateral-force derivative, $\partial C_Y/\partial\beta$

α angle of attack referred to fuselage reference line, deg

β angle of sideslip, deg

APPARATUS AND METHODS

Tunnel

The investigation was conducted in the Langley 8-foot transonic pressure tunnel, which is a single-return system with a rectangular slotted test section permitting continuous operation throughout the transonic speed range. The slots are located in both the upper and the lower walls (fig. 2). Automatic stagnation-temperature controls maintain a constant and uniform air temperature of 120° F. Tunnel dewpoint is maintained at 0° F or lower. Through automatic stagnation-temperature and dewpoint control, the effects of humidity are greatly minimized.

Local Mach number distributions over the test section length occupied by the model are shown in figure 3. These distributions were obtained by an axial survey tube, provided with static-pressure orifices along its length, positioned in the center of the tunnel. Local Mach number deviations over the length of the model were no greater than 0.005 at subsonic speeds and 0.010 at supersonic speeds.

Through the design of the sting-support system (fig. 2), the model is essentially located at the center line of the test section throughout the angle range tested.

Model

A three-view drawing of the 0.10-scale model of the Douglas A4D-1 airplane is shown in figure 4 and geometric characteristics are listed in table I. Tables II and III list the ordinates of the wing and tail sections, respectively. Figure 5 gives the cross-sectional area distribution for the basic model and area modifications thereof. Photographs of the model sting mounted in the Langley 8-foot transonic pressure tunnel are shown in figure 6. The model and all modifications were supplied by the contractor.

The term "basic model" hereinafter refers to the model with the following components:

(1) Wing (no movable surfaces)

(2) Fuselage with twin inlets and internal ducting

(3) Canopy

(4) Horizontal stabilizer (movable elevators fixed at zero deflection)

(5) Vertical stabilizer (no rudder)

(6) Closed landing gear fairing

(7) Wing guns

(8) Arresting hook

(9) Fuselage center line pylon

The initial tests were performed with the original tail cone, which corresponds geometrically to the full-scale airplane. When internal flow difficulties were encountered with the original tail cone, which

are discussed in detail in a subsequent section of this paper, the modified tail cone, which increased the internal duct exit area, was used for the remainder of the tests. The modified tail cone (fig. 4) was obtained by reducing the length of the original tail cone 1.93 inches and boring out the latter to increase the duct-exit area from 0.39 square inch to 1.07 square inches. (See table I.)

The area modifications consisted of a full bump, modified full bump combined with a wing trailing-edge extension sweptforward 10°, and a wing trailing-edge extension alone (figs. 7 and 8). (The trailing edge is referred to as T.E. in the figures.) The full bump and modified full bump modifications were based upon the transonic area rule of reference 1. As much area as possible was added by the bumps behind the wing to smooth out the aft portion of the area distribution curve of figure 5 without creating excessive longitudinal model surface curvature resulting in adverse pressure gradients. The modified full bump was obtained by removing from the full bump above the wing chord plane that area added by the trailing-edge extensions. The wing trailing-edge extension was formed by strips of metal clamped to the trailing edge of the basic wing. Filler was used to build up the trailing-edge extension so that the upper and lower wing surfaces were flat from the swept trailing-edge forward to a point of tangency on the basic wing (fig. 8). Since the trailing edge extension ended below the bottom of the fuselage, it was necessary to include a fuselage fairing to fill in the existing gap (fig. 7). The extended internal flow duct inlets are the same geometrically as the basic inlets and were obtained by moving the basic inlets forward 0.9 inch (fig. 4).

The modifications to the wing leading edge consisted of a tapered chord-extension with camber and a constant chord-extension with camber hereinafter referred to as leading edge I and leading edge II, respectively (fig. 9 and table IV). (The leading edge is referred to as L.E. in the figures.)

The tail cone fairing, whose exposed surface is circular in cross-section shape, formed a fairing at the tail of the model between the original tail cone and vertical tail (fig. 4).

Measurements and Accuracies

Force and moment measurements were made by a six-component electrical strain-gage balance internally mounted within the model. Moments are referred to the assumed center of gravity of the airplane (25 percent of the mean aerodynamic chord). All coefficients were based on the wing area and mean aerodynamic chord of the basic wing, 2.60 square feet and 12.96 inches, respectively. Through consideration of the static calibrations of the electrical strain-gage balance and repeatability of data, the estimated accuracy of the coefficients at a Mach number of 0.60 is as follows:

C_L	±0.01
C_D	±0.0015
C_m	±0.002
C_l	±0.0008
C_n	±0.001
C_Y	±0.004

Since the accuracy is inversely proportional to dynamic pressure, these values decrease with Mach number.

Angle of attack and angle of sideslip were determined with a pendulum-type strain-gage unit located in the support strut of the model support system. Model loaded deflections were corrected by a calibration of sting and strain-gage balance deflections with respect to model forces and moments. The estimated accuracy of the angle of attack and angle of sideslip is within ±0.1°. For lateral tests at constant angles of attack or constant angles of sideslip, these angles were measured by the deflection of a light source reflected from the model sting directly behind the model base and corrected by a calibration of balance deflections with respect to model forces and moments. The values stated for these constant angles are nominal values.

Internal-drag and mass-flow measurements were obtained by pressure survey rakes located at the duct exit. Four rakes were spaced 45°, 135°, 225°, and 315° around and beginning at the top of the base annulus. Each rake consisted of four total pressure tubes and one static pressure tube. The tube spacing was such that each tube sampled an equal segment of the annular area. One static pressure tube was placed in the strain-gage balance chamber of the model and used to obtain the balance-chamber buoyancy force. Both internal drag and balance-chamber buoyancy force have been removed from the drag values measured by the strain-gage balance before presentation in this paper.

Corrections

Boundary interference at subsonic velocities has been minimized by the slotted test section and no corrections have been applied. At Mach numbers above 1.025 and below 1.20, boundary-reflected disturbances were present and data in this range were not taken. At a Mach number of 1.20, unpublished schlieren photographs showed that the boundary-reflected disturbances had passed downstream of the model base approximately 2.2 model base diameters.

With a ratio of model sting area to model base area of 0.292, sting interference on lift and pitching-moment coefficients should be negligible

(ref. 3). The effect of the sting on the drag coefficients has been reduced by the removal of internal drag which contains base-pressure measurements.

Tests

Static longitudinal tests of the basic model including area modifications, wing leading-edge modifications, and tail cone fairing were conducted at Mach numbers from 0.60 to 1.20 and an angle-of-attack range which varied with configuration up to a maximum of approximately -3° to 11° (maximum angle of attack limited by load limits of the internal strain-gage balance). In order to obtain lift coefficients of at least 0.4, the tests were conducted at a reduced tunnel pressure of 0.8 atmosphere. The Reynolds number for these tests was of the order of 3.5×10^6 based on the wing mean aerodynamic chord (fig. 10).

Static lateral tests of the model with and without horizontal and vertical tail were conducted at Mach numbers of 0.80 to 1.20 for constant angles of sideslip from 0° to 5° (0°, 2.4°, and 5° for the model without empennage and 0°, 2°, and 5° for the model with empennage). The test angle-of-attack range varied up to a maximum of approximately -3° to 11°. Lateral tests were also conducted at constant nominal angles of attack of 0° and 6° with angle of sideslip varying up to a maximum range of approximately -12° to 10°. In order to obtain the large angles of sideslip at an angle of attack of 6°, the lateral tests were conducted at a reduced tunnel pressure of 0.5 atmosphere (due to load limits of the internal strain-gage balance). The Reynolds number for these tests was of the order of 2.25×10^6 based on the wing mean aerodynamic chord (fig. 10).

Tuft studies of the basic model with and without full bumps were made for a Mach number range of 0.80 to 0.95 through an angle-of-attack range of 0° to 6°.

Test data of the model with fixed transition were obtained by adding 1/8-inch strips of no. 60 (0.0117-inch-diameter) carborundum particles applied sparsely along the 5-percent-chord lines of the wing (upper and lower surfaces), horizontal tail (upper and lower surfaces), vertical tail (both sides), around the duct inlet 1.75 inches from the inlet lip and around the fuselage nose 1.75 inches back from the nose leading edge.

RESULTS

In order to obtain satisfactory external drag measurements in wind-tunnel tests of a model with internal ducting, the internal mass-flow

ratio for the model should be approximately the same as the operational mass-flow ratio of the full-scale airplane. In the case of the Douglas A4D-1 airplane the operational mass-flow ratio is approximately 0.75 for an altitude of 35,000 feet at a Mach number of 0.90. At the beginning of the present wind-tunnel tests, the mass-flow ratio measured for the model with the original tail cone was 0.26 for a Mach number of 0.90 (fig. 11(a)). Subsequent tests of the model with the modified tail cone resulted in a mass-flow ratio of approximately 0.75 at a Mach number of 0.90 (fig. 11(b)). Upon comparing the drag data of the basic model with the original tail cone (fig. 12) with that of the basic model with the modified tail cone (fig. 13), it is noted that the original tail cone with the low mass-flow ratio resulted in an increase of approximately 0.0025 in zero-lift drag coefficient. It is believed that the higher drag values for the model with the original tail cone primarily resulted from external spillage at the inlet as the result of the low mass-flow ratio. It was therefore decided to use the modified tail cone for the remainder of the tests.

The data from this investigation are presented in the following figures:

The use of staggered scales has been employed extensively in the presentation of data and care should be exercised in the selection of the zero axis for each curve.

DISCUSSION

Longitudinal Force and Moment Characteristics

Cross-sectional area modifications.- The purpose of the cross-sectional area modifications was to improve the transonic drag characteristics of the model and to determine to what extent they affected lift and pitching-moment characteristics. The full bump provided the necessary addition of area to the total area distribution of the basic model (fig. 5) in order to conform to the principles of the transonic area-rule concept (refs. 1 and 2). The wing trailing-edge extension provided a swept trailing edge in an attempt to extend the drag-rise Mach number of the model by relieving the abrupt discontinuity of the area-distribution curve at the juncture of the wing trailing edge and fuselage (fig. 5). The modified full bump was designed to fill in the total area distribution of the basic model with trailing-edge extension resulting in essentially the same total area distribution of the basic model with full bump (fig. 5). This involved the removal of area from the full bump equal to the cross-sectional area added by the trailing-edge extension. The loss of lift experienced by the addition of the full bump (fig. 14) was believed to be caused by local velocity gradients created on the upper surface of the wing by the curvature at the beginning of the bump. It was therefore decided that the area removed from the full bump to obtain the modified full bump would be taken from above the wing to reduce the bump curvature and thereby reduce the intensity of the local velocity gradient. The inlets were extended to improve the forward portion of the total area distribution curve (fig. 5).

In general, the full bump, wing trailing-edge extensions, and trailing-edge extension combined with modified full bump resulted in reductions in zero-lift drag over a Mach number range from approximately 0.975 to 1.00 (fig. 18). The modified full bump with wing trailing-edge extension produced the largest maximum reduction in zero-lift drag coefficient of 0.0100 around a Mach number of 0.975. Although the wing trailing-edge extension did not increase the drag-rise Mach number, it did produce a zero-lift drag coefficient reduction of approximately 0.0040 from Mach numbers of 0.975 to 1.00. Above a Mach number of 1.05, the full bump and wing trailing-edge extension combined with modified full bump increased the drag coefficient at least up to a lift coefficient of 0.4 (figs. 18 and 19). Generally, the full bump, wing trailing-edge extension, and trailing-edge extension combined with modified full bump provided only a slight decrease in the rate of rise of the zero-lift drag coefficient with increasing Mach number up to a Mach number of 1.05 (fig. 18). It is of practical importance to note that the zero-lift drag reductions produced by the full bump, wing trailing-edge extension, and trailing-edge extension combined with modified full bump were essentially maintained up to a lift coefficient of 0.4 (fig. 19). At a lift coefficient of 0.4, the wing trailing-edge extension resulted in approximately twice the maximum drag coefficient reduction obtained at zero-lift conditions and a drag coefficient decrease of about 3 percent at a Mach number of 1.20. No appreciable improvements in drag characteristics were realized by the extended inlets (fig. 13).

The full bump and wing trailing-edge extension had no appreciable effect upon the maximum lift-drag ratio or lift coefficient for maximum lift-drag ratio over the Mach number range tested (fig. 20). The wing trailing-edge extension combined with modified full bump resulted in the greatest change in maximum lift-drag ratio at a Mach number of 0.80 (a decrease of approximately 12 percent) and it is possible that this reduction may continue at lower subsonic speeds.

The full bump resulted in a loss in lift coefficient of approximately 0.05 (fig. 14) around an angle of attack of 0° throughout the Mach number range. The loss in lift may possibly be attributed to adverse upper wing surface pressure gradients previously mentioned. Some indication of the rapid loss in lift-curve slope exhibited by the basic model (fig. 21) at a Mach number around 0.95 and recovered by the addition of the full bump may be seen in the tuft studies of the basic model with and without the full bump in figure 31. Except for a Mach number of 0.95 (fig. 31(d)), the flow over the wing for both configurations with and without full bump appears to be similar. At a Mach number of 0.95, flow separation has occurred in the vicinity of the wing-fuselage juncture for the basic model near the trailing edge of the wing over both the wing and the body and appears to become more severe with angle of attack, thus resulting in loss of lift-curve slope. Upon addition of the full bump, the degree of separation appears to be reduced, thereby recovering

the loss in lift-curve slope. The wing trailing-edge extension and trailing-edge extension combined with modified full bump also removed the abrupt discontinuity in lift-curve slope experienced by the basic model (fig. 21). It appears that these modifications may be as beneficial as the full bump in alleviating the flow separation near the wing trailing edge and fuselage juncture. The wing trailing-edge extension increased the lift-curve slope approximatly 5 percent over the Mach number range tested (figs. 15 and 21) except at a Mach number of 1.20 where an increase of 11 percent resulted. This percentage increase in lift-curve slope is considerably less than the 14-percent increase in wing area due to the wing trailing-edge extension. The manner in which the area was removed from the full bump to produce the modified full bump, previously mentioned, was not effective in recovering the loss of lift (figs. 14 and 15). The wing trailing-edge extension and modified full bump combined increased the lift-curve slope from approximately 3 to 17 percent over the Mach number range tested (fig. 21). The extended inlets had no significant effect upon the lift characteristics (fig. 13).

The effect of the full bump, wing trailing-edge extensions, and trailing-edge extension combined with modified full bump on the pitching-moment coefficient (figs. 14 and 15) and static longitudinal stability parameter (fig. 21) as compared with the basic model is associated with the effects each had upon the lift characteristics. The extended inlets had no significant effect upon the pitching-moment characteristics (fig. 13).

Wing-leading-edge modifications.- Both leading edge I and leading edge II resulted in a slightly higher zero-lift drag level (figs. 16 and 22) over the Mach number range tested as compared with the basic leading edge. The small increase in wing area (approximately 1.5 percent for leading edge I and 4.5 percent for leading edge II) would partially account for the increase in drag level due to the expected increase in skin friction drag. At a lift coefficient of 0.2 no beneficial drag reductions were realized from either leading-edge modification. At a lift coefficient of 0.4, leading edge I resulted in a small decrease in drag coefficient of approximately 0.0025 which slowly diminished up to a Mach number of 0.95 where leading edge I ceased to be effective. Leading edge II realized a drag coefficient reduction which varied from approximately 0.0050 to 0.0075 over the Mach number range except around Mach numbers of 1.00 and 1.025 where no reduction is evident.

In order to give some insight into the effectiveness of the leading-edge modifications, the values of $(L/D)_{max}$ for the wing realizing full and no leading-edge suction have been plotted in figure 23. Values for full and no leading-edge suction were computed from $(L/D)_{max} = \frac{1}{2\sqrt{KC_{D_o}}}$

where K (drag-due-to-lift factor) for full leading-edge suction was taken as $\frac{1}{\pi A}$ at subsonic speeds and obtained from reference 4 for supersonic speeds. For no suction, K was assumed to be equal to $\frac{1}{57.3C_{L_\alpha}}$. Values for C_{D_o} and C_{L_α} were obtained from experimental data. Throughout the Mach number range, neither leading-edge modification improved the leading-edge suction over that of the basic leading edge except for Mach numbers near 0.95 where leading edge II realized approximately 33 percent of full leading-edge suction. Neither leading edge I nor leading edge II had any appreciable effect upon the lift coefficient for maximum lift-drag ratio when compared with the basic leading edge.

In general, neither leading-edge modification resulted in more than slight changes in lift or pitching-moment characteristics (fig. 24).

Tail cone fairing.- The tail cone fairing is expected to alleviate the tail buffet loads without appreciably affecting the force and moment characteristics of the basic model. In figure 12 it is shown that the tail cone fairing had no appreciable effect upon the lift or drag characteristics but decreased the trim-lift coefficient slightly over the Mach number range. Since the tail cone fairing is located directly beneath the horizontal tail (fig. 4) it could be expected to influence the lift on the tail surface and, thus, to affect the pitching-moment characteristics until the formation of the wing trailing-edge shock at supersonic speeds could possibly change the tail lift characteristics.

Transition.- Figures 17 and 25 show that the addition of transition increased the zero-lift drag coefficient approximately 0.002 to 0.003 over the Mach number range tested. Transition had little or no effect upon the lift or pitching-moment characteristics (fig. 17).

Lateral Force and Moment Characteristics

Effective dihedral.- At negative lift coefficients and angles of attack (figs. 26 and 29(a)), the basic model including leading edge I without horizontal or vertical tail exhibited negative effective dihedral $\left(\text{positive values of } C_{l_\beta}\right)$. At positive lift coefficients and angles of attack the model exhibited positive effective dihedral $\left(\text{negative values of } C_{l_\beta}\right)$ up to a Mach number of 0.95, and above this Mach number either neutral or slightly negative effective dihedral. The model without

horizontal or vertical tail revealed slightly positive effective dihedral, for constant lift coefficients of approximately 0.1 and 0.5, up to a Mach number of 1.00, and above this speed exhibited slightly negative effective dihedral (figs. 28 and 30). Addition of the horizontal and vertical tail resulted in positive effective dihedral over the lift and Mach number range tested (figs. 29(a) and 30, respectively). In figure 30, as the lift coefficient increases from 0.1 to 0.5, there is an approximate loss in positive effective dihedral of 33 percent throughout the Mach number range.

Directional stability.- The basic model including leading edge I without horizontal and vertical tail was directionally unstable $\left(\text{negative values for } C_{n_\beta}\right)$ throughout the lift range (figs. 26 and 29(b)) and Mach number range for approximate lift coefficients of 0.1 and 0.5 (figs. 28 and 30). Upon addition of the tails the model became directionally stable throughout the lift range (figs. 27 and 29(b)) and throughout the Mach number range for lift coefficients of approximately 0.1 and 0.5 (figs. 28 and 30).

Lateral-force derivative.- Little or no effect on the lateral-force derative was noted due to lift (fig. 29(c)) or Mach number (fig. 30) for the model with or without tails. The incremental lateral-force derivative contributed by the vertical tail was approximately 0.014 throughout the Mach number range.

CONCLUSIONS

From transonic wind-tunnel tests of a 0.10-scale model of the Douglas A4D-1 airplane to investigate the static longitudinal characteristics of wing and fuselage modifications and static lateral characteristics of the basic model, the following conclusions are indicated:

1. Addition of cross-sectional area to the aft fuselage section, extension of the wing trailing edge, and the combination of the two were effective in reducing the zero-lift drag coefficient around a Mach number of 0.975. These reductions were essentially maintained at least up to a lift coefficient of 0.4. Above a Mach number of 1.05 up to a lift coefficient of 0.4, addition of cross-sectional area to the aft fuselage section resulted in an increase in drag coefficient. The extension of the internal-flow duct inlets had no appreciable effect upon the drag characteristics of the model.

2. Modifications involving the addition of cross-sectional area to the aft fuselage section and wing trailing-edge extension resulted in

the recovery of a loss in lift-curve slope and static longitudinal stability exhibited by the basic model around a Mach number of 0.95.

3. Wing leading-edge modifications consisting of a tapered chord-extension with camber and a constant chord-extension with camber slightly improved the drag at lifting conditions.

4. The addition of a tail cone fairing had no appreciable effect upon the longitudinal aerodynamic characteristics of the model.

5. The basic model with a tapered chord-extension with camber on the wing leading edge exhibited positive directional stability and positive effective dihedral through the angle-of-attack and Mach number ranges tested.

Langley Aeronautical Laboratory,
National Advisory Committee for Aeronautics,
Langley Field, Va., July 6, 1956.

Dewey E. Wornom
Aeronautical Research Scientist

Approved: Eugene C. Draley
Eugene C. Draley
Chief of Full-Scale Research Division

Thomas V. Bollech
Thomas V. Bollech
Aeronautical Engineer

pf

REFERENCES

1. Whitcomb, Richard T.: A Study of the Zero-Lift Drag-Rise Characteristics of Wing-Body Combinations Near the Speed of Sound. NACA RM L52H08, 1952.

2. Holdaway, George H.: Comparison of Theoretical and Experimental Zero-Lift Drag-Rise Characteristics of Wing-Body-Tail Combinations Near the Speed of Sound. NACA RM A53H17, 1953.

3. Osborne, Robert S.: High-Speed Wind-Tunnel Investigation of the Longitudinal Stability and Control Characteristics of a 1/16-Scale Model of the D-558-2 Research Airplane at High Subsonic Mach Numbers and at a Mach Number of 1.2. NACA RM L9C04, 1949.

4. Jones, Robert T.: Estimated Lift-Drag Ratios at Supersonic Speed. NACA TN 1350, 1947.

TABLE I

GEOMETRIC CHARACTERISTICS OF THE 0.10-SCALE MODEL

OF THE DOUGLAS A4D-1 AIRPLANE

Basic wing:		
Airfoil sections:		
Root		NACA 0008 (modified)
Tip		NACA 0005 (modified)
Area, total, sq ft		2.60
Aspect ratio		2.91
Mean aerodynamic chord, in.		12.96
Location of assumed center of gravity, percent $\bar{c}$		25.00
Incidence, deg		0
Dihedral, deg		2.67
Geometric twist, deg		0
Span, in.		33.00
Leading-edge sweep, deg		41.11
Trailing-edge sweep, deg		0
Root chord, in.		18.60
Tip chord, in.		4.20
Fuselage:		
Overall length, in.:		
With original tail cone		44.43
With modified tail cone		42.50
Maximum frontal area (free-stream area of 3.56 sq in. removed), sq in.		26.97
Empennage:		
	Horizontal	Vertical
Airfoil section		
Root	NACA 0007 (modified)	NACA 0007 (modified)
Tip	NACA 0004 (modified)	NACA 0004 (modified)
Area, including control surfaces, sq ft	0.4585	0.4995
Span, in.	13.60	9.44
Root chord, in.	8.00	12.83
Tip chord, in.	1.80	2.495
Mean aerodynamic chord, in.	5.59	8.86
Aspect ratio	2.80	1.24
Taper ratio	0.225	0.1945
Leading-edge sweep, deg	42.36	49.60
Dihedral, deg	0	0
Incidence, deg	0	0
Geometric twist, deg	0	0
Engine ducts:		
Inlet area (both), sq in.		4.89
Exit area (excluding sting), sq in.:		
Original tail cone		0.39
Modified tail cone		1.07
Equivalent body of revolution:		
Maximum frontal area (free-stream area of 3.56 sq in. removed), sq in.		42.98
Fineness ratio (free-stream area of 3.56 sq in. removed)		6.23

TABLE II

BASIC WING ORDINATES FOR 0.10-SCALE DOUGLAS A4D-1 AIRPLANE

Modified NACA 0008

Root chord ordinates, percent c		
Station	Upper	Lower
0	0	0
1.1	1.50	-----
1.4	----	-1.14
2.3	2.19	-----
2.7	----	-1.53
4.8	3.15	-----
5.2	----	-2.00
7.3	3.80	-----
7.7	----	-2.31
9.9	4.25	-----
10.1	----	-2.54
15.0	4.72	-2.88
20.0	4.85	-3.08
25.0	4.83	-3.17
30.0	4.75	-3.20
40.0	4.46	-3.13
50.0	4.01	-2.90
60.0	3.41	-2.53
70.0	2.70	-2.04
80.0	1.89	-1.45
90.0	.99	-.77
95.0	.52	-.41
100.0	0	0
L.E. radius: 0.70 percent c		

Modified NACA 0005

Tip chord ordinates, percent c		
Station	Upper	Lower
0	0	0
1.2	.83	-----
1.3	----	-.47
2.4	1.22	-----
2.6	----	-.55
4.9	1.77	-----
5.1	----	-.61
7.4	2.15	-----
7.6	----	-.65
10.0	2.41	-----
10.1	----	-.71
15.0	2.73	-.90
20.0	2.89	-1.12
25.0	2.98	-1.33
30.0	3.05	-1.50
40.0	3.10	-1.78
50.0	3.05	-1.95
60.0	2.86	-1.98
70.0	2.47	-1.81
80.0	1.85	-----
90.0	1.04	-.82
95.0	.59	-.48
100.0	0	0
L.E. radius: 0.21 percent c		

TABLE III

HORIZONTAL AND VERTICAL TAIL ORDINATES FOR 0.10-SCALE

DOUGLAS A4D-1 AIRPLANE

Station, percent c	Root chord ordinates, percent c modified NACA 0007	Tip chord ordinates, percent c modified NACA 0004
0	0	0
1	1.043	.473
2	1.469	.646
5	2.259	.954
7	2.605	1.092
10	2.972	1.252
15	3.322	1.452
20	3.468	1.603
25	3.500	1.724
30	3.479	1.821
40	3.321	1.953
50	3.019	2.000
60	2.594	1.934
70	2.060	1.692
80	1.432	1.250
90	.745	.652
100	0	0
L.E. radius: 0.539 percent c		L.E. radius: 0.132 percent c

TABLE IV

ORDINATES FOR LEADING-EDGE MODIFICATIONS[a]

Basic wing ordinates at 0.2425b/2, percent c			Leading edge II ordinates at 0.2425b/2, percent c			Leading edge I and leading edge II ordinates at 0.873b/2, percent c		
Station	Upper	Lower	Station	Upper	Lower	Station	Upper	Lower
0	0	0	-3.78	-0.31	-0.31	-9.48	-2.65	-2.65
.05	.28	-.28	-3.72	-.05	-.59	-9.42	-2.39	-2.92
.10	.39	-.40	-3.66	.12	-.71	-9.33	-2.25	-3.03
.20	.56	-.56	-3.54	.29	-.85	-9.18	-2.07	-3.13
.50	.89	-.77	-3.19	.66	-1.14	-8.75	-1.71	-3.32
1.01	1.30	-1.05	-2.60	1.08	-1.43	-8.02	-1.31	-3.43
2.02	1.90	-1.40	-1.43	1.69	-1.74	-6.55	-.70	-3.41
3.03	2.37	-1.65	-.25	2.13	-1.94	-5.57	-.18	-3.32
4.04	2.73	-1.86	.92	2.47	-2.08	-3.61	.27	-3.18
6.06	3.32	-2.16	3.27	3.03	-2.26	-.66	1.01	-2.90
8.08	3.71	-2.39	5.62	3.50	-2.37	2.27	1.59	-2.67
10.10	4.04	-2.43	7.98	3.83	-2.50	5.20	2.09	-2.49
12.12	4.25	-2.68	10.32	4.12	-2.62	8.14	2.49	-2.37
14.14	4.40	-2.80	12.68	4.33	-2.74	11.07	2.80	-2.27
16.17	4.51	-2.91	15.03	4.49	-2.88	14.01	3.07	-2.24
18.19	4.57	-3.02	17.37	4.56	-3.01	16.96	3.22	-2.25
20.21	4.60	-3.07	19.73	4.59	-3.09	19.89	3.28	-2.35

[a]Stations and ordinates referenced to the leading edge and wing reference plane of the basic wing.

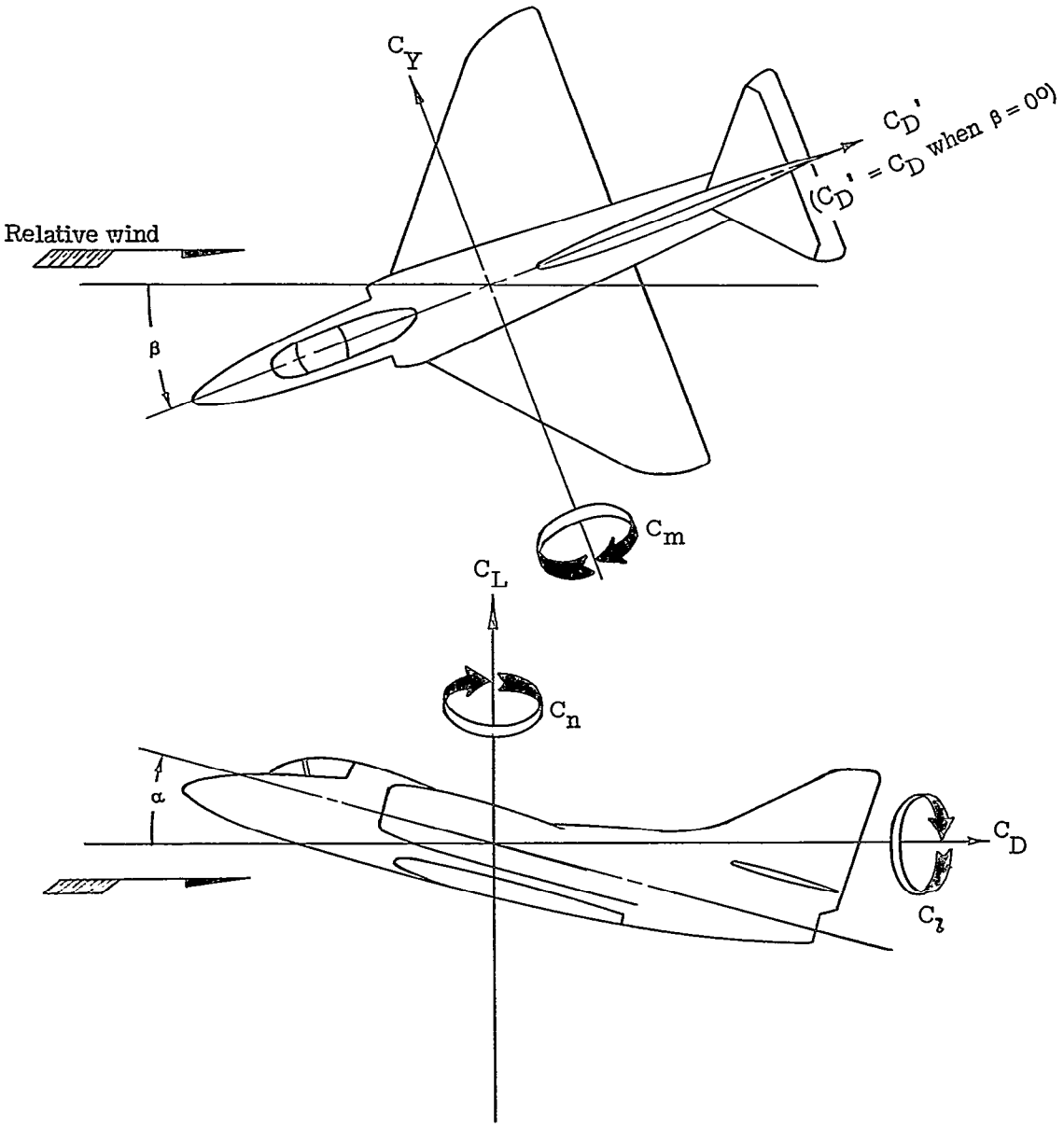

Figure 1.- System of axes. Arrows denote positive direction of force, moment, and angular measurements.

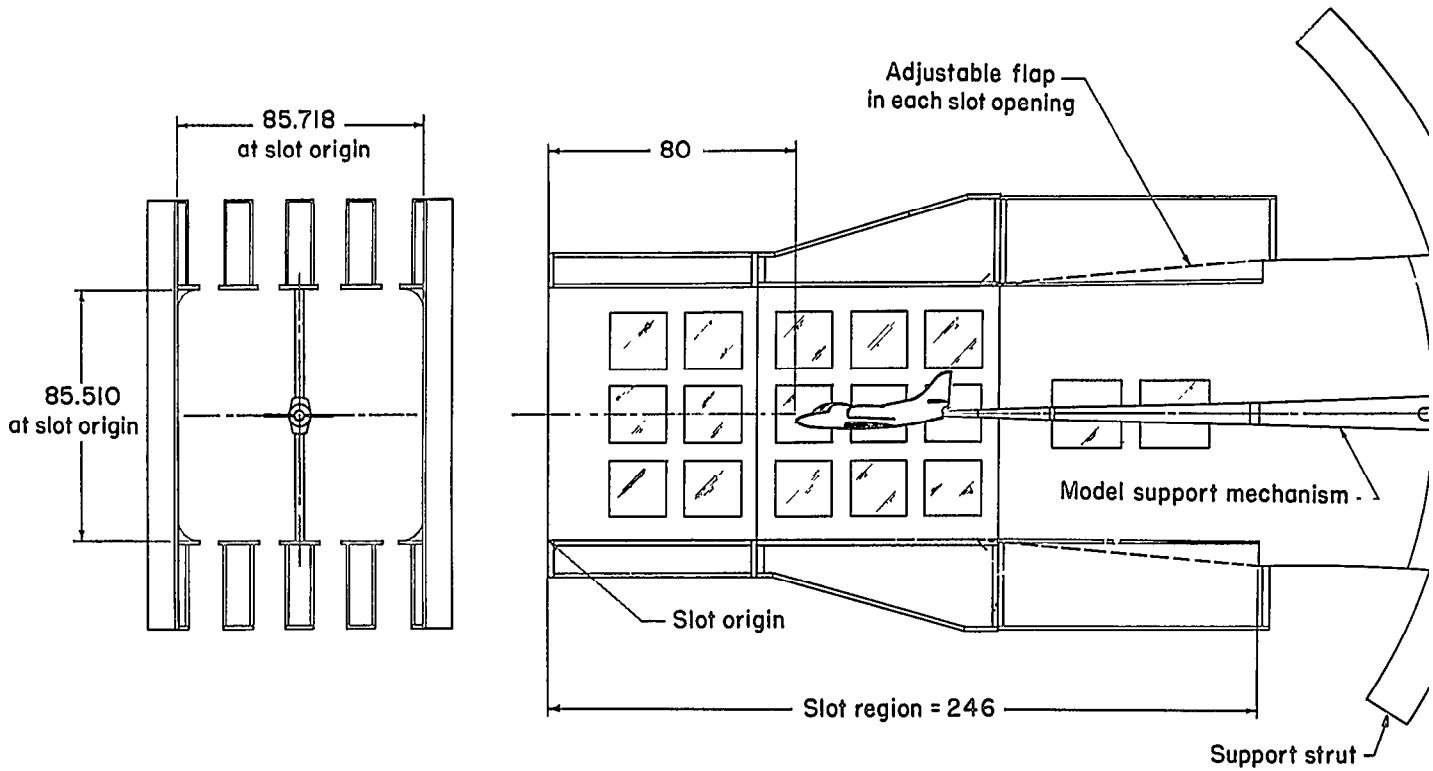

Figure 2.- Details of test section and location of model in the Langley 8-foot transonic pressure tunnel. All dimensions in inches.

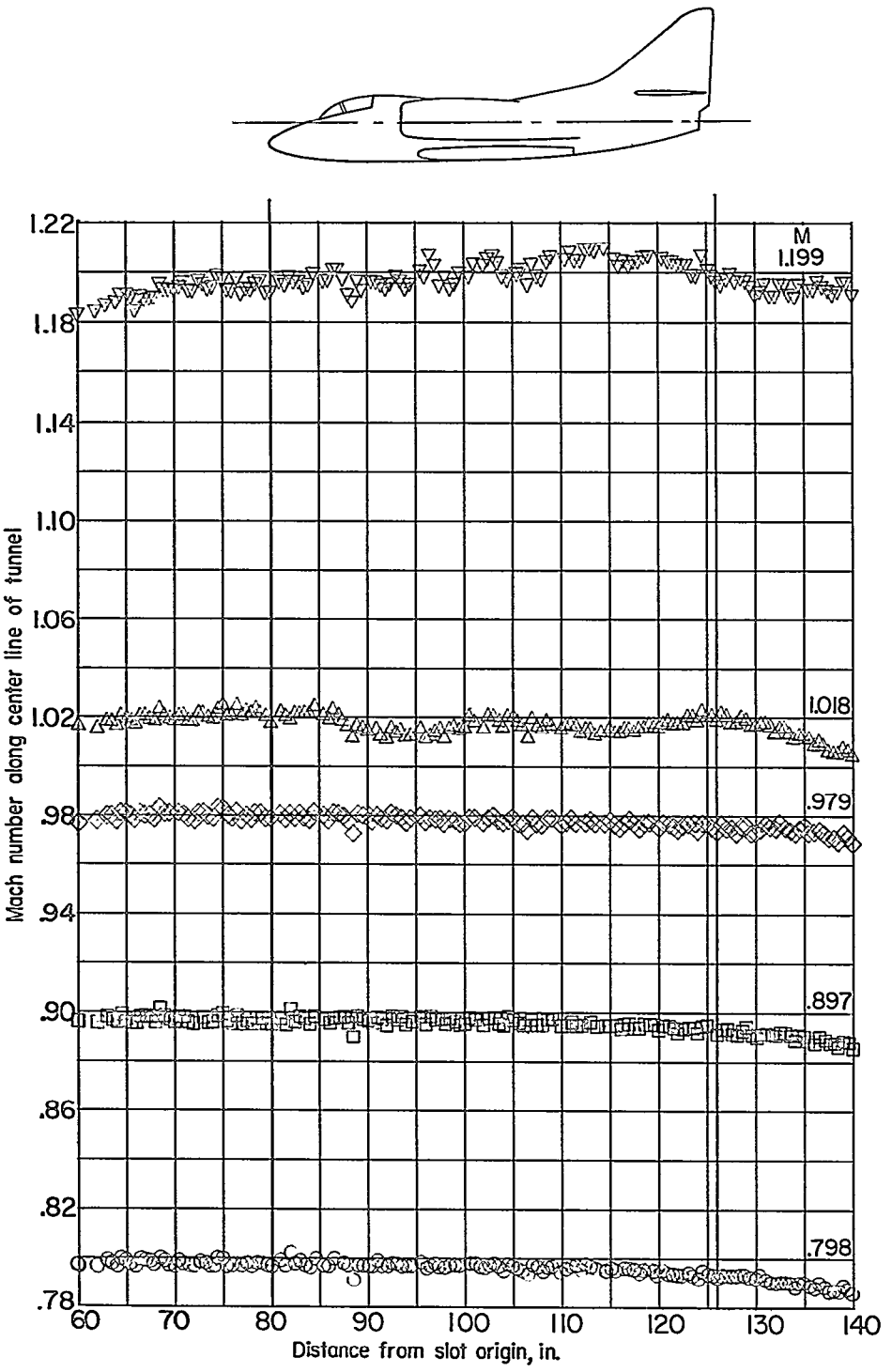

Figure 3.- Mach number distribution along center line of tunnel test section.

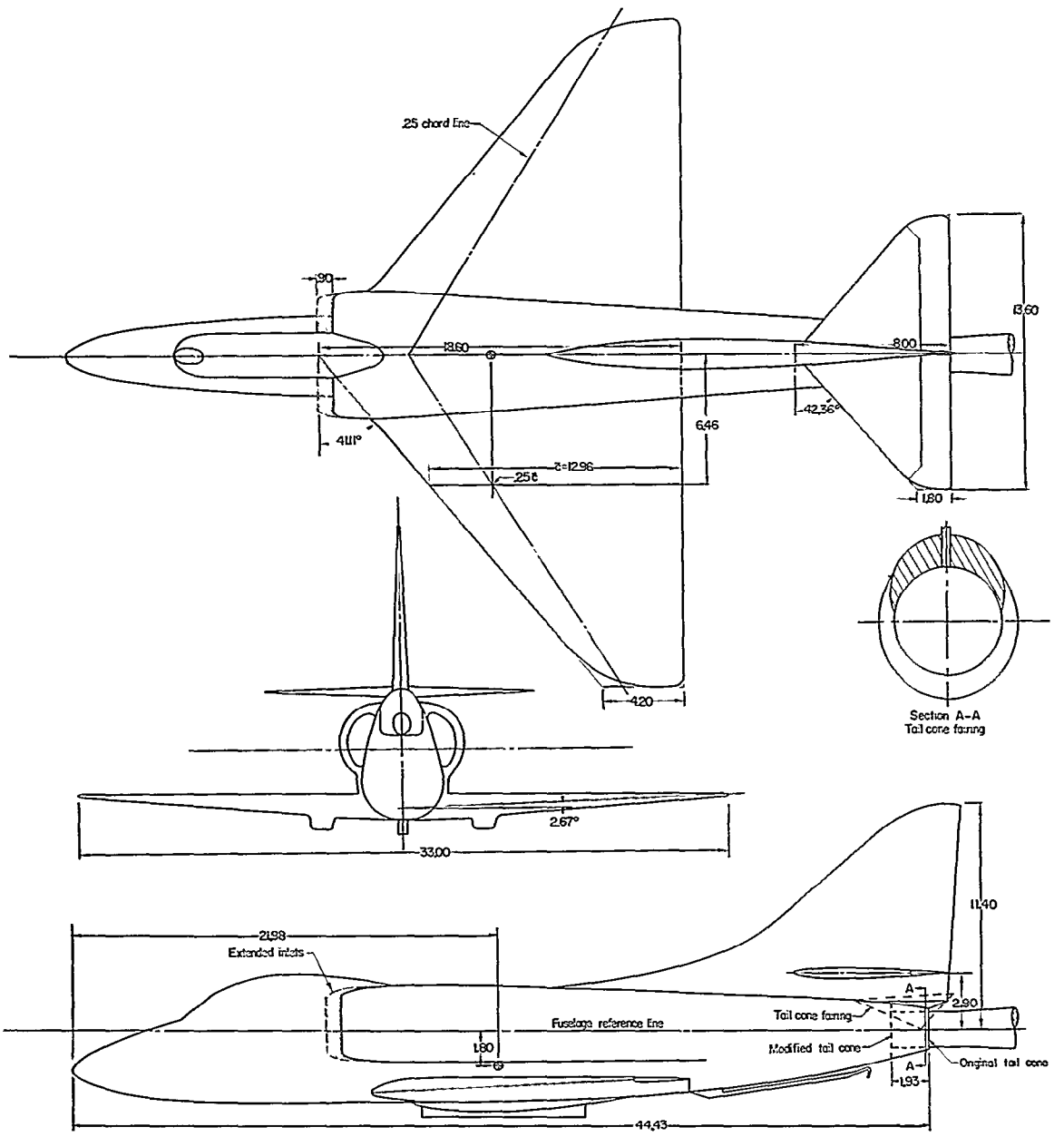

Figure 4.- Three-view drawing of the 0.10-scale Douglas A4D-1 airplane. All dimensions in inches unless otherwise noted.

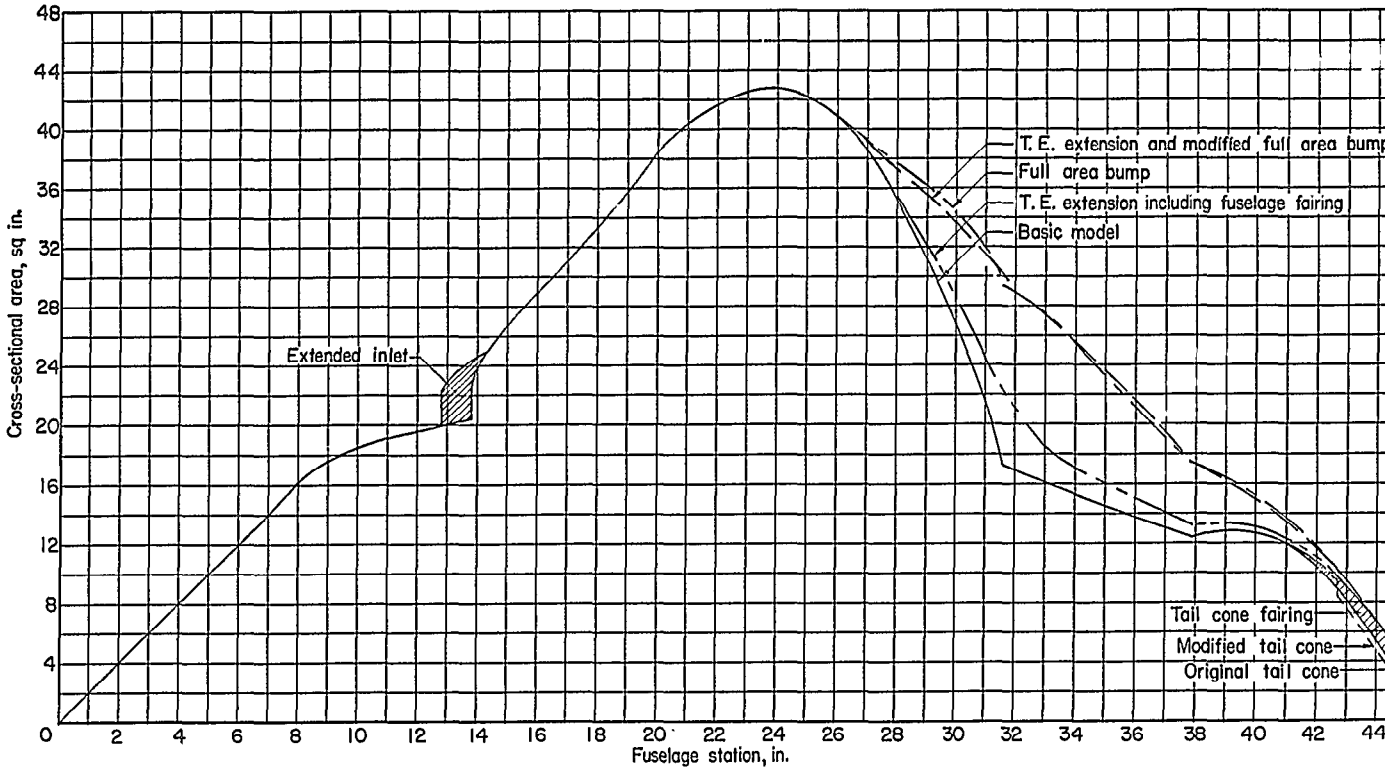

Figure 5.- Axial distribution of cross-sectional area for the 0.10-scale Douglas A4D-1 airplane model and various area modifications. Free-stream area of 3.56 square inches removed.

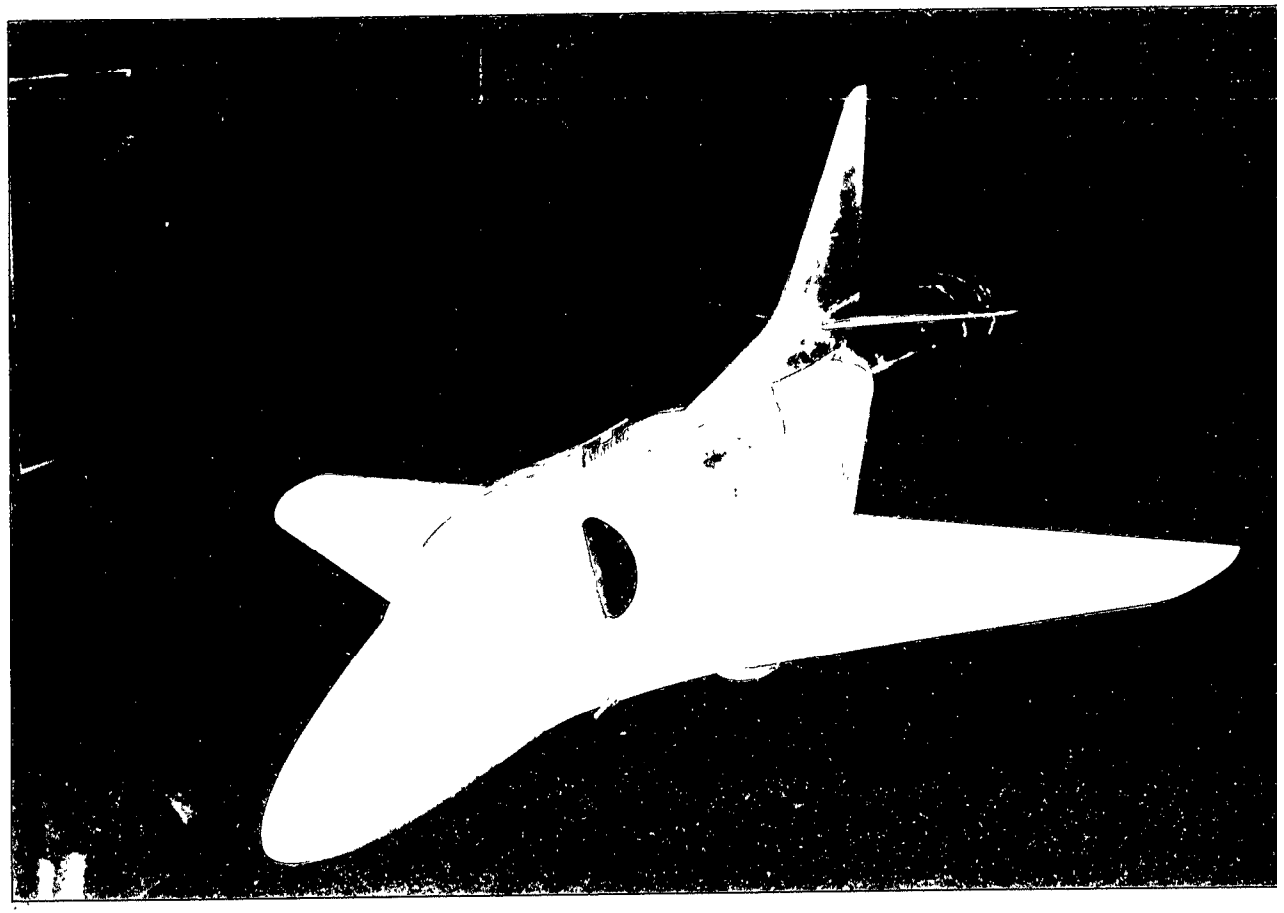

L-90011

(a) Basic model with modified tail cone, leading edge I, trailing-edge extension, and modified full bump.

Figure 6.- The 0.10-scale Douglas A4D-1 airplane installed in the 8-foot transonic pressure tunnel.

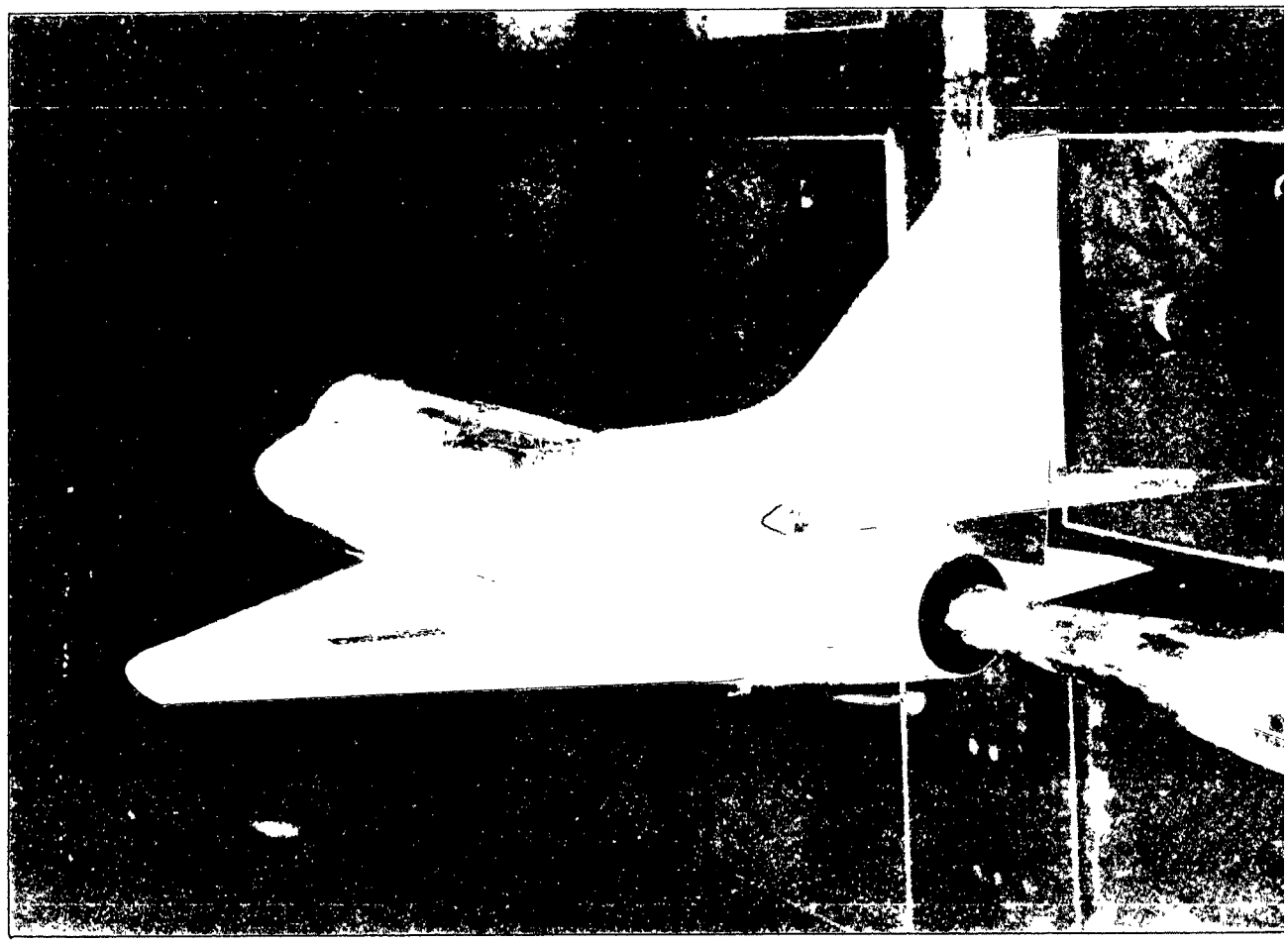

L-90081

(b) Basic model with modified tail cone, leading edge I, and trailing-edge extension.

Figure 6.- Concluded.

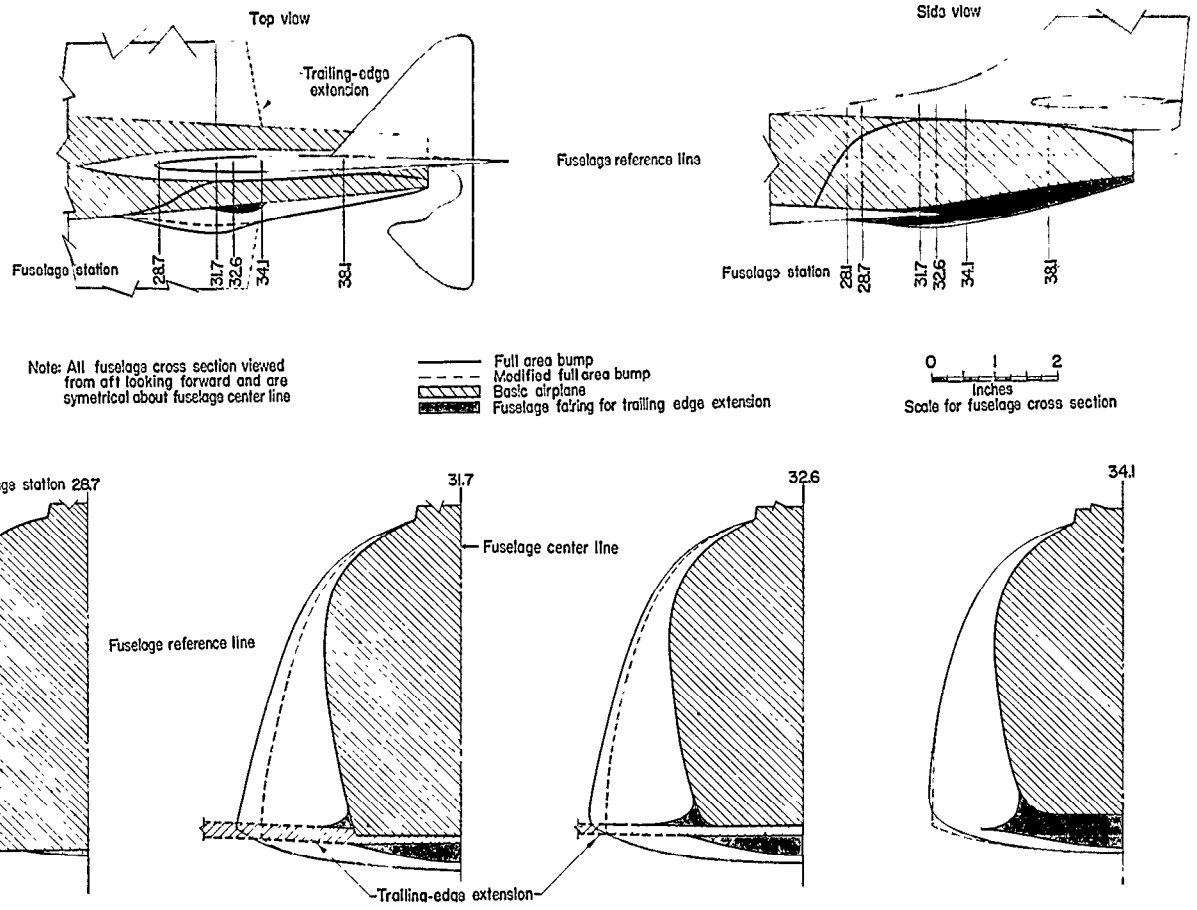

Figure 7.- Details of fuselage modifications.

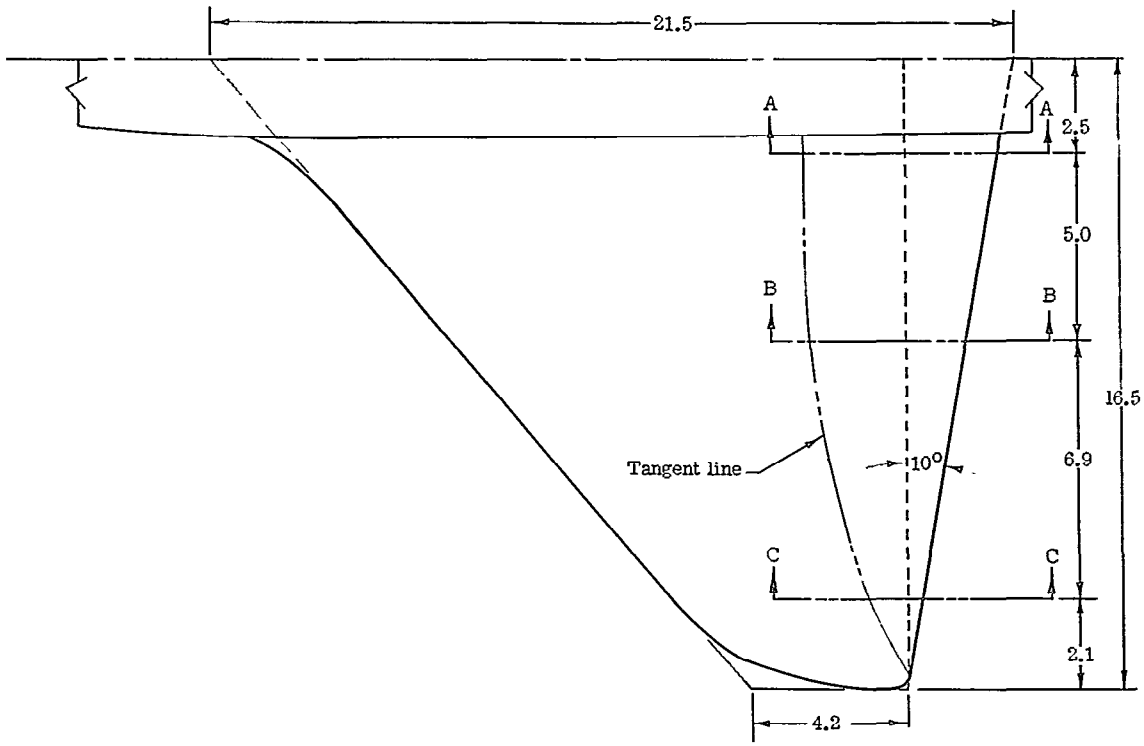

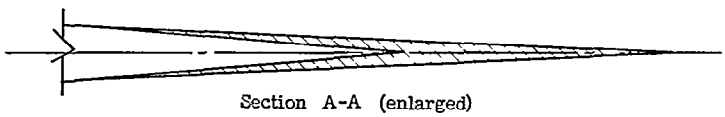

Section A-A (enlarged)

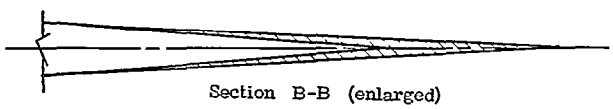

Section B-B (enlarged)

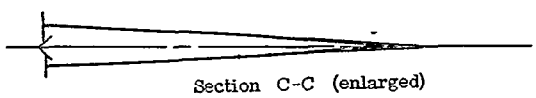

Section C-C (enlarged)

Figure 8.- Dimensional details of trailing-edge extension. All dimensions in inches unless otherwise noted.

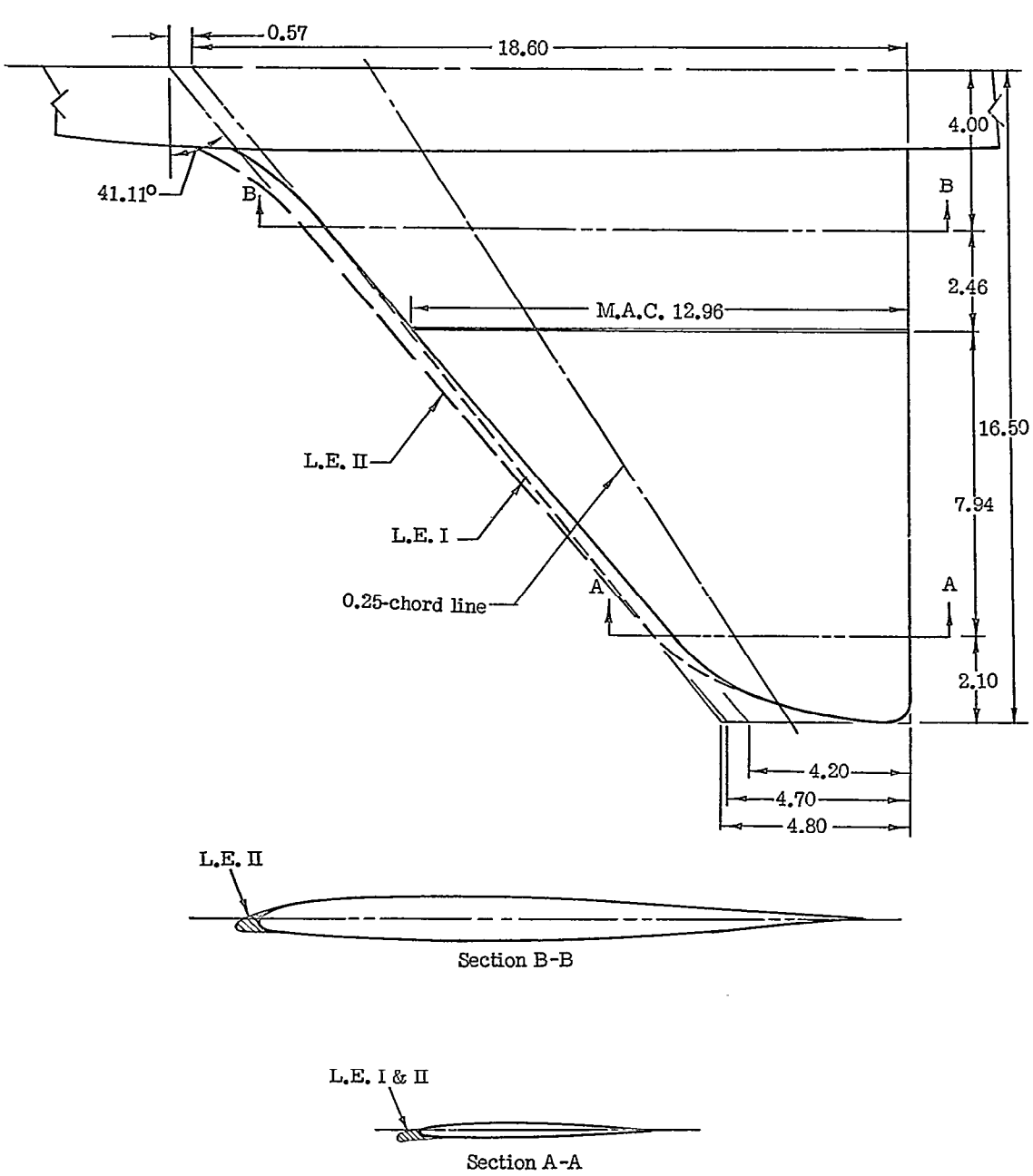

Figure 9.- Dimensional details of leading-edge modifications. All dimensions in inches unless otherwise noted.

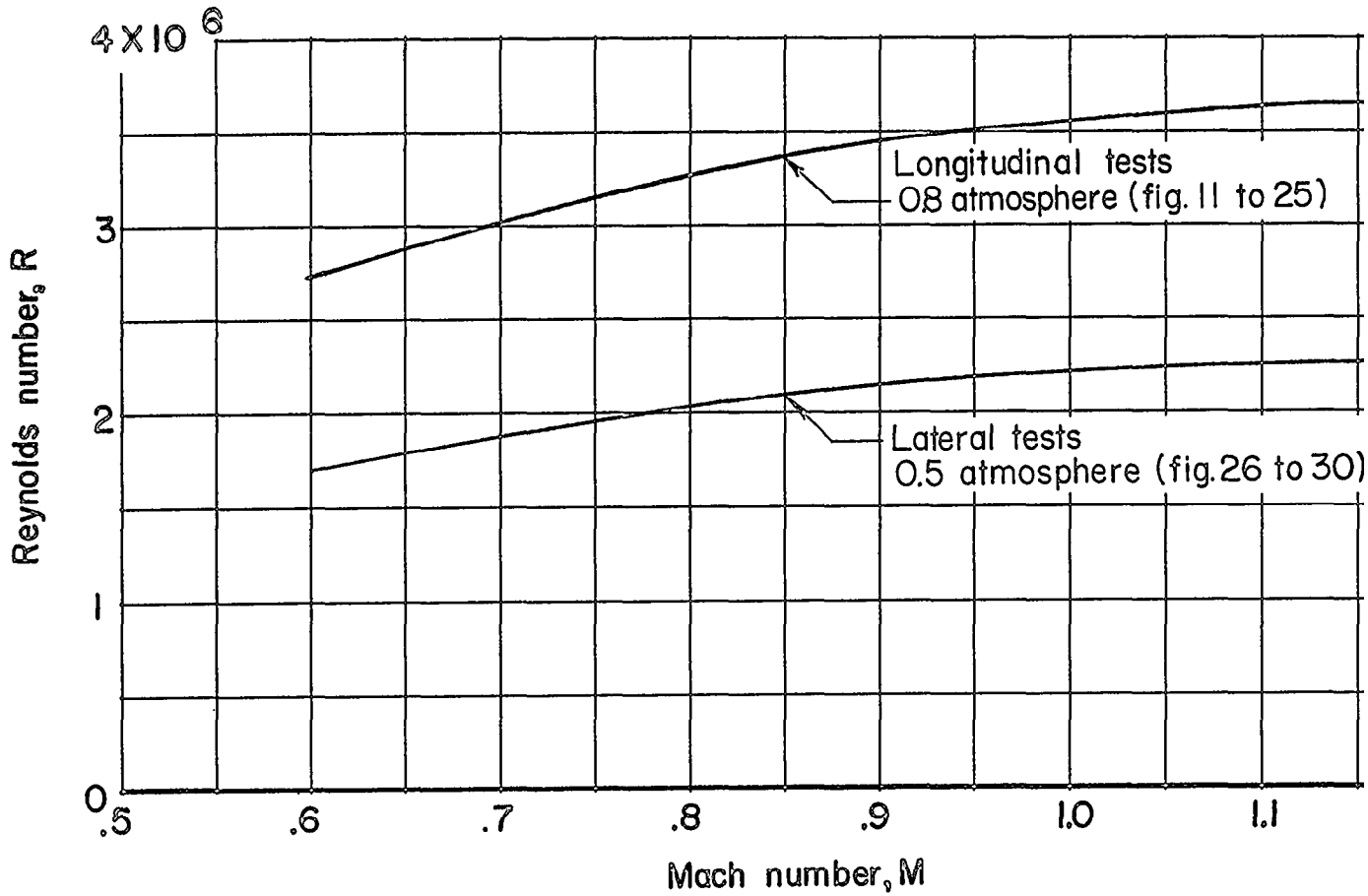

Figure 10.- Variation with Mach number of approximate test Reynolds number based on $\bar{c}$ = 12.96 inches.

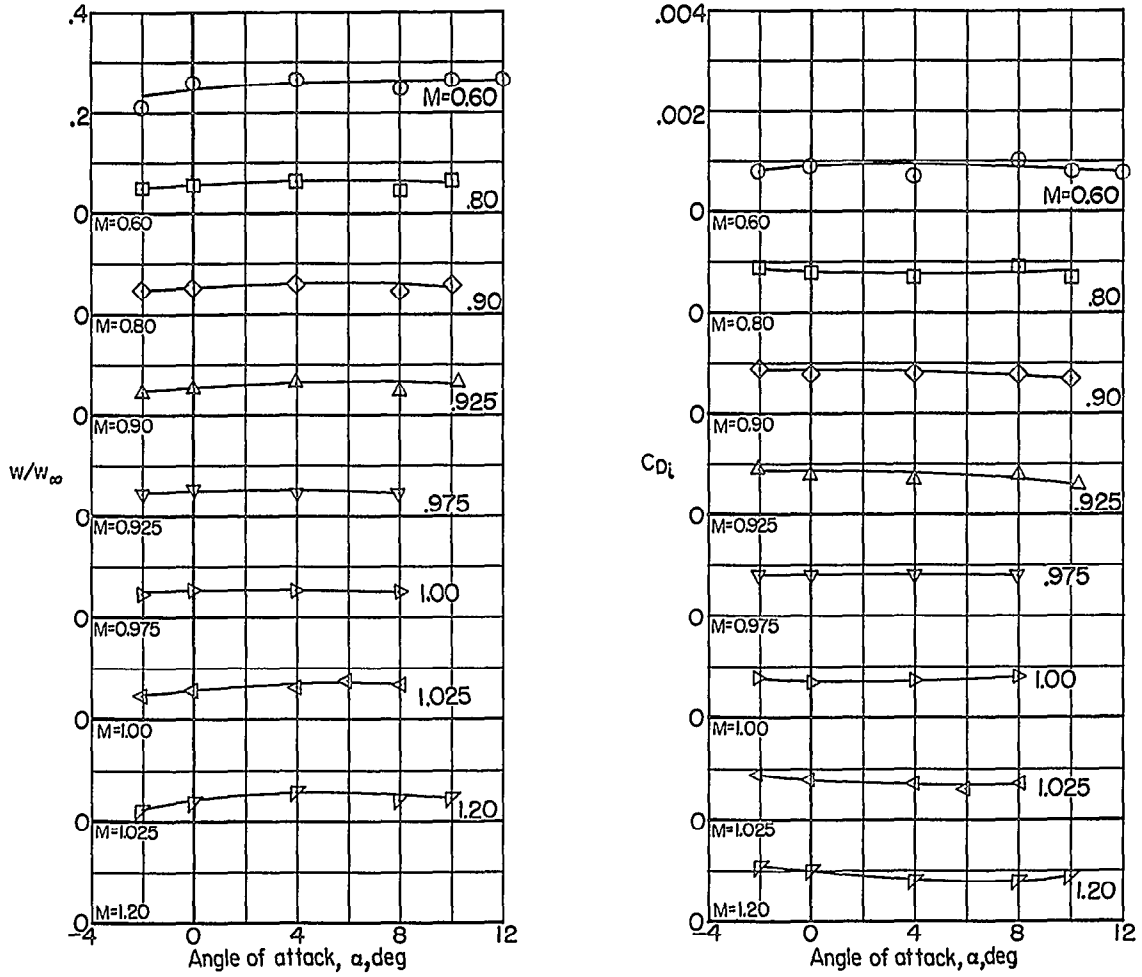

(a) Original tail cone and tail cone fairing.

Figure 11.- Mass-flow ratios and internal-drag coefficients for the basic model.

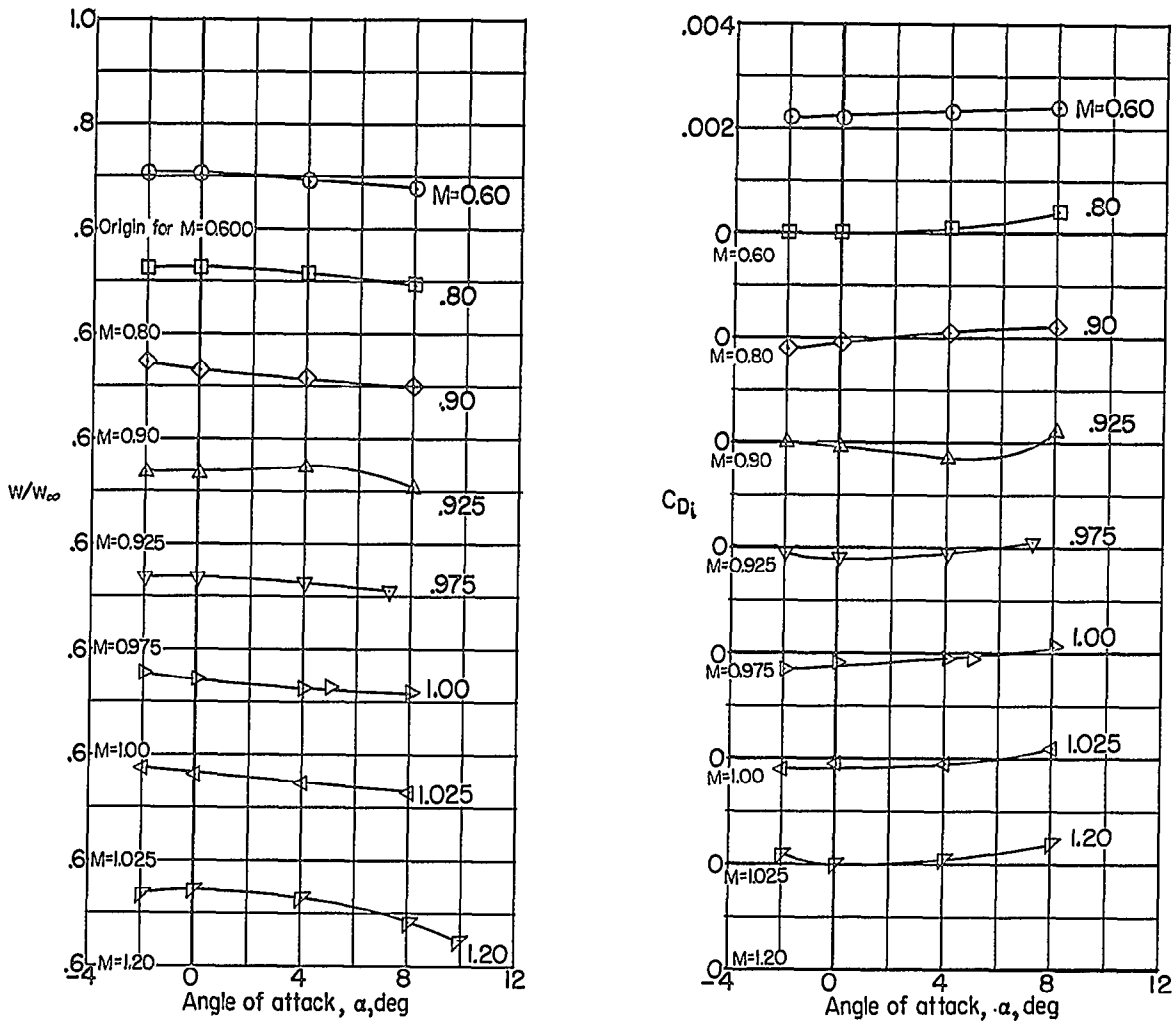

(b) Modified tail cone.

Figure 11.- Concluded.

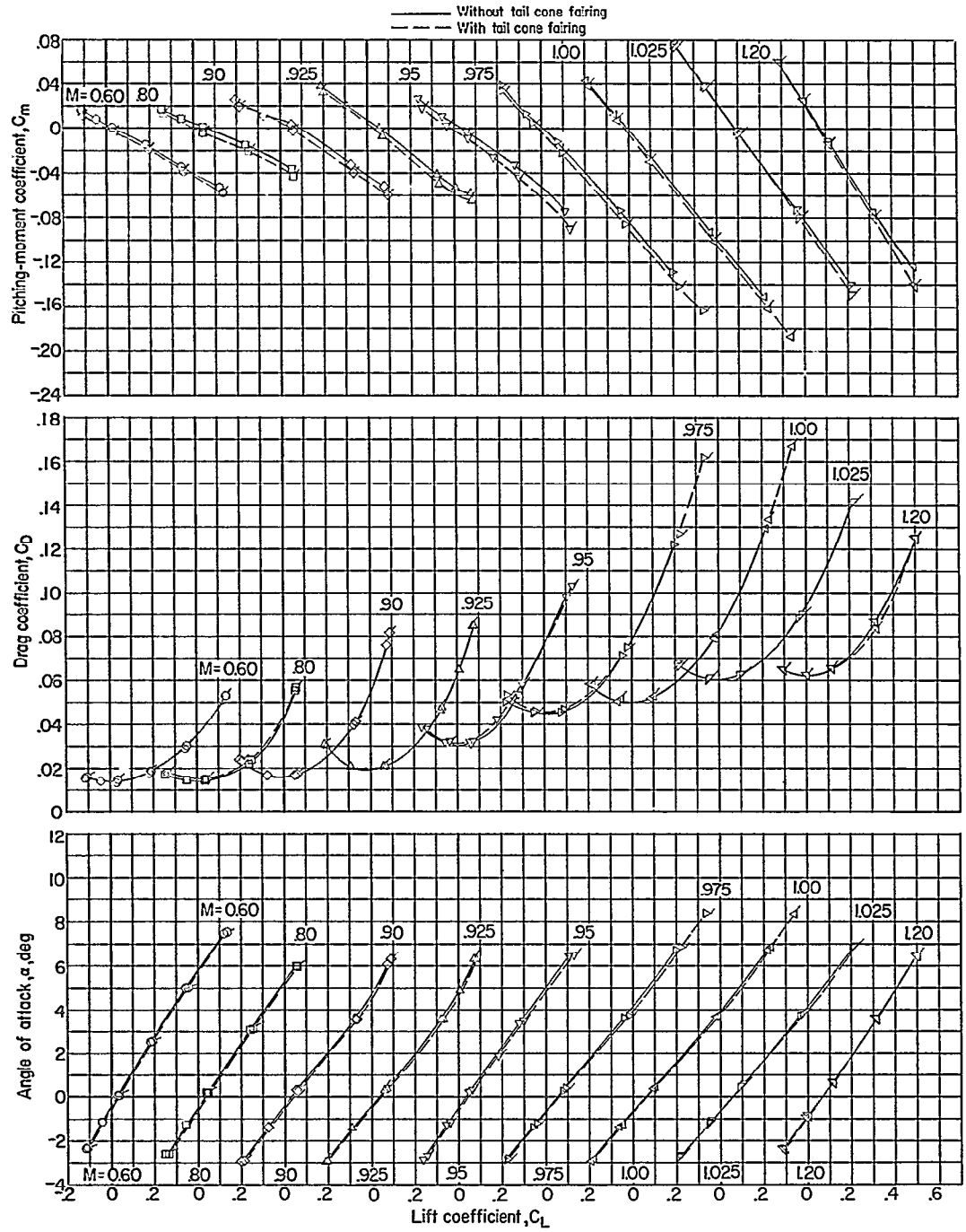

Figure 12.- Force and moment characteristics of the basic model (original tail cone) with and without tail cone fairing. Plain symbols indicate without tail cone fairing and flagged symbols indicate with tail cone fairing.

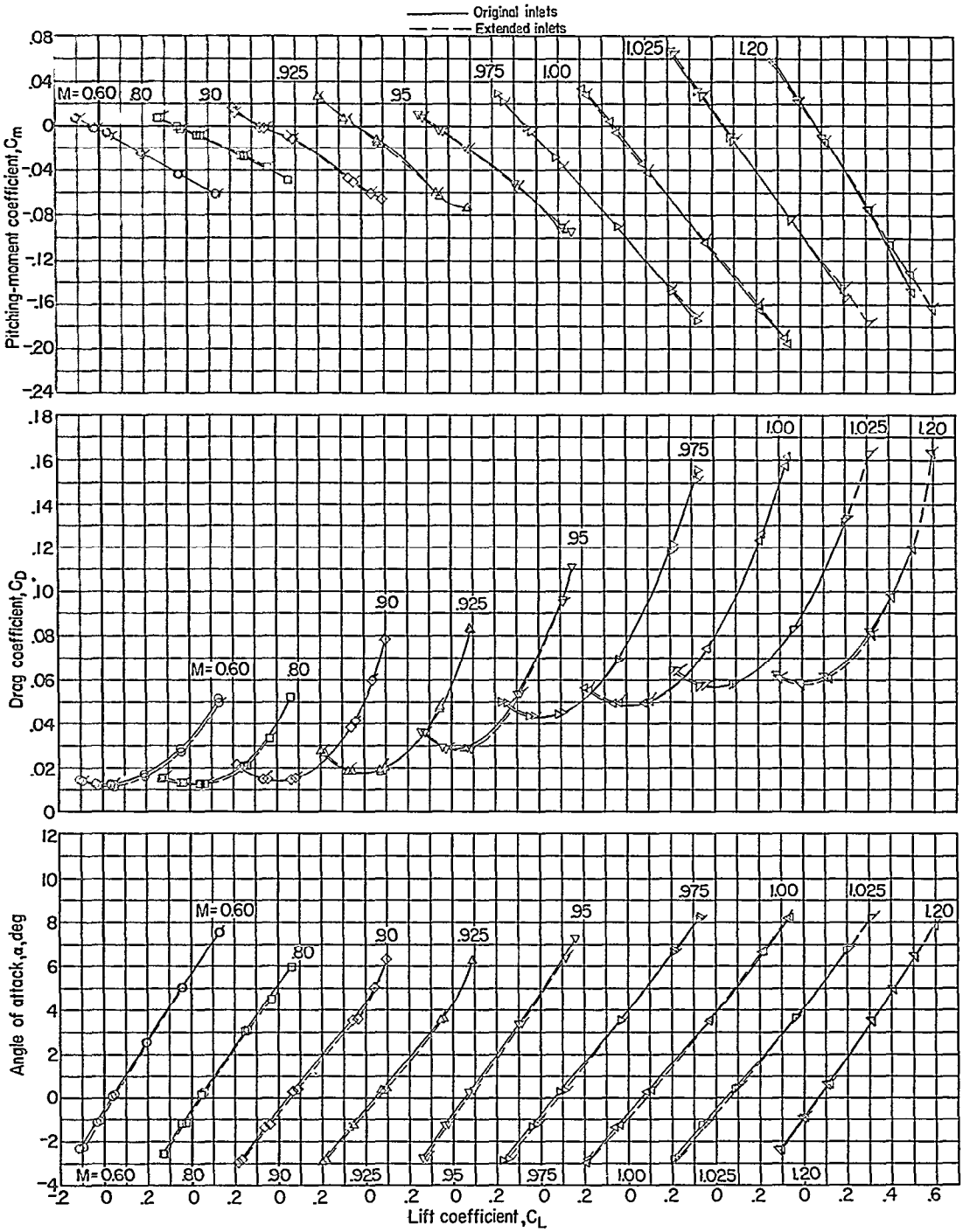

Figure 13.- Force and moment characteristics of the basic model (modified tail cone) with and without extended inlets. Plain symbols indicate original inlets and flagged symbols indicate extended inlets.

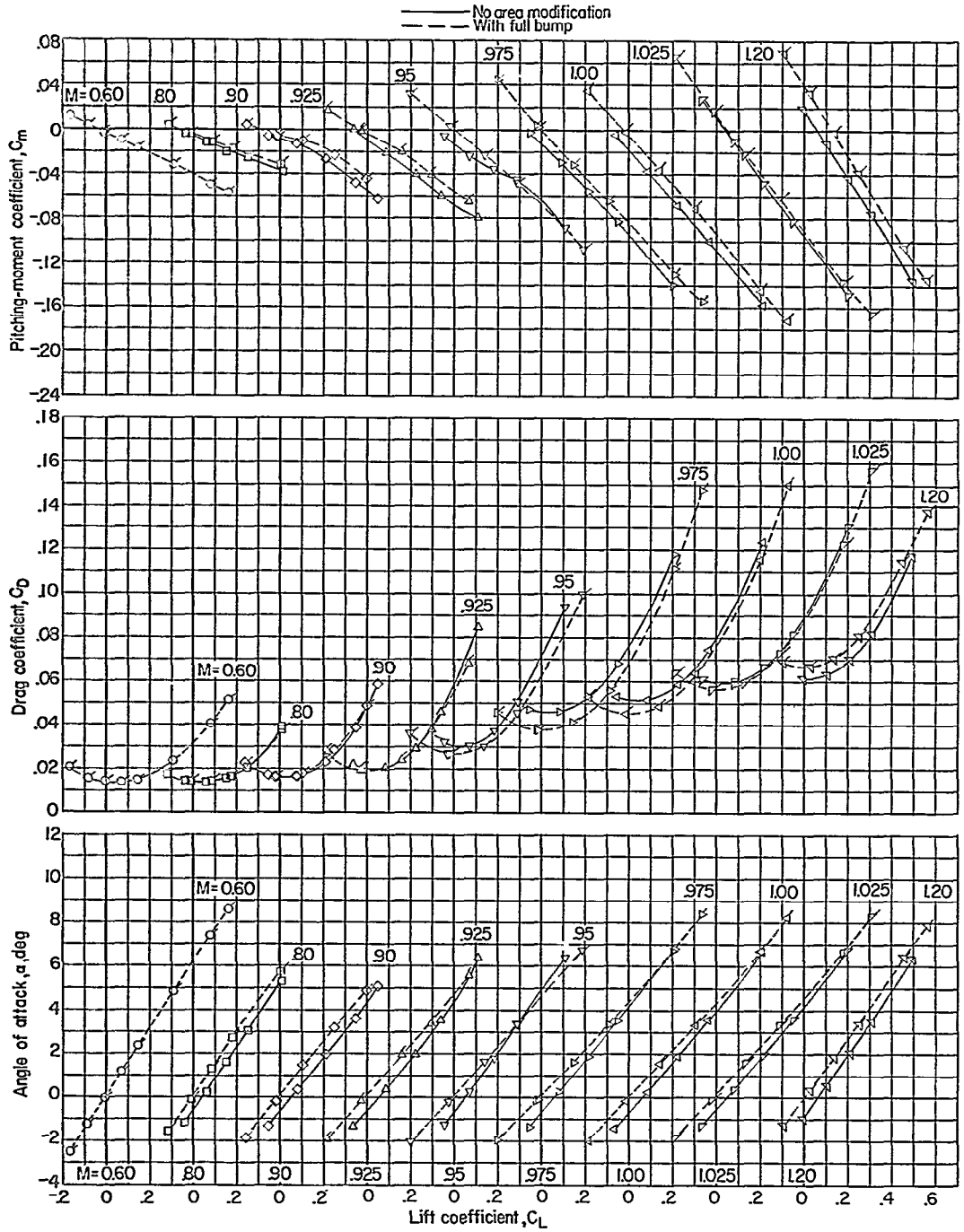

Figure 14.- Force and moment characteristics of the basic model (modified tail cone) including leading edge I with and without full bump. Plain symbols indicate no area modification and flagged symbols indicate full bump.

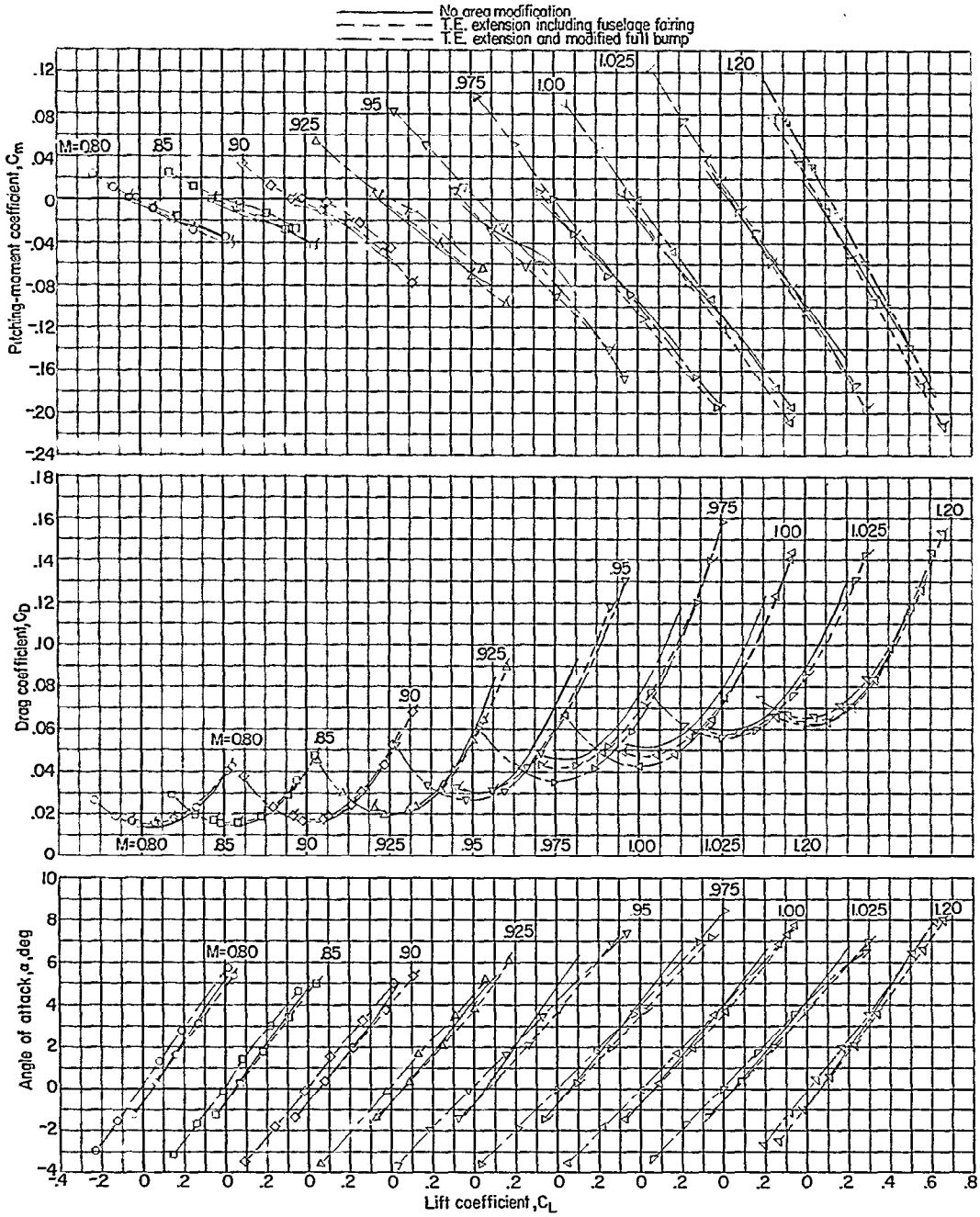

Figure 15.- Force and moment characteristics of the basic model (modified tail cone) including leading edge I with and without modified full bump and wing trailing-edge extension. Plain symbols indicate trailing-edge extension with modified full bump and flagged symbols indicate trailing-edge extension including fuselage fairing.

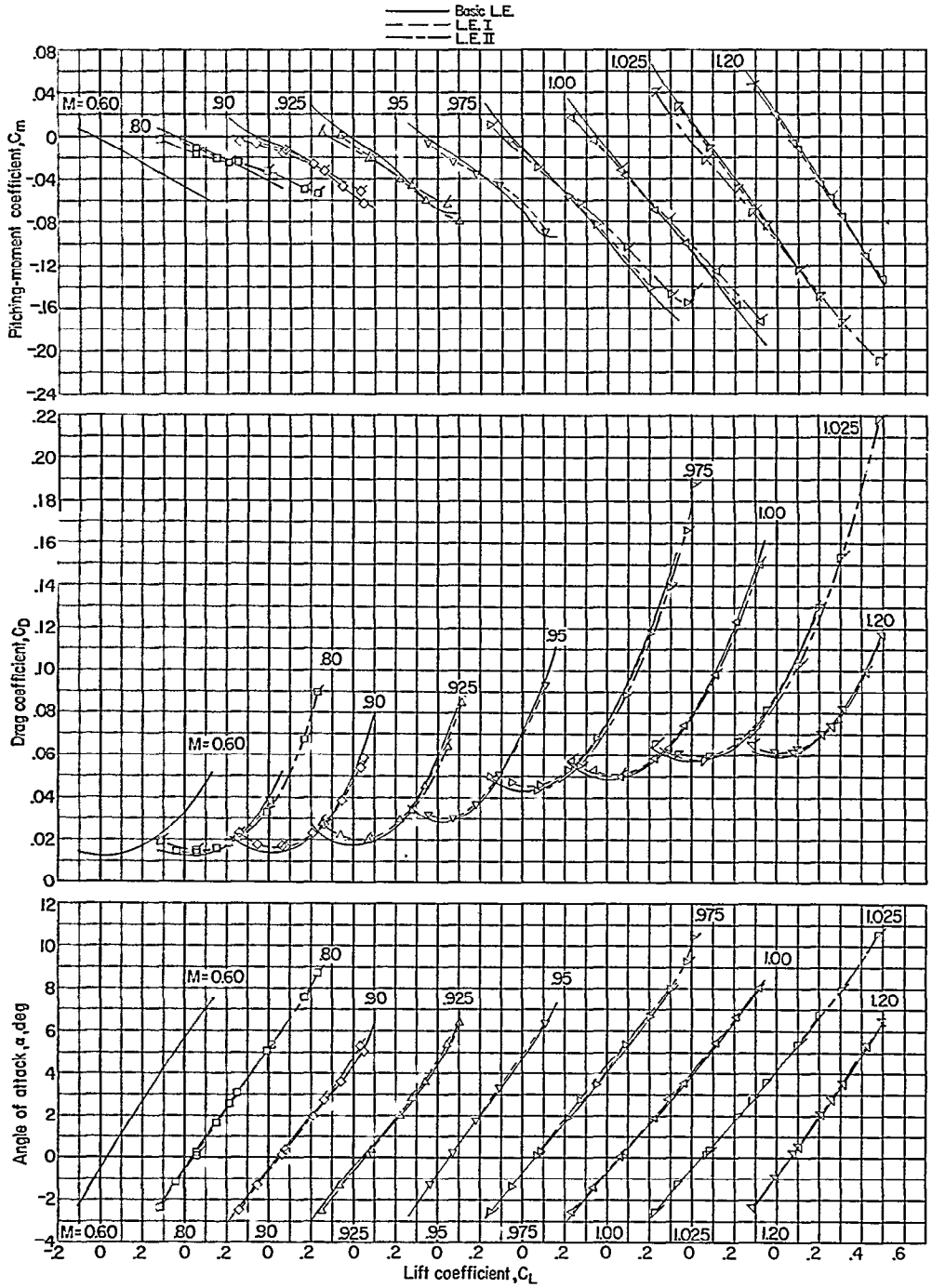

Figure 16.- Force and moment characteristics of the basic model (modified tail cone) with and without wing leading-edge modifications. Plain symbols indicate leading edge I and flagged symbols indicate leading edge II.

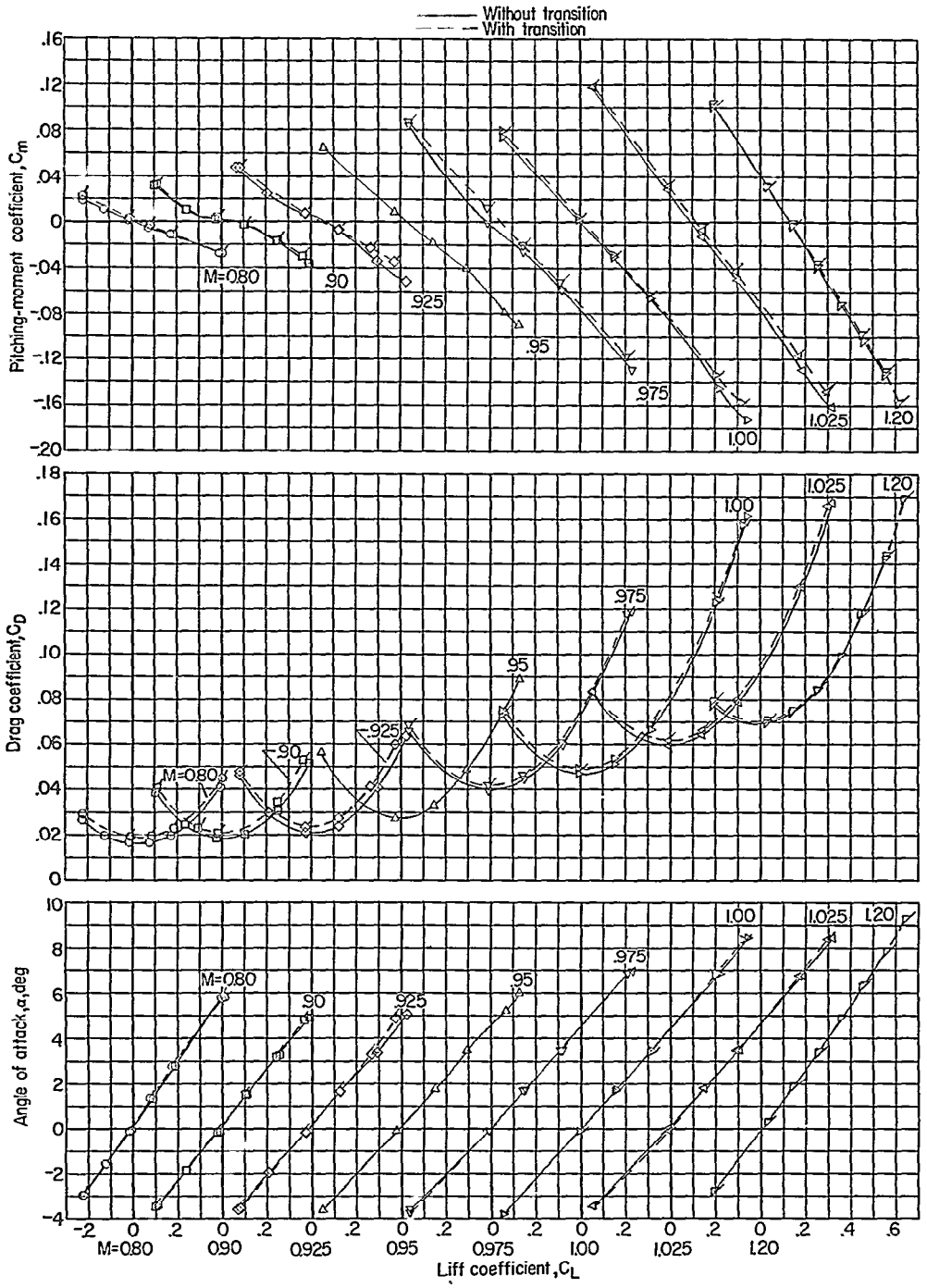

Figure 17.- Force and moment characteristics of the basic model including original tail cone and tail cone fairing with and without fixed transition. Plain symbols indicate without fixed transition and flagged symbols indicate with fixed transition.

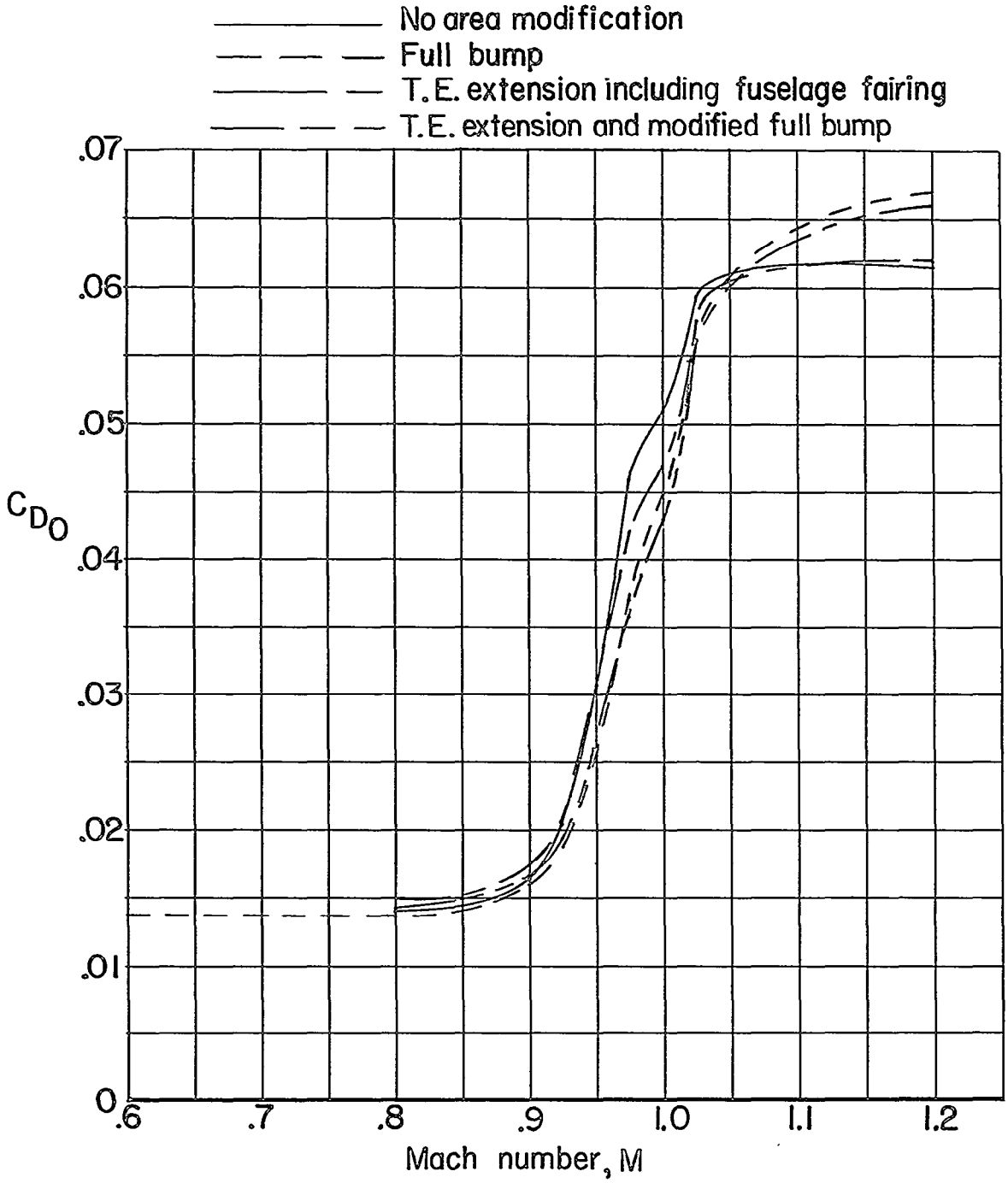

Figure 18.- Effect of full bump, trailing-edge extension, and modified full bump in combination with the trailing-edge extension on the zero-lift drag coefficient of the basic model (modified tail cone) including leading edge I.

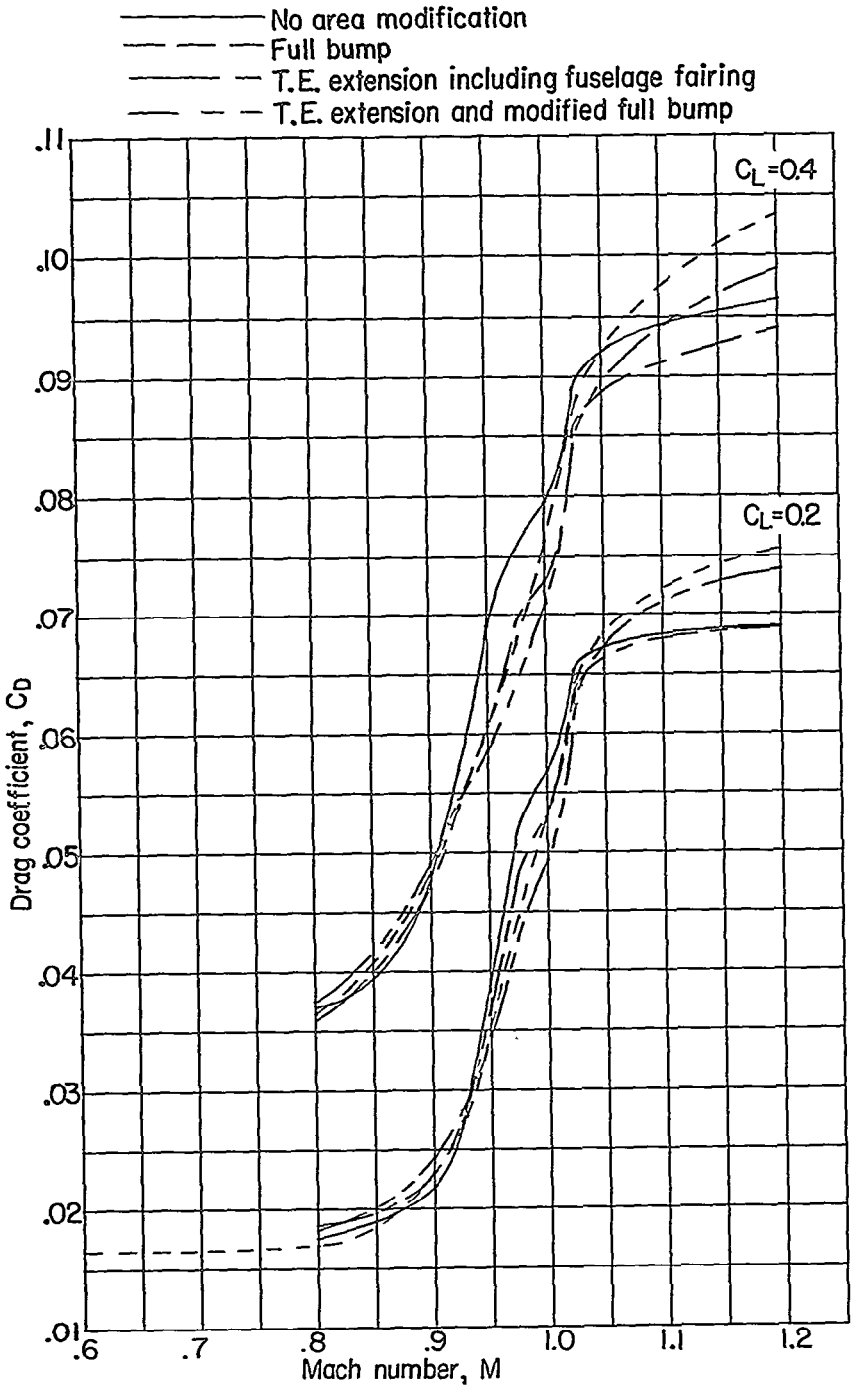

Figure 19.- Effect of full bump, trailing-edge extension, and modified full bump in combination with the trailing-edge extension on the drag coefficient at lifting conditions of the basic model (modified tail cone) including leading edge I.

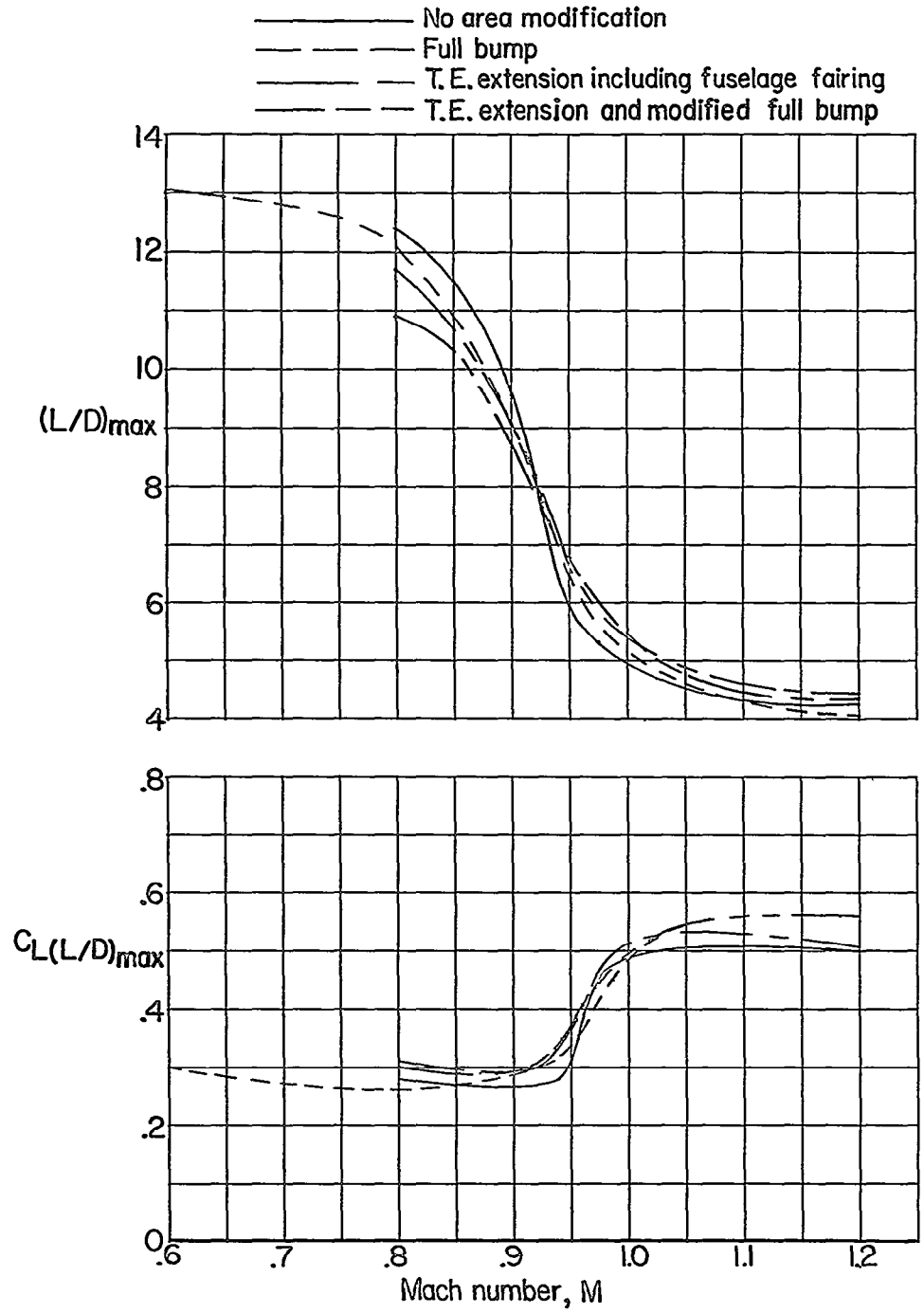

Figure 20.- Effect of full bump, trailing-edge extension, and modified full bump in combination with the trailing-edge extension on the maximum lift-drag ratio and lift coefficient for maximum lift drag ratio of the basic model (modified tail cone) including leading edge I.

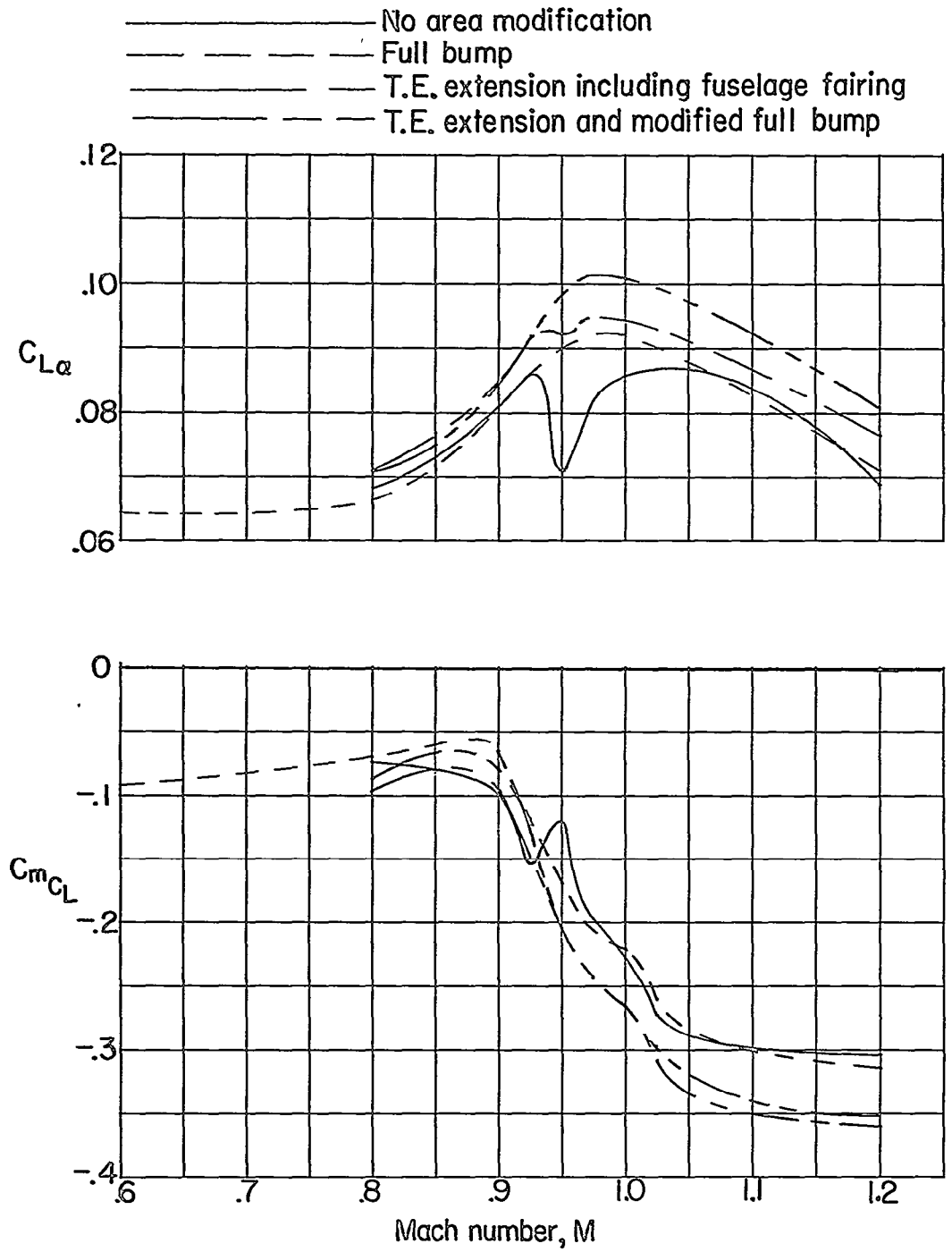

Figure 21.- Effect of full bump, trailing-edge extension, and modified full bump in combination with the trailing-edge extension on the lift-curve slope and static longitudinal stability parameter of the basic model (modified tail cone) including leading edge I.

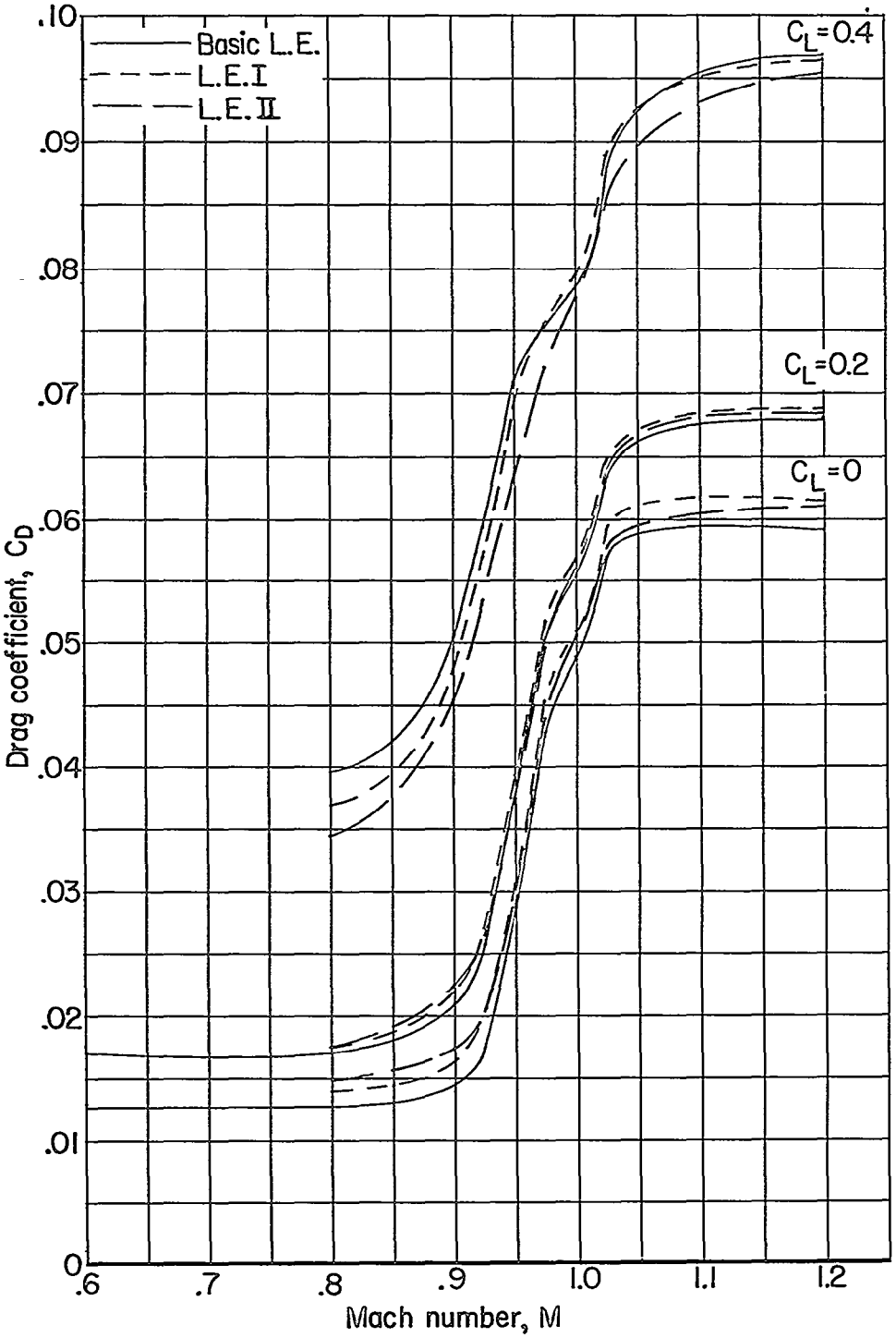

Figure 22.- Effect of wing leading-edge modifications on drag coefficient of the basic model (modified tail cone).

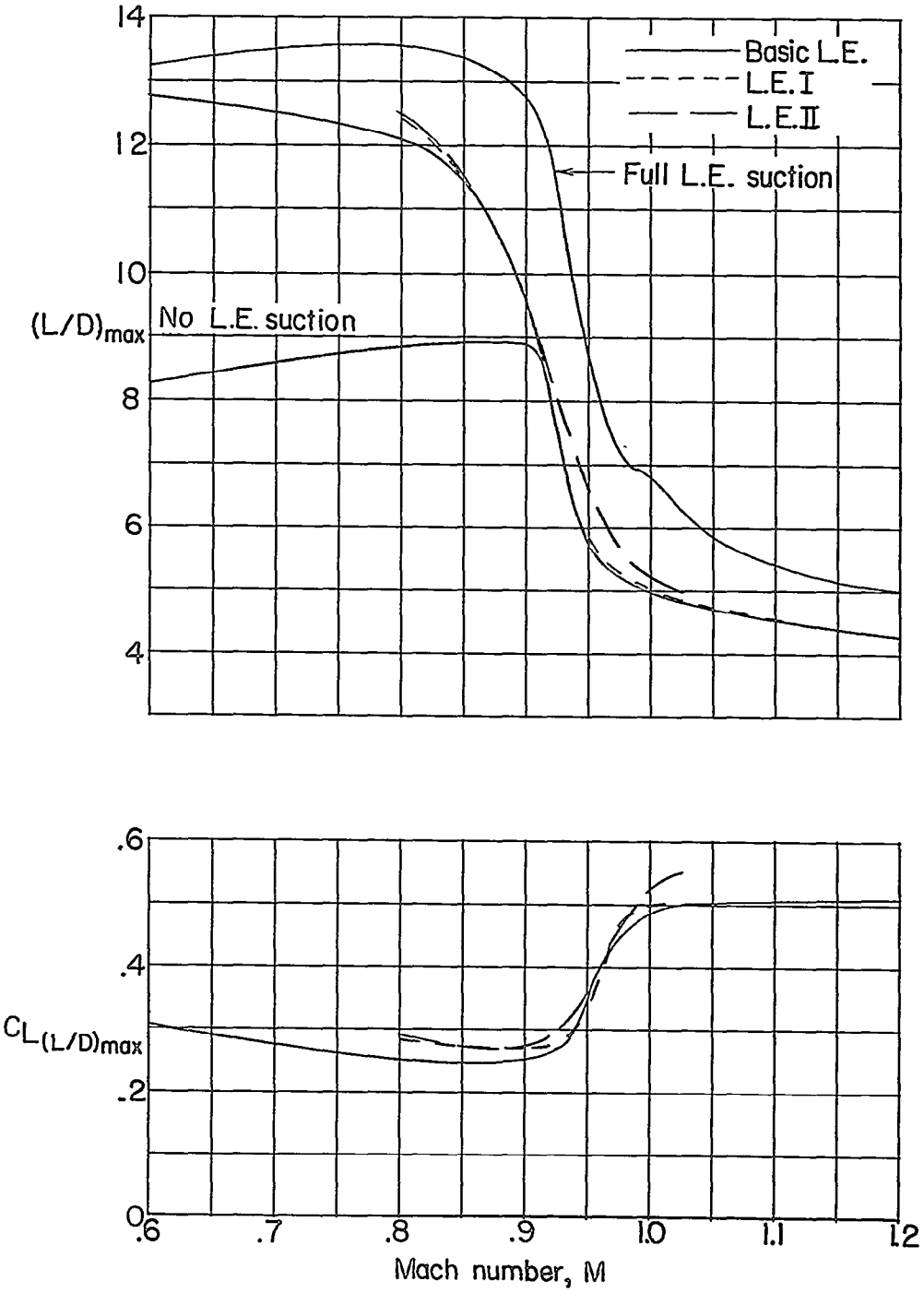

Figure 23.- Effect of wing leading-edge modifications on the maximum lift-drag ratio and lift coefficient for maximum lift-drag ratio of the basic model (modified tail cone).

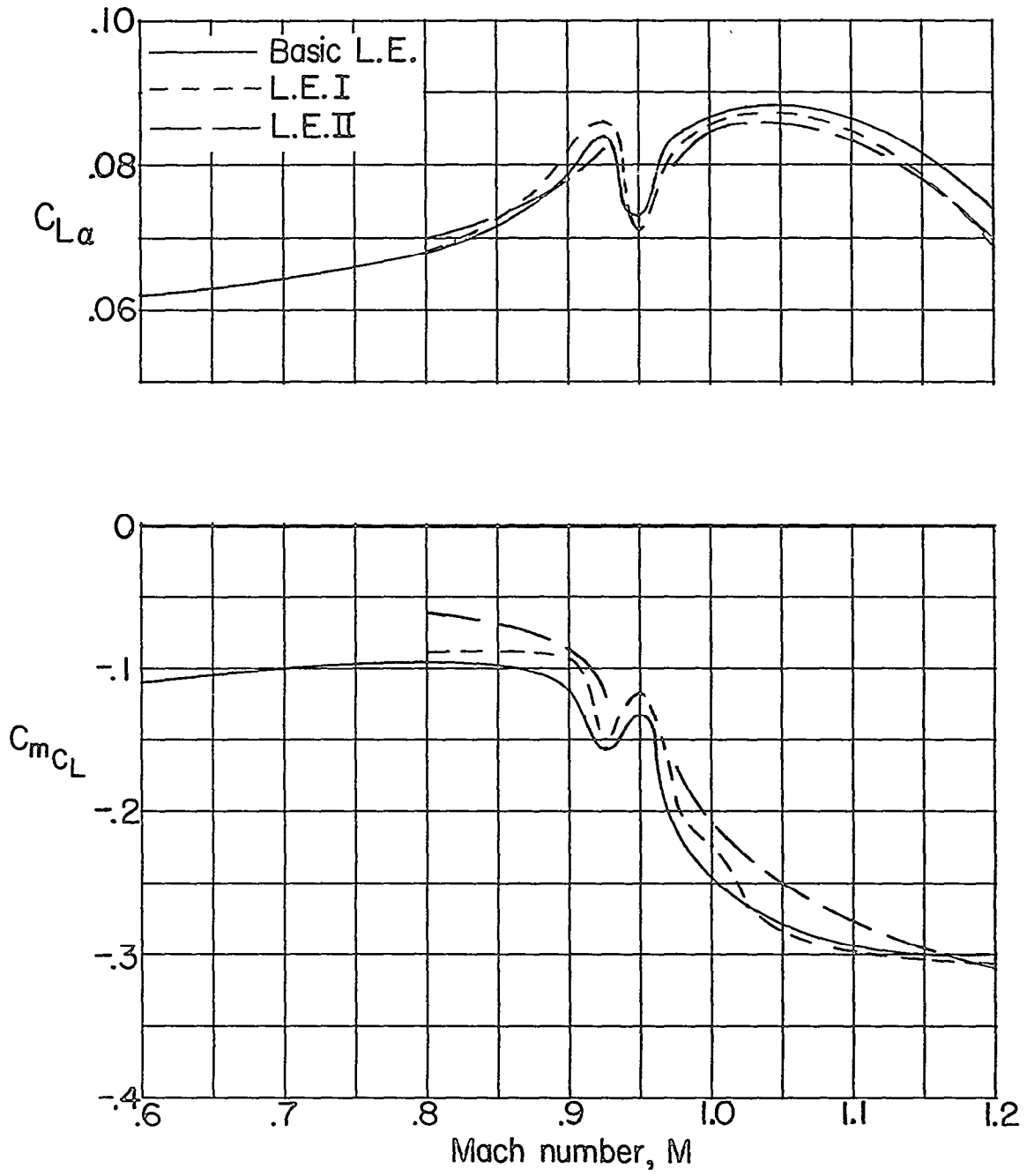

Figure 24.- Effect of wing leading-edge modifications on the lift-curve slope and static-longitudinal-stability parameter for the basic model (modified tail cone).

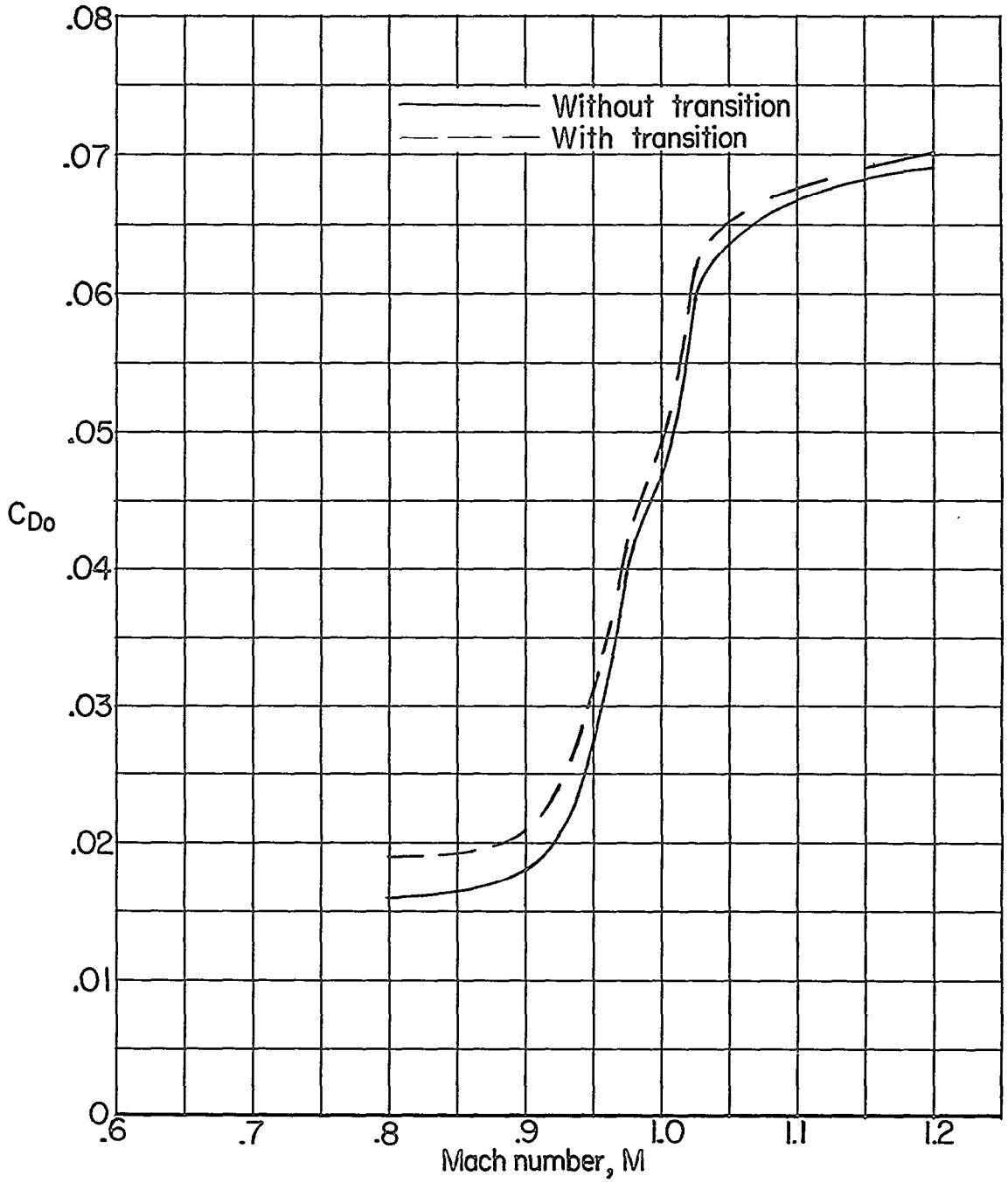

Figure 25.- Variation with Mach number of the zero-lift drag coefficient of the basic model including original tail cone, leading edge I, and tail cone fairing with and without fixed transition.

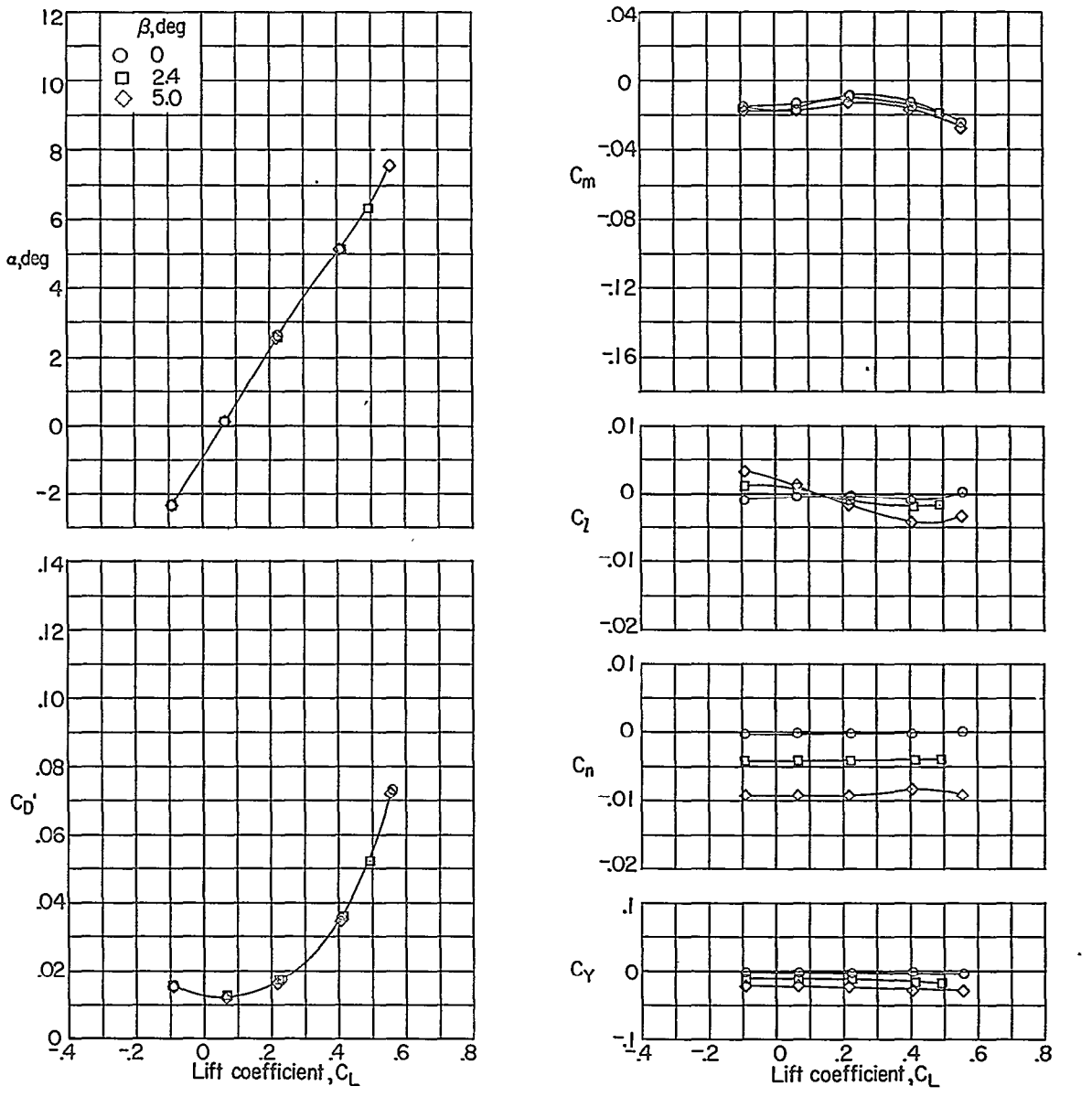

(a) M = 0.80.

Figure 26.- Variation with lift coefficient of the aerodynamic characteristics of the basic model (modified tail cone) with leading edge I for various angles of sideslip. Horizontal and vertical tails off.

[redacted]

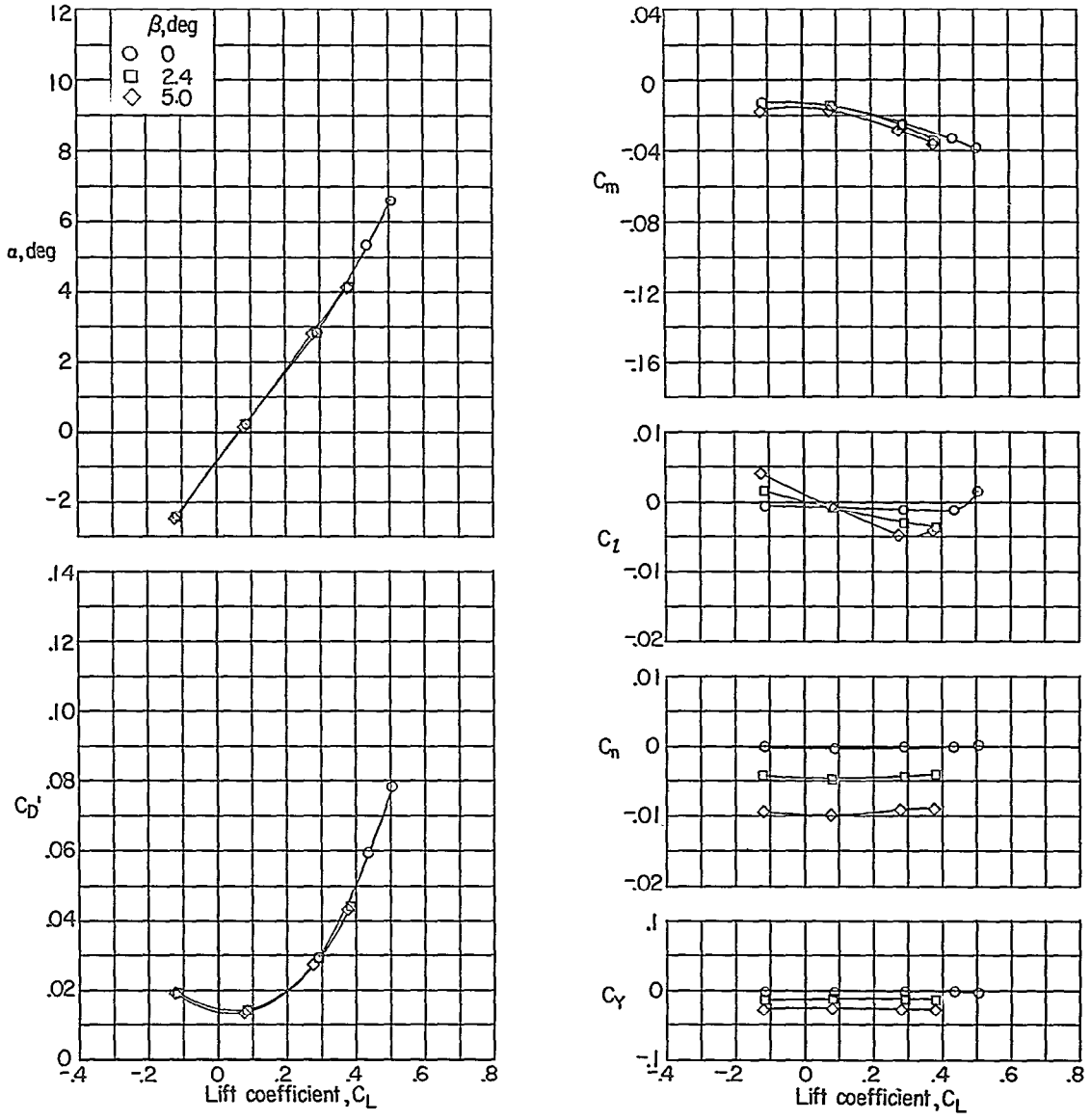

(b) M = 0.90.

Figure 26.- Continued.

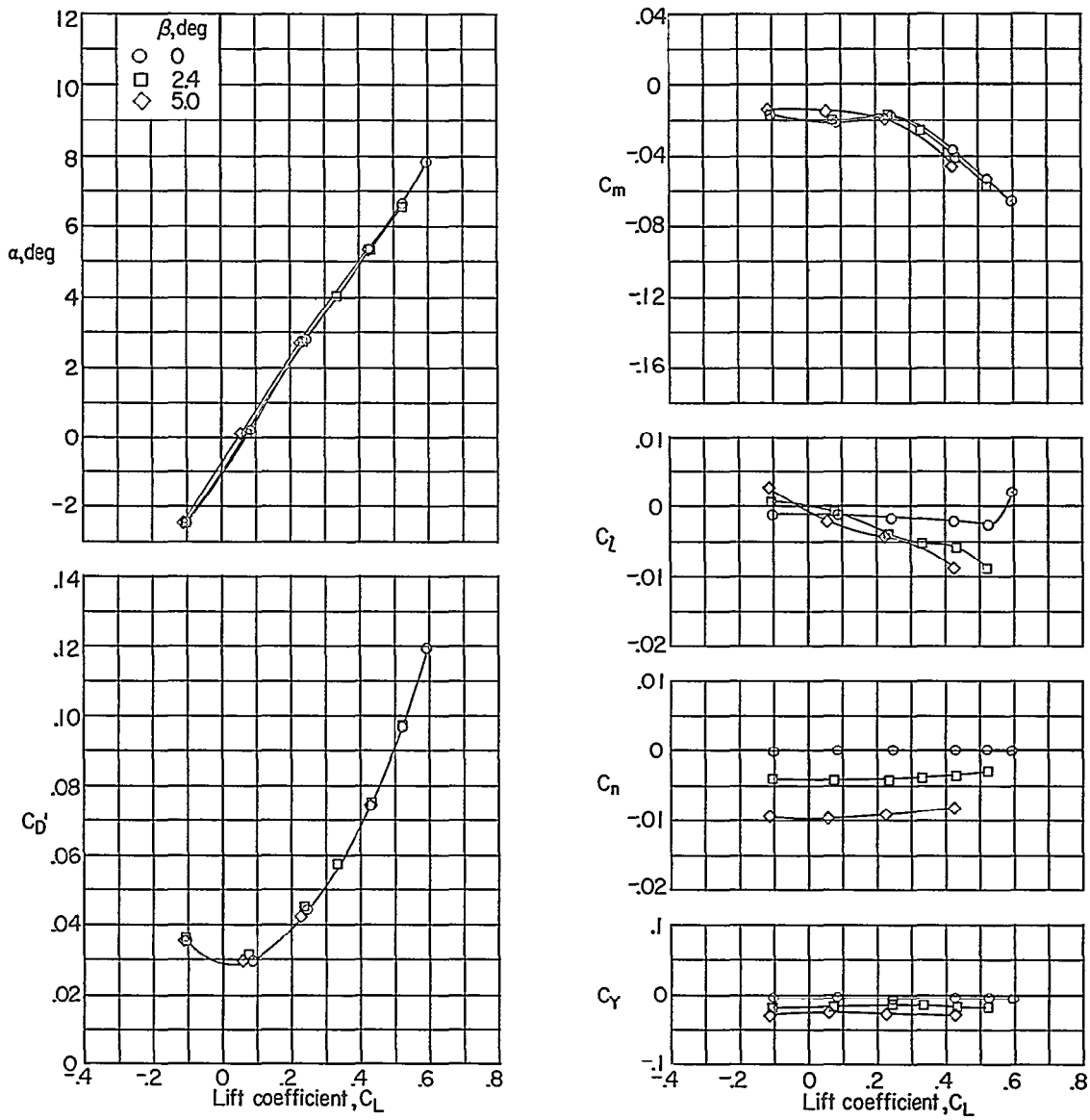

(c) M = 0.95.

Figure 26.- Continued.

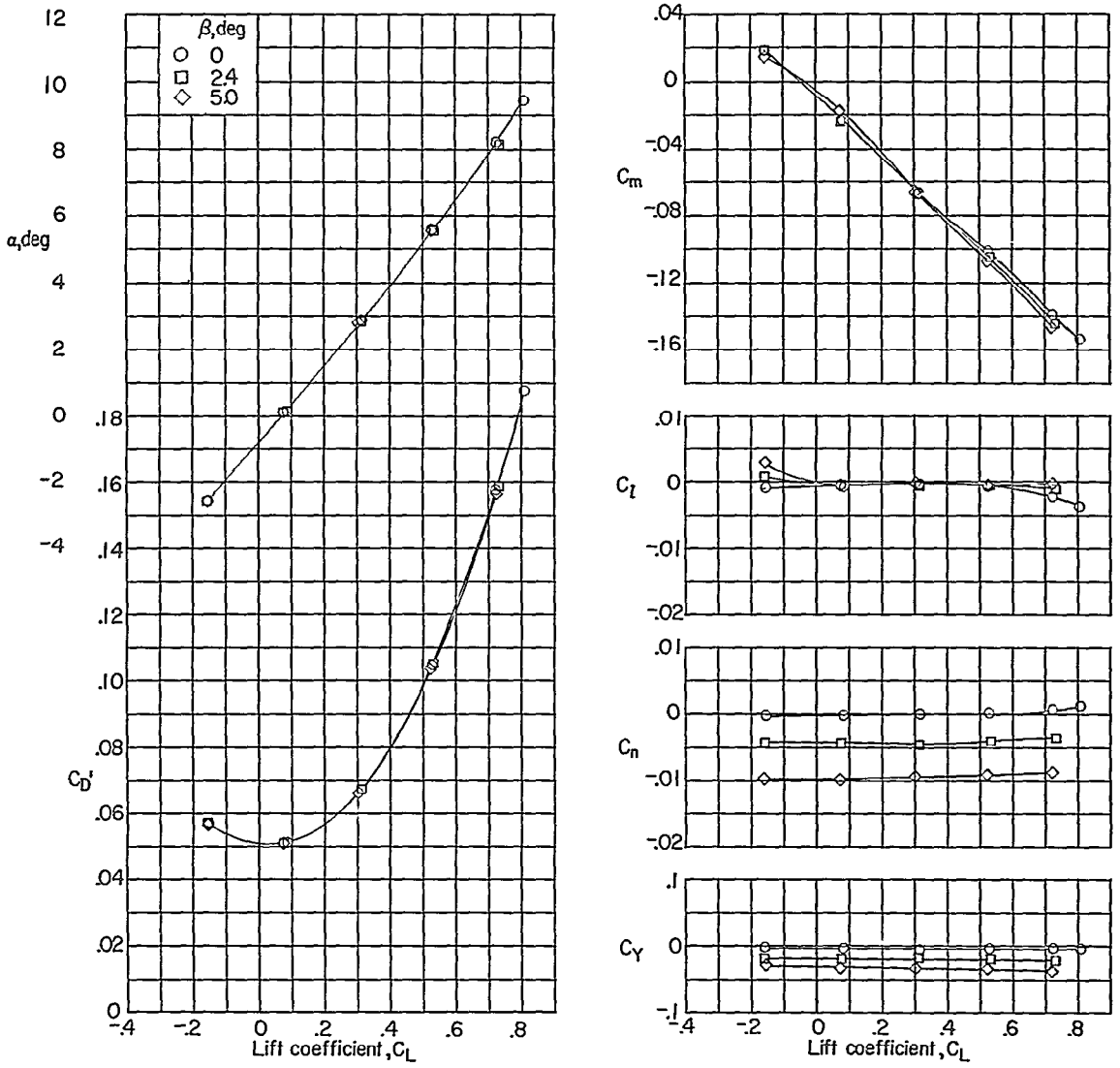

(d) M = 1.00.

Figure 26.- Continued.

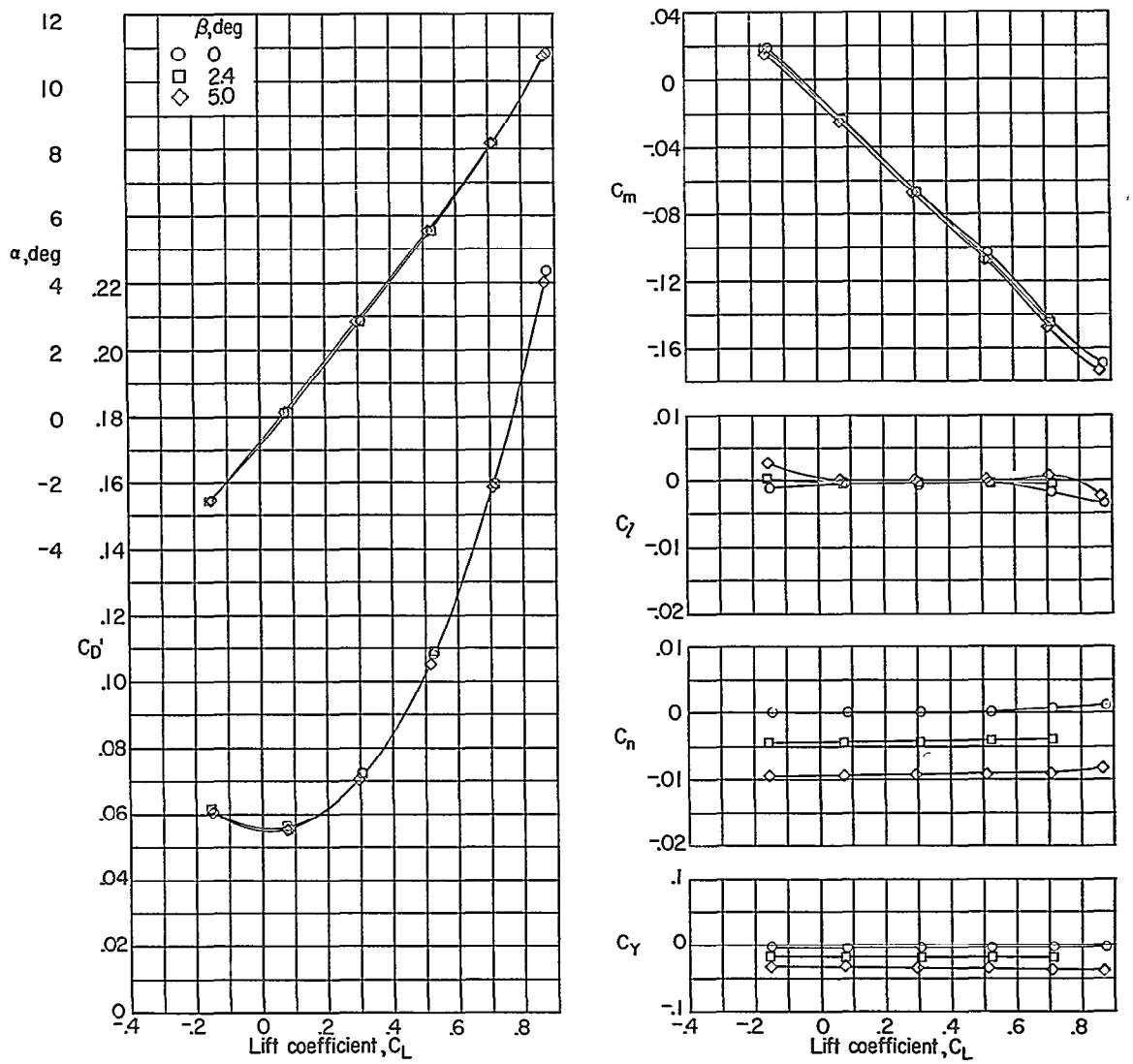

(e) M = 1.025.

Figure 26.- Continued.

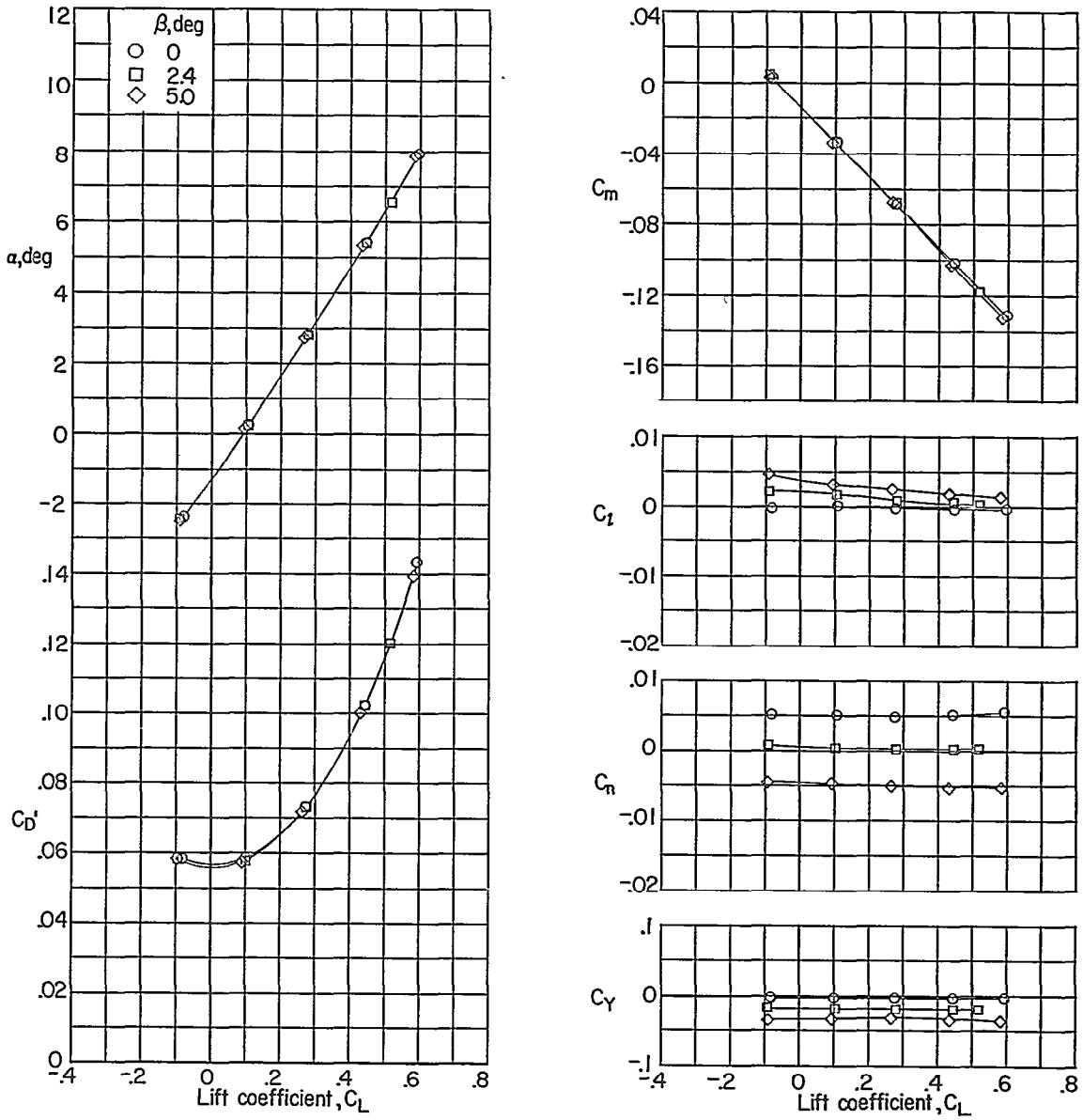

(f) M = 1.20.

Figure 26.- Concluded.

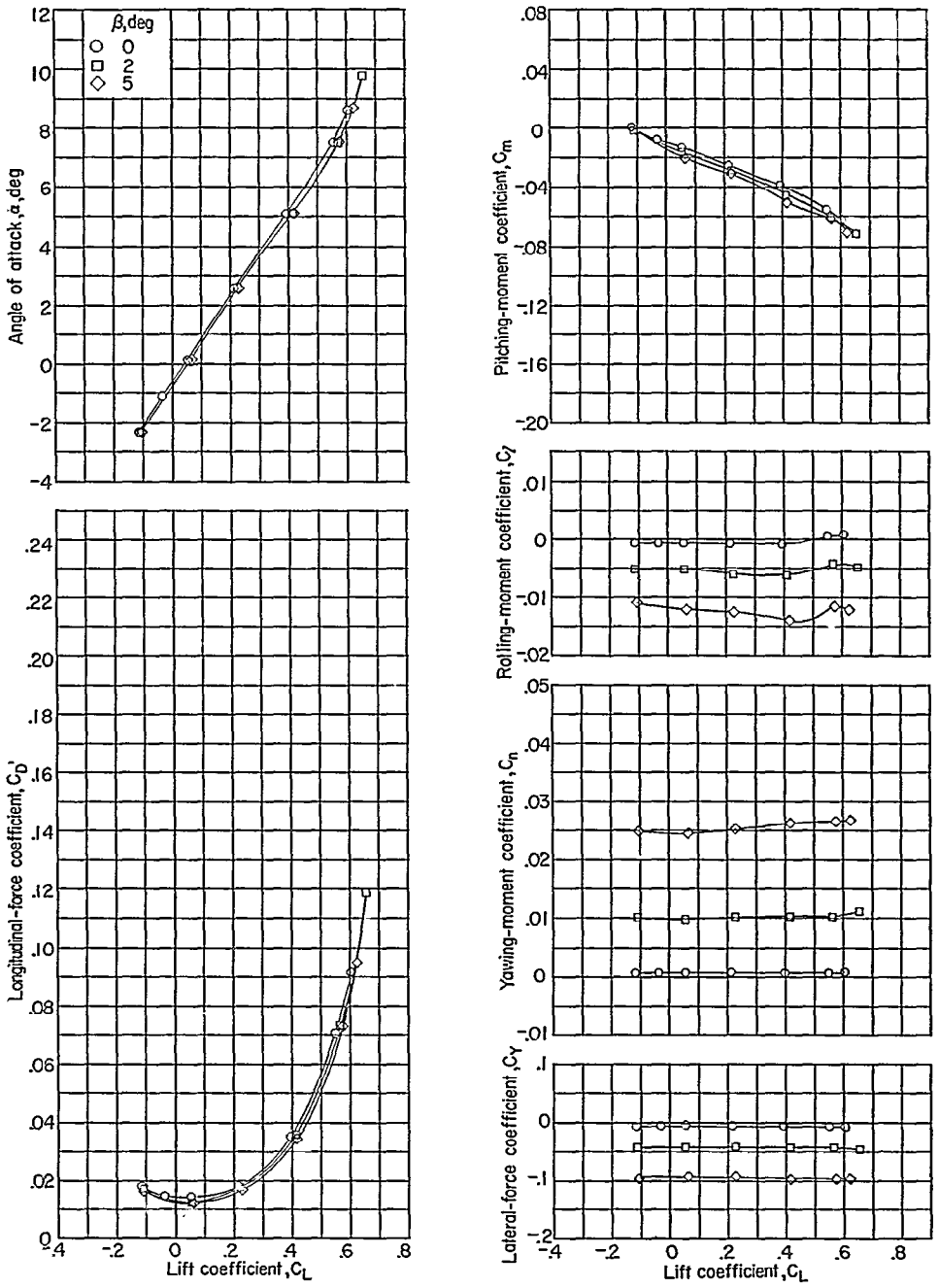

(a) M = 0.80.

Figure 27.- Variation with lift coefficient of the aerodynamic characteristics of the basic model (modified tail cone) with leading edge I for various angles of sideslip. Horizontal and vertical tails on.

[redacted]

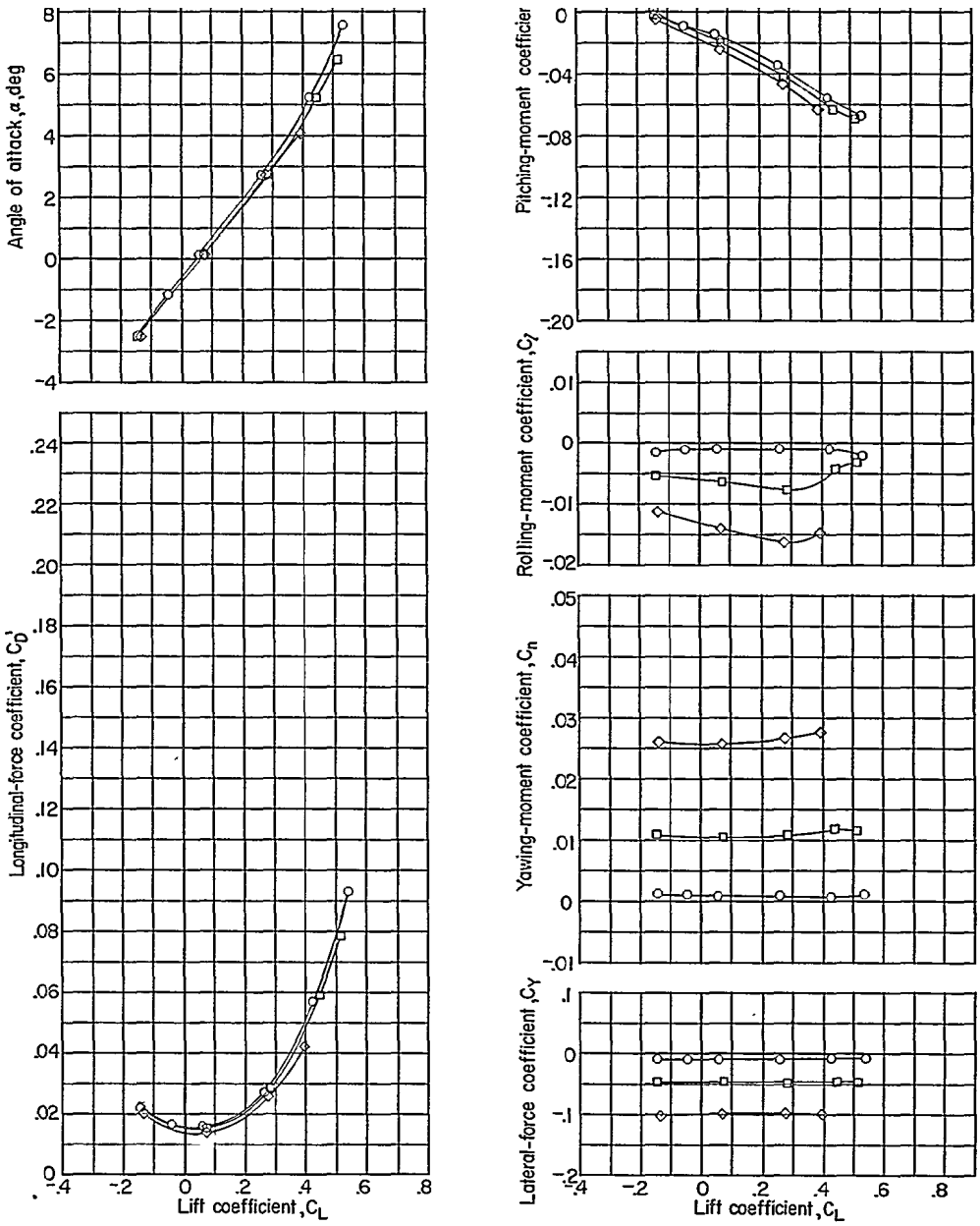

(b) M = 0.90.

Figure 27.- Continued.

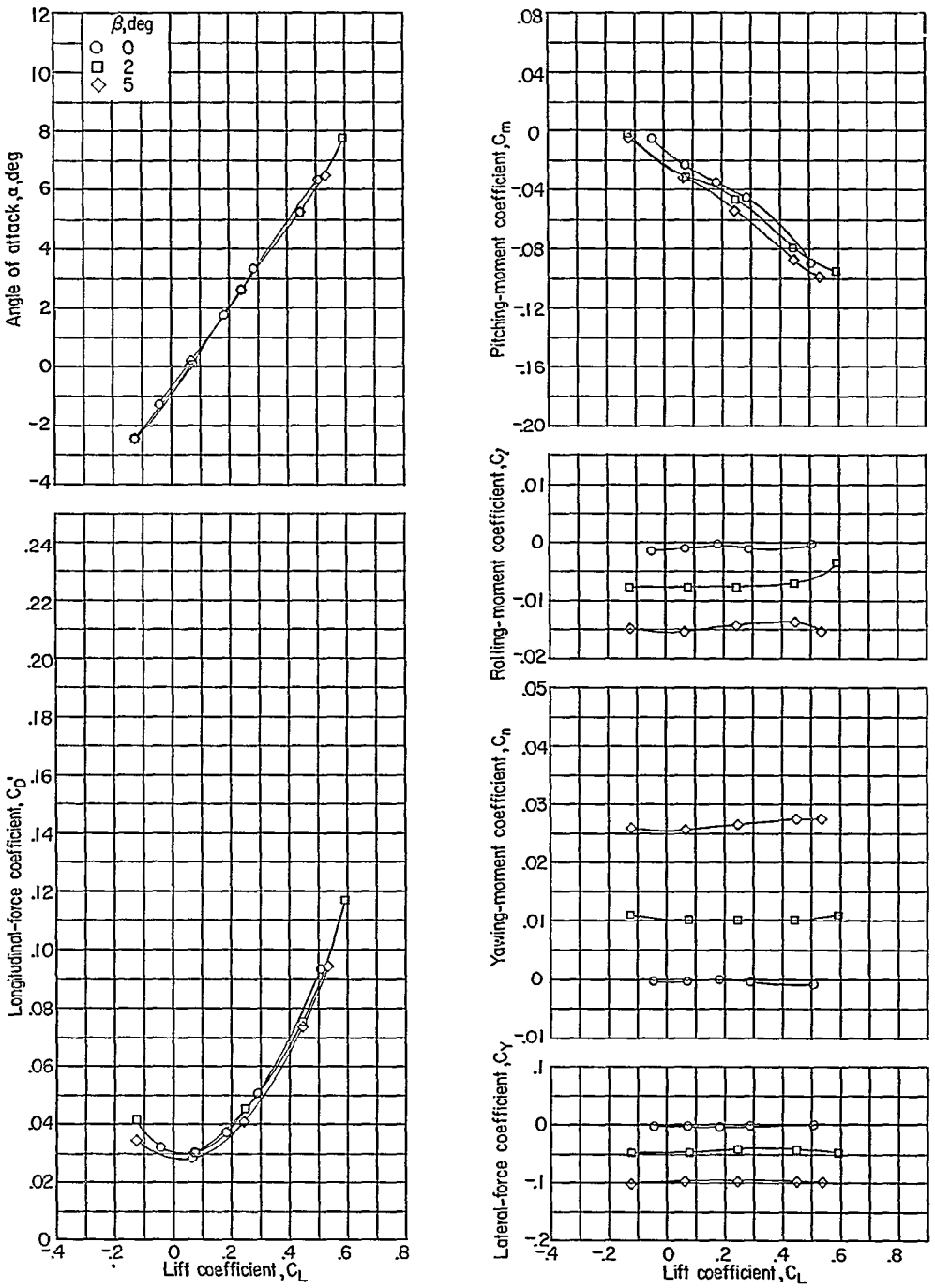

(c) M = 0.95.

Figure 27.- Continued.

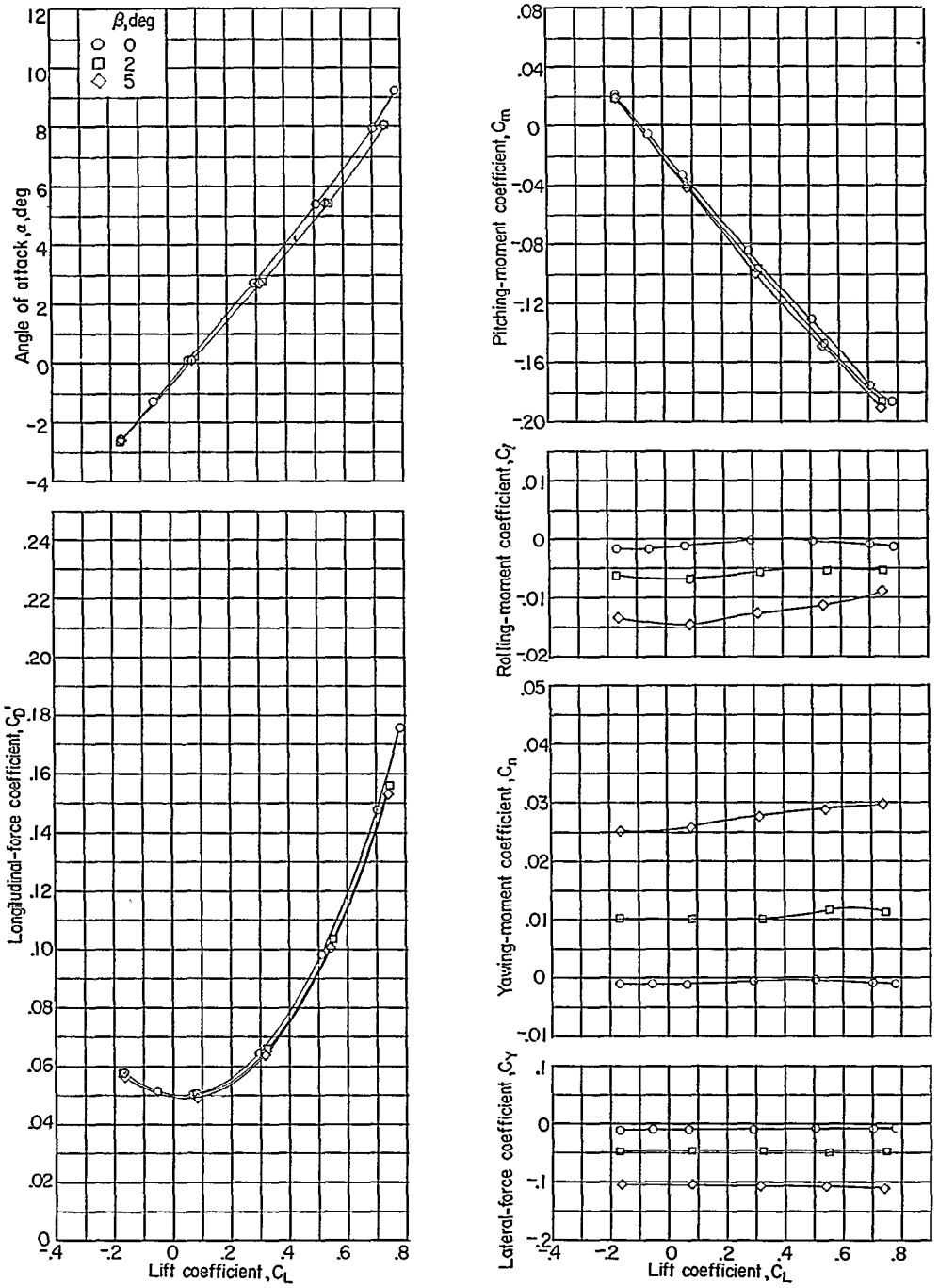

(d) M = 1.00.

Figure 27.- Continued.

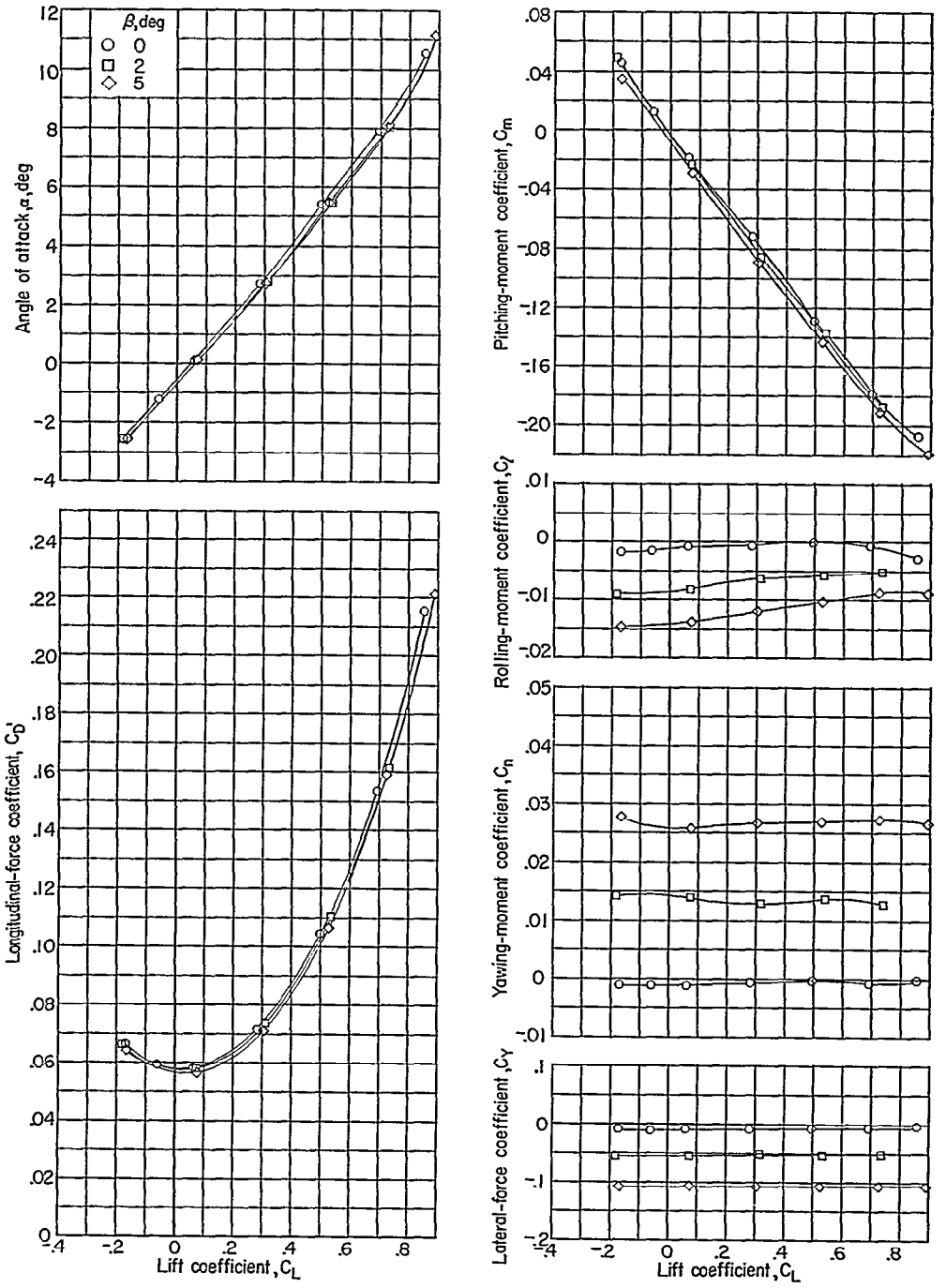

(e) M = 1.025.

Figure 27.- Continued.

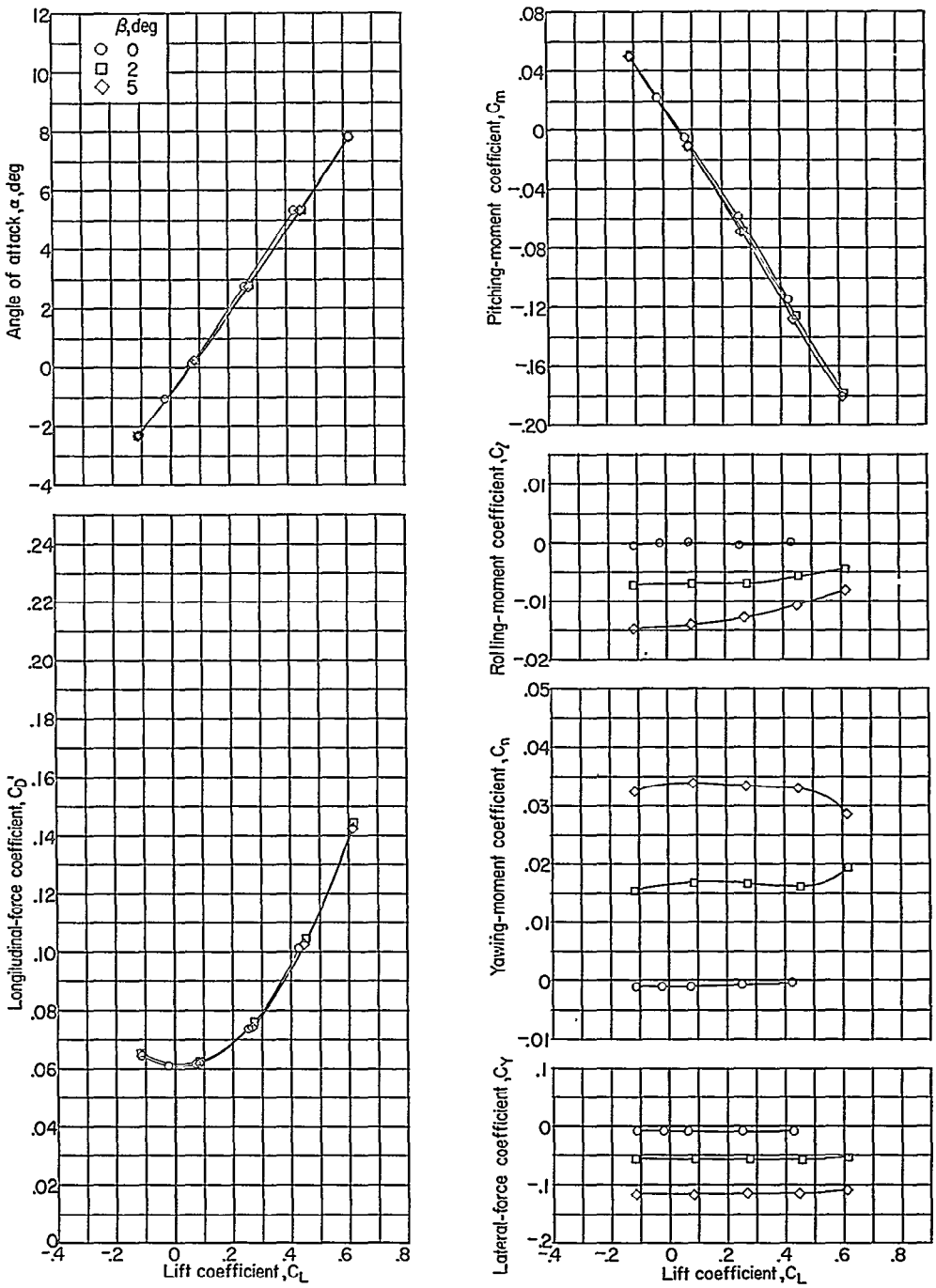

(f) M = 1.20.

Figure 27.- Concluded.

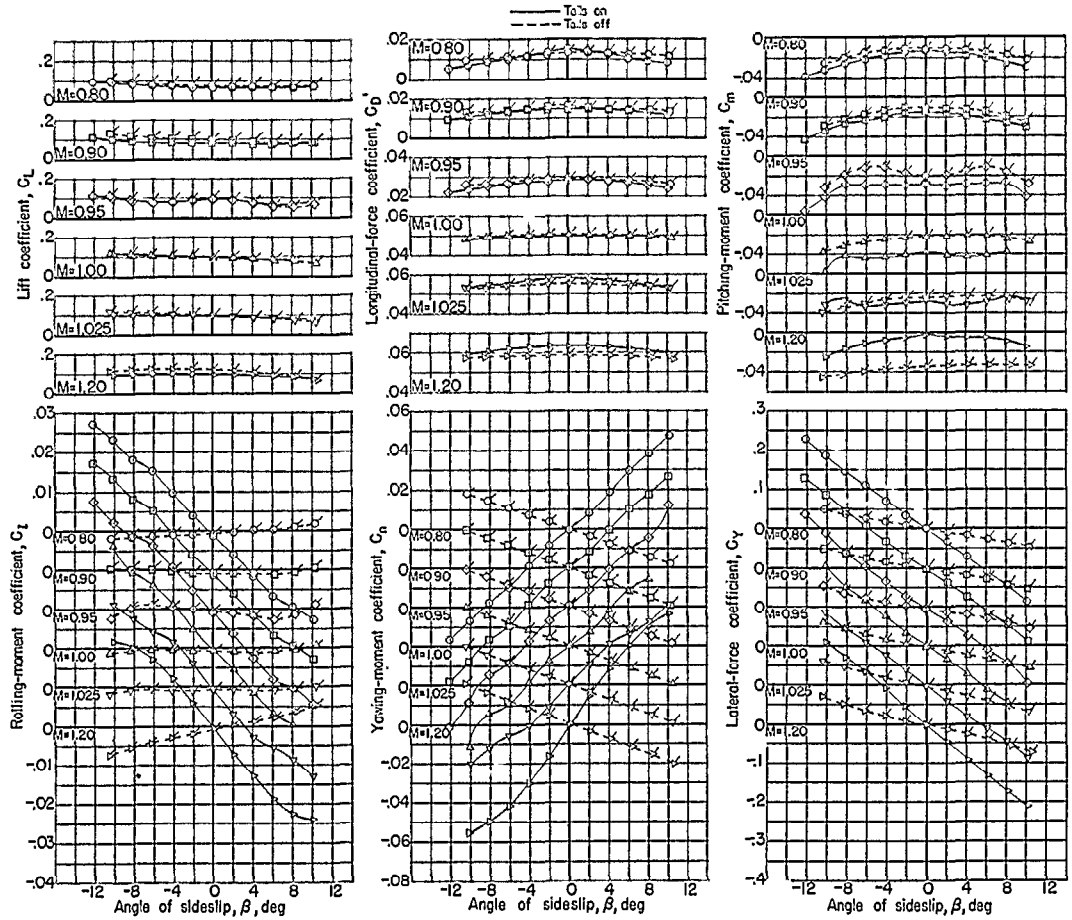

(a) $\alpha \approx 0.3°$.

Figure 28.- Variation with angle of sideslip of the aerodynamic characteristics of the basic model (modified tail cone) with leading edge I Horizontal and vertical tails on and off. Plain symbols indicate tails on and flagged symbols indicate tails off.

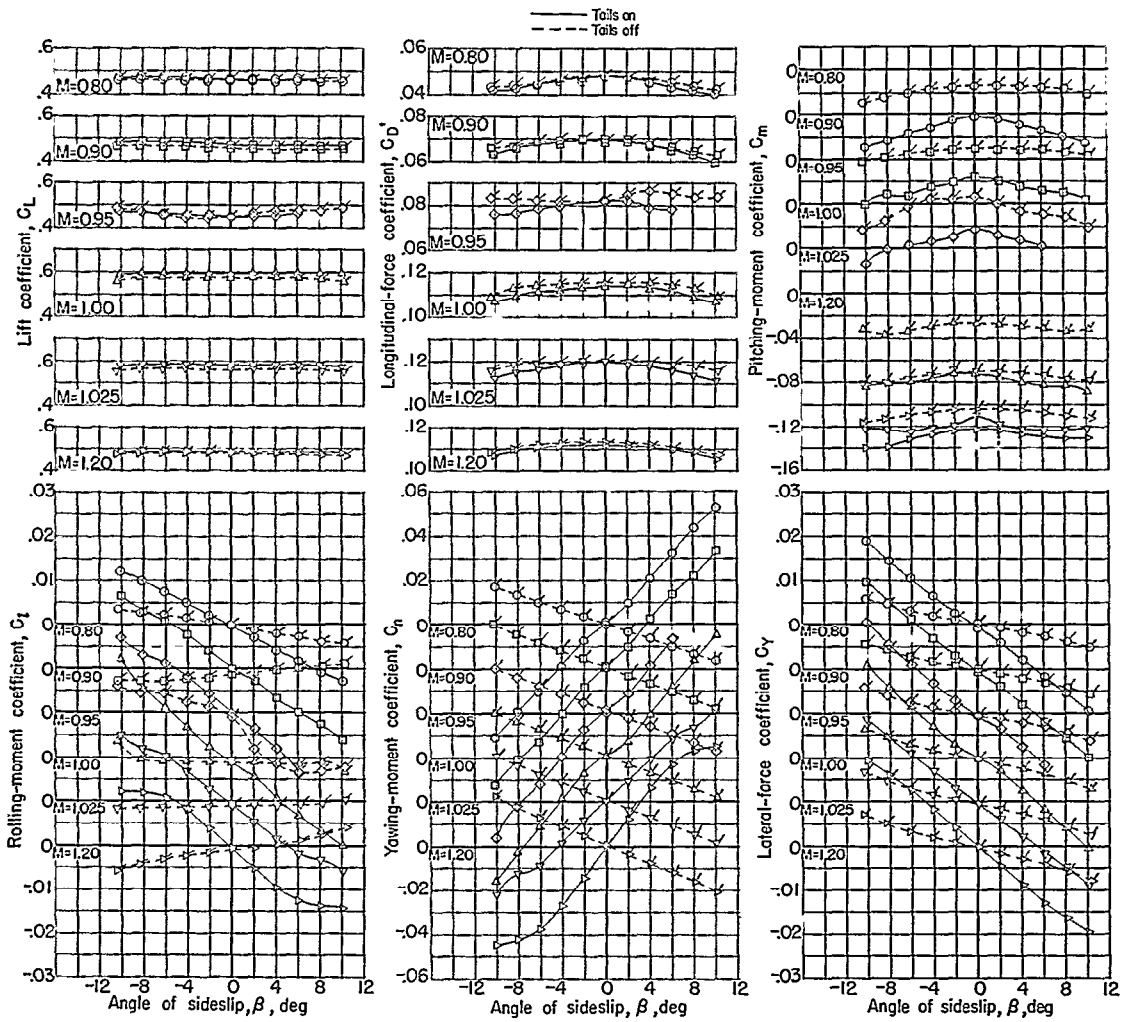

(b) $\alpha \approx 6.0°$.

Figure 28.- Concluded.

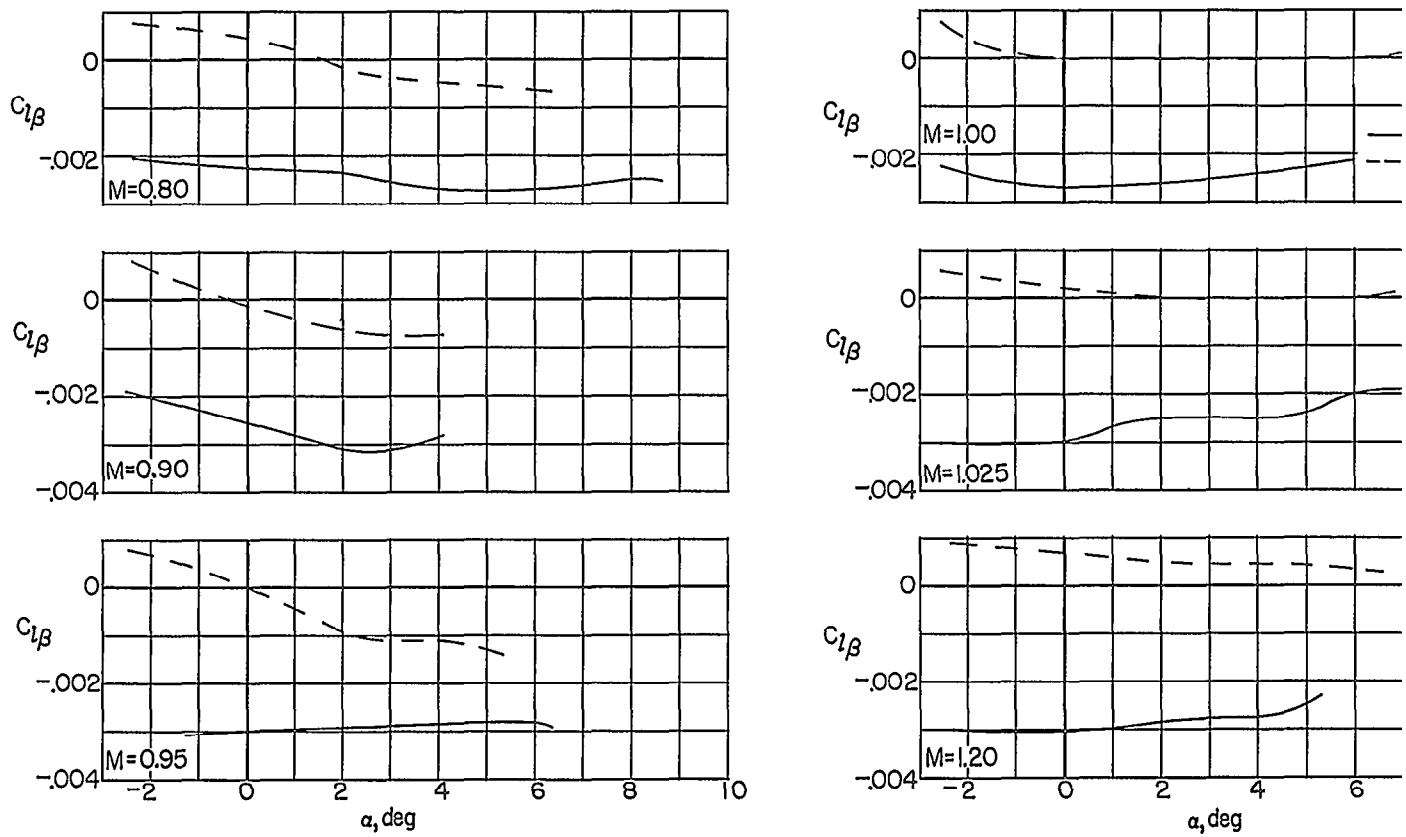

(a) Effective-dihedral derivative.

Figure 29.- Variation with angle of attack of the lateral stability derivatives for the basic model (modified tail cone) with leading edge I. Horizontal and vertical tails on and off.

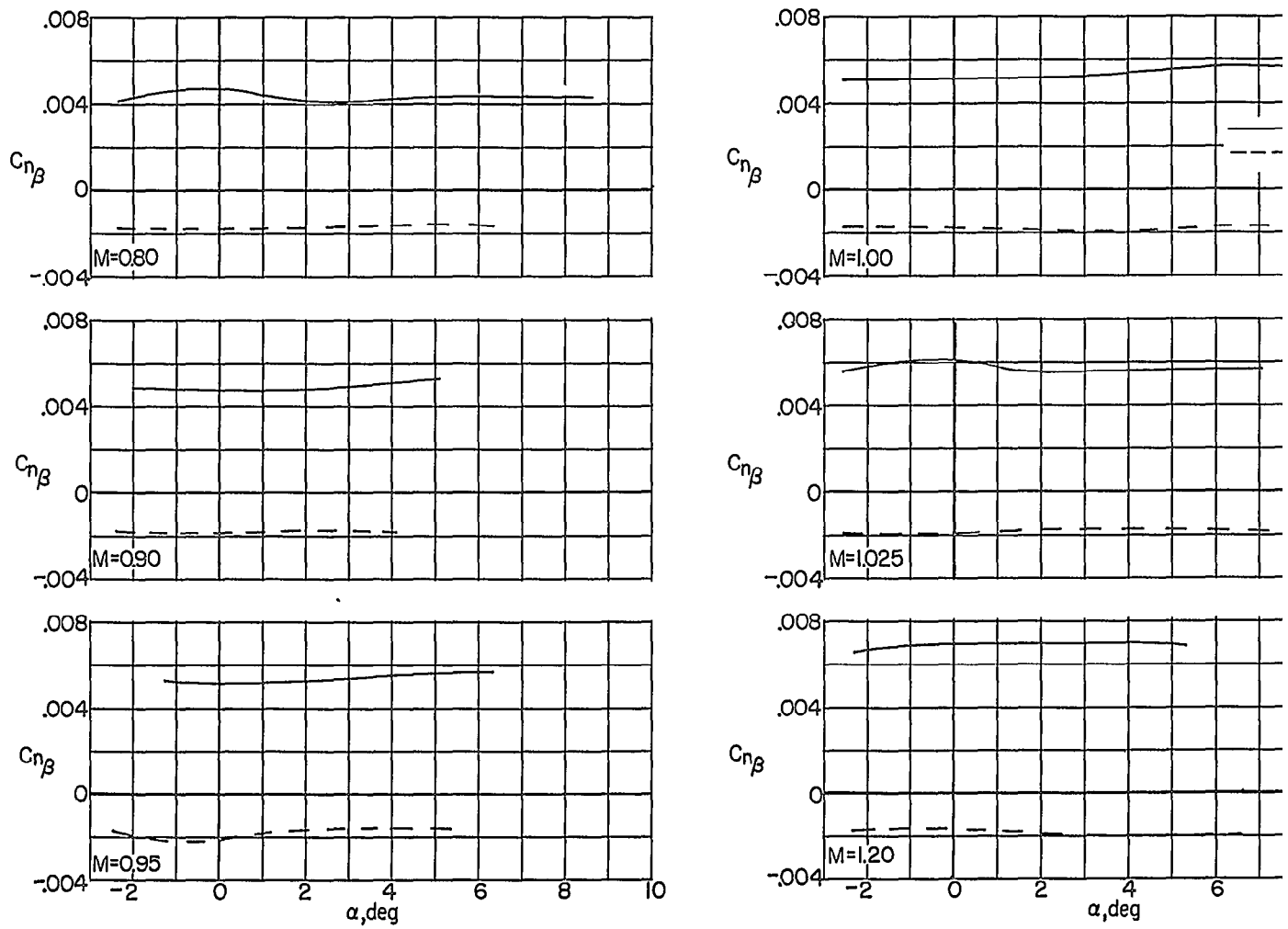

(b) Directional stability derivative.

Figure 29.- Continued.

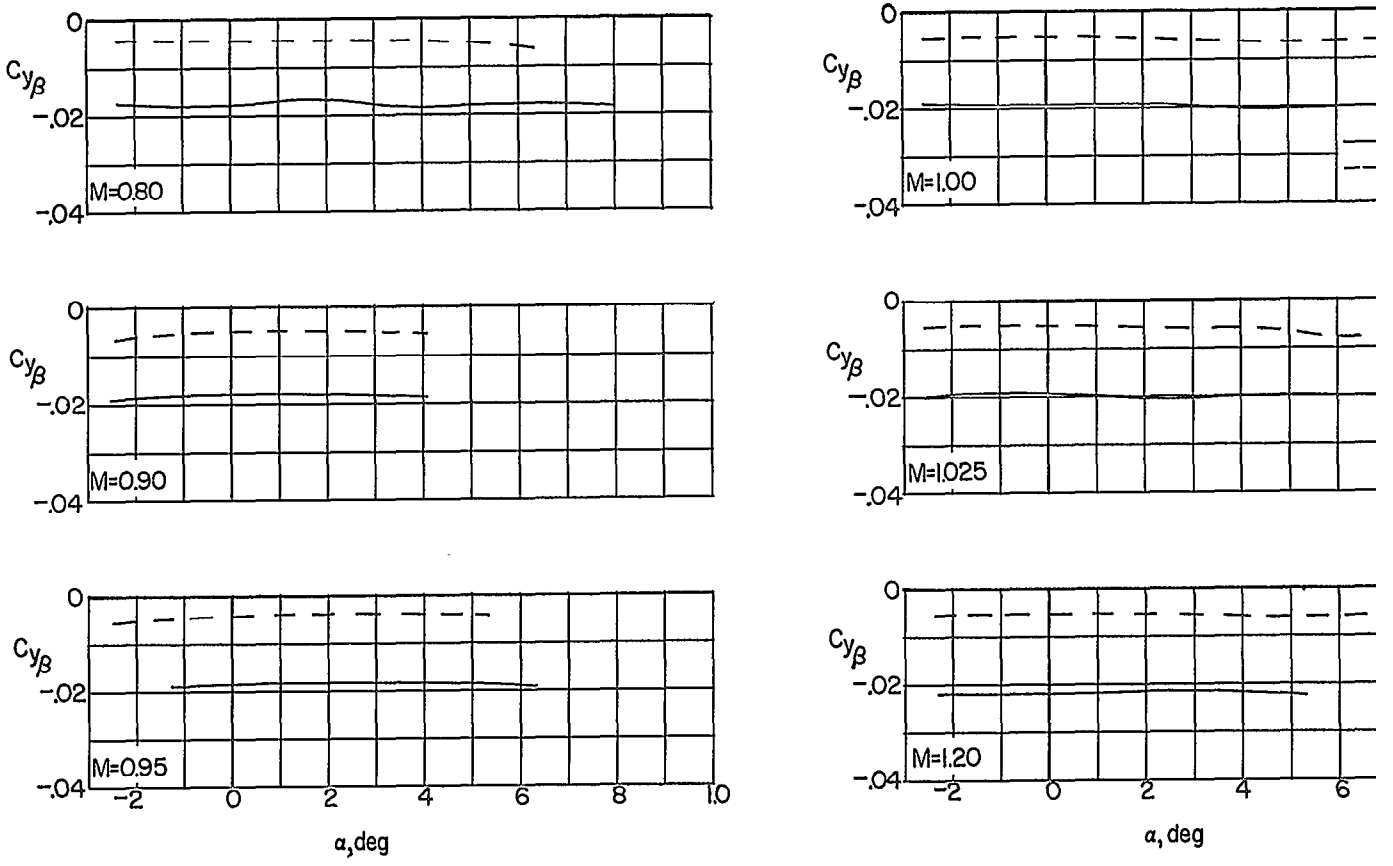

(c) Lateral-force derivative.

Figure 29.- Concluded.

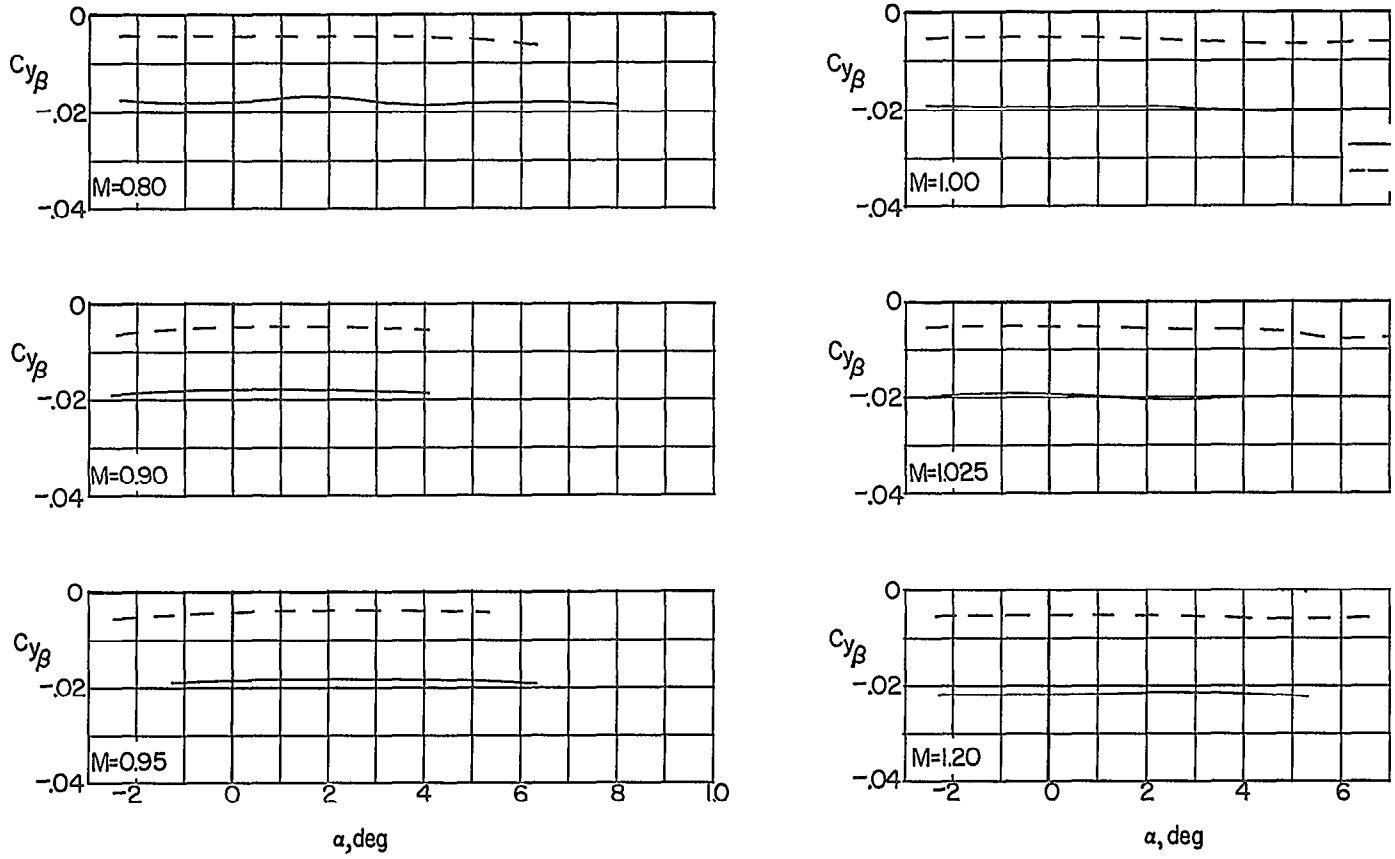

(c) Lateral-force derivative.

Figure 29.- Concluded.

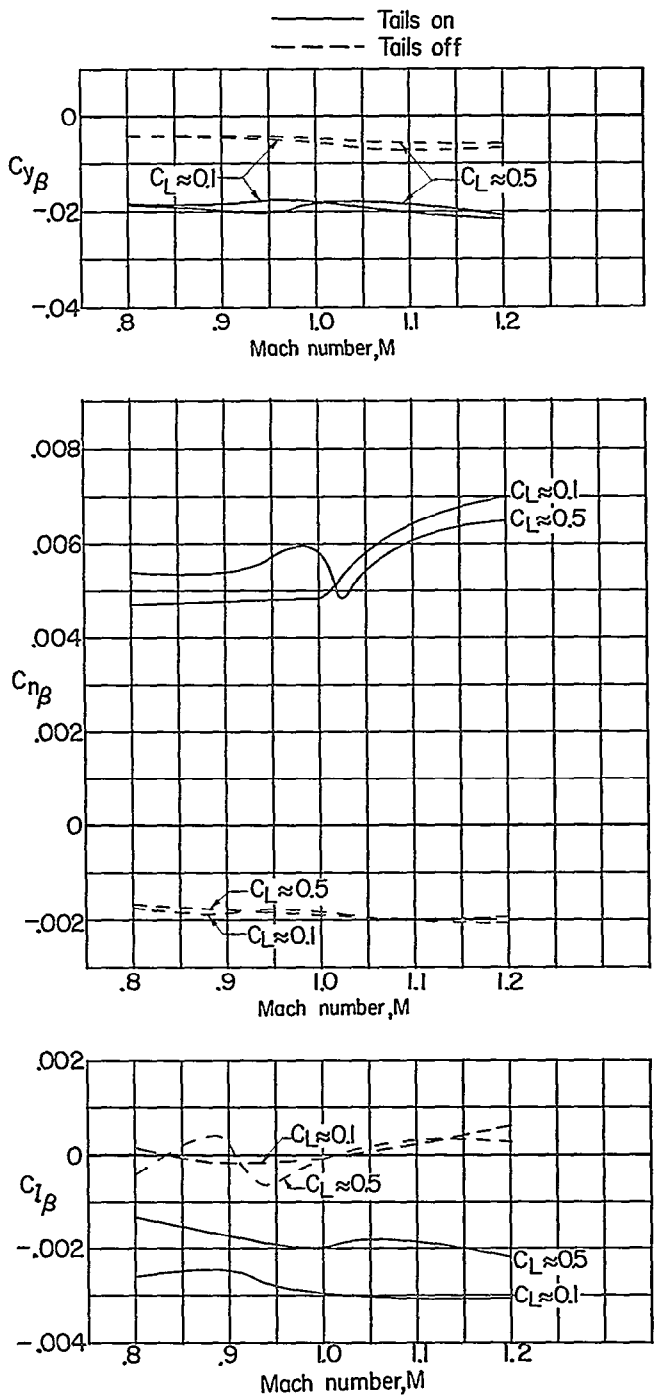

Figure 30.- Variation with Mach number of the lateral stability derivatives for the basic model (modified tail cone) with leading edge I. Horizontal and vertical tails on and off.

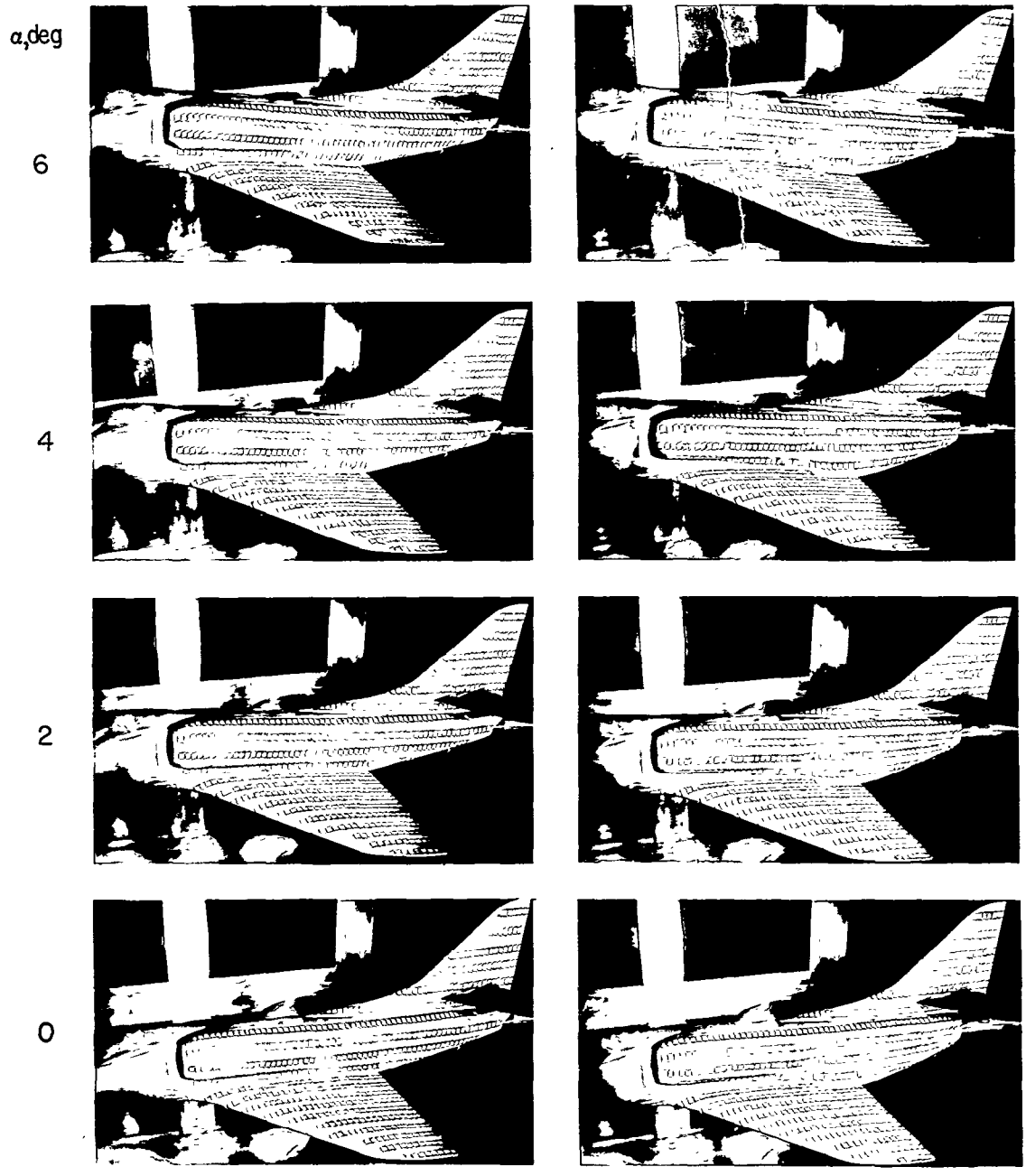

L-93576

(a) M = 0.80.

Figure 31.- Tuft photographs of the basic model with leading edge I with and without full bump.

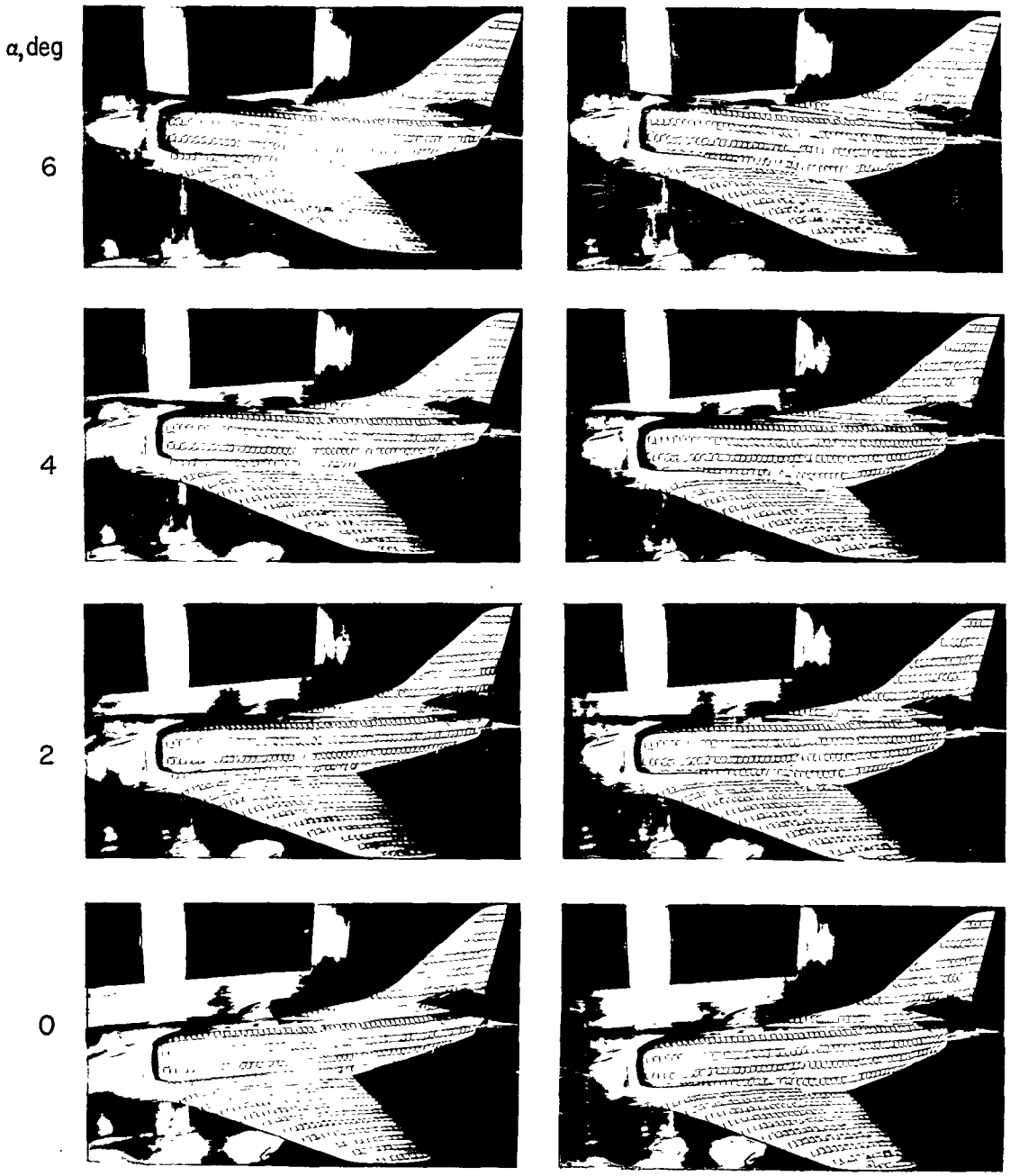

L-93577

(b) M = 0.85.

Figure 31.- Continued.

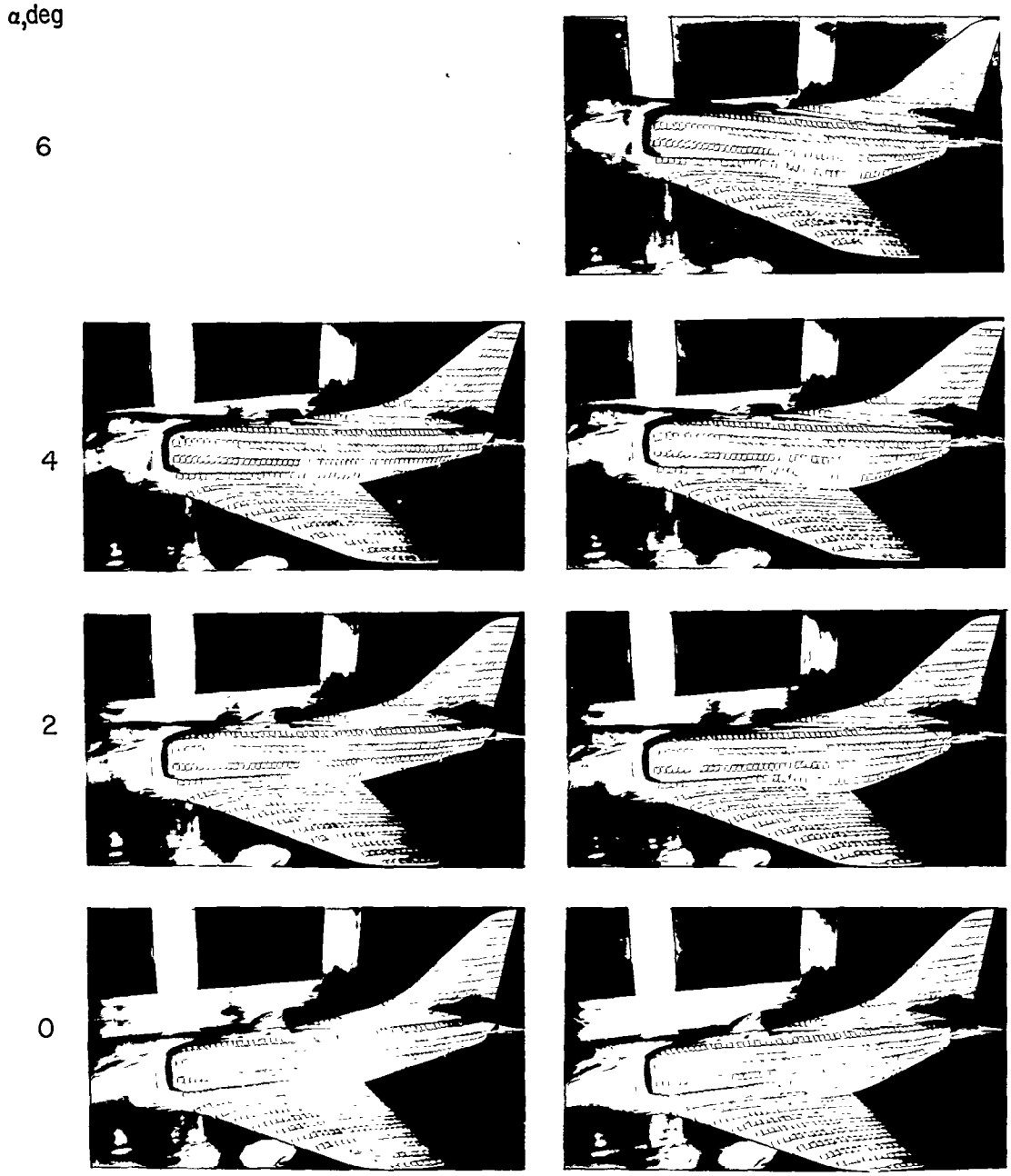

L-93578

(c) M = 0.90.

Figure 31.- Continued.

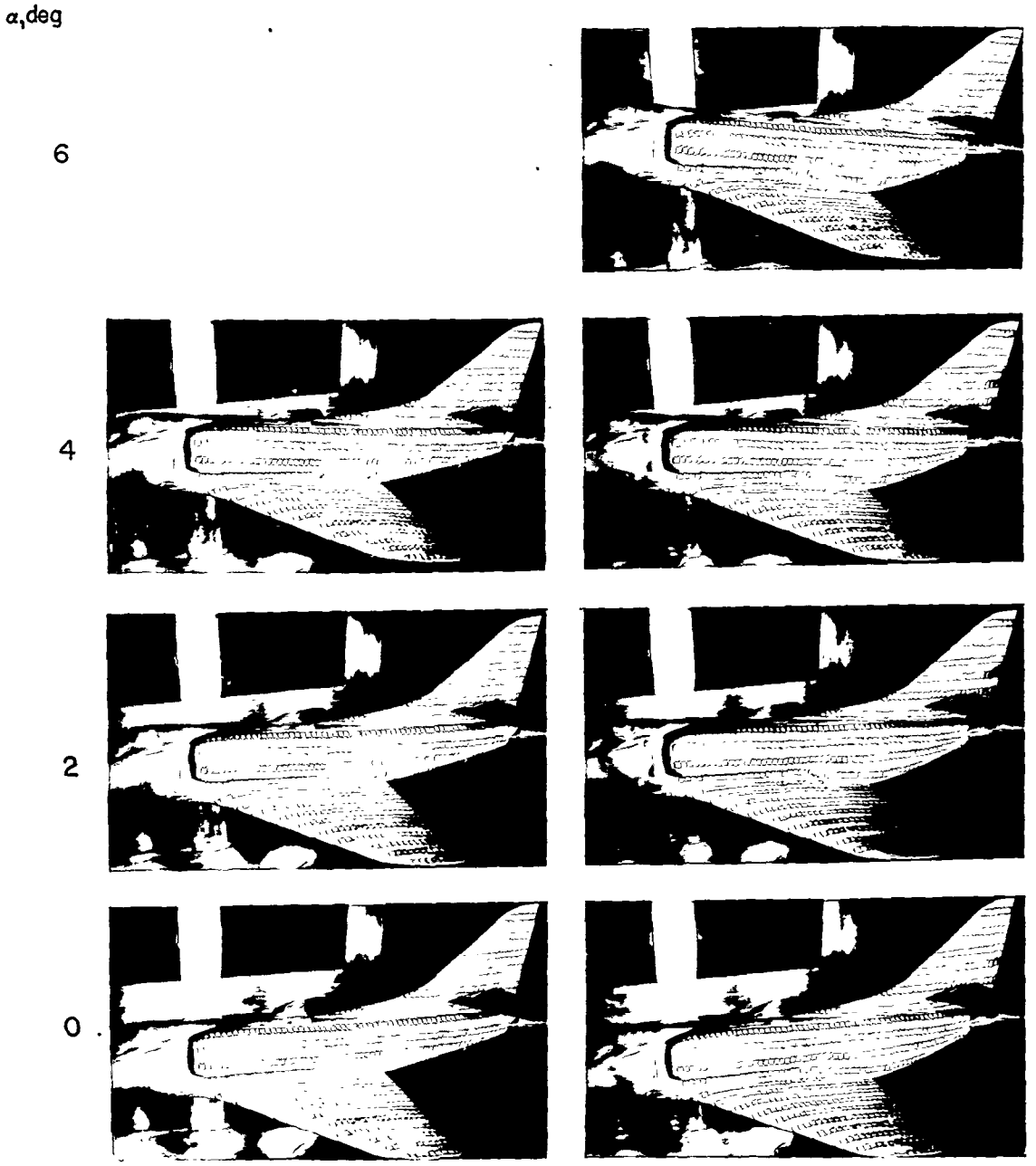

L-93579

(d) M = 0.95.

Figure 31.- Concluded.

INDEX

Subject	Number
Wings, Complete	1.2.2
Bodies - Cross Section	1.3.2.2
Airplanes - Specific Types	1.7.1.2
Airplanes - Performance	1.7.1.3
Stability, Static	1.8.1.1

ABSTRACT

Transonic wind-tunnel force and moment tests of a 0.10-scale model of the Douglas A4D-1 airplane were performed to investigate the static longitudinal characteristics of wing and fuselage modifications and the static lateral characteristics of the basic model. Tests were conducted at Mach numbers from 0.60 to 1.20, a maximum angle-of-attack range of approximately -3° to 11°, and at Reynolds numbers from approximately 2×10^6 to 3.5×10^6. Area-rule modifications to the fuselage and sweptforward wing trailing edge were beneficial to drag at Mach numbers around 0.975. Wing leading-edge modifications were only slightly successful in improving drag at lifting conditions. Lateral stability tests of the basic model revealed positive directional stability and positive effective dihedral throughout the tested angle-of-attack and Mach number ranges.

AL